MATERIAL CHARACTERISTICS AND DETERIORATION PROBLEMS OF ROMAN MOSAICS IN ANTANDROS ANCIENT CITY

A Thesis Submitted to the
the Graduate School of Engineering and Sciences of
İzmir Institute of Technology
in Partial Fulfillment of the Requirements for the Degree of

MASTER OF SCIENCE

in Architectural Restoration

by
Zişan KARAYAZILI

July 2013
İZMİR

We approve the thesis of **Zişan KARAYAZILI**

Examining Committee Members:

Prof.Dr. Hasan BÖKE
Department of Architectural Restoration, İzmir Institute of Technology

Prof.Dr. Başak İPEKOĞLU
Department of Architectural Restoration, İzmir Institute of Technology

Prof.Dr. Zeynep MERCANGÖZ
Department of Art History, Ege University

Prof.Dr. Sedat AKKURT
Department of Mechanical Engineering, İzmir Institute of Technology

Assoc.Prof.Dr. Gürcan POLAT
Department of Classical Archaeology, Ege University

12 July 2013

Prof.Dr. Hasan BÖKE
Supervisor,
Department of Architectural Restoration
İzmir Institute of Technology

Prof.Dr. Başak İPEKOĞLU
Co-supervisor,
Department of Architectural Restoration
İzmir Institute of Technology

Prof.Dr. Başak İPEKOĞLU
Head of the Department of
Architectural Restoration

Prof.Dr. R.Tuğrul SENGER
Dean of the Graduate School of
Engineering and Sciences

ACKNOWLEDGMENTS

First of all, I would like to express my gratitude to my supervisor Prof. Dr. Hasan Böke and co-supervisor Prof. Dr. Başak İpekoğlu for their invaluable supervision, guidance and care throughout this thesis. I specially thank to Prof. Dr. Hasan Böke for his scientific support, encouragement and incredible patient during this study.

I am also grateful to Assoc. Prof. Dr. Gürcan Polat, Head of the Antandros Excavations, for his permission and sharing his knowledge during site survey of this study. I would like express my special thanks to the jury members; Prof. Dr. Zeynep Mercangöz, Prof. Dr. Sedat Akkurt and Assoc. Prof. Dr. Gürcan Polat for their attendance at my thesis defence seminar and for their valuable suggestions to this study.

I would like to thank the researchers of the Centre for Materials Research at the Izmir Institute of Technology for XRD, XRF, TGA and SEM-EDS analyses during the experimental stage of this study. Also my special thanks are for Spec. Dr. Elif Uğurlu Sağın and Spec. Kerem Şerifaki for their help and moral support during this study.

My special thanks to my dear friend Funda Uygun for her endless support, patient and friendship, working with her in same office is invaluable for me. Furthermore, my special thanks to my special friend Selçuk Kaplan for his endless patient encouragement during this study. Finally, I would like to express my special thanks to my beloved family for their endless love and patient throughout my life and especially my dear sister Dişan Karayazılı who made me to overcome all the difficulties with her encouragement, support and love. This thesis dedicated to her.

ABSTRACT

MATERIAL CHARACTERISTICS AND DETERIORATION PROBLEMS OF ROMAN MOSAICS IN ANTANDROS ANCIENT CITY

In Roman period, fascinating, colorful and highly detailed mosaics were formed by laying small colored stones, pieces of marble, ceramics and glass tesserae on setting bed. Their conservation requires knowledge concerning the construction techniques, properties of the used materials as well as the problems of deterioration.

In this study material characteristics and deterioration problems of Roman mosaics found in a Roman Villa in Antandros Ancient city (Altınoluk, Balıkesir) have been determined in order to define the properties of the original mortars and tesserae, and the main characteristics of the intervention materials, which will be used in the conservation works of mosaics. For this purpose, basic physical properties, mineralogical, chemical and microstructural characteristics of preparatory mortars and tesserae were determined by color spectrometer, standard RILEM test methods, XRD, XRF, SEM-EDS and TGA analyses.

Results indicated that mosaics had a multilayered system composed of tesserae, bedding layer, nucleus and rudus from the surface to bottom. Tesserae were small cubes of stone, ceramic and opaque glasses. Stone tesserae were limestones and dolomites. Ceramic tesserae were produce from different raw clay sources by heating them at high temperatures. Glass tesserae were natron based and classified as soda-lime, lead, and soda-lime lead glasses. They were opacified with Ca and Pb-antimonates typical of Roman period and colored with transition metals. The thin bedding layer in which the tesserae were embedded was non-hydraulic lime mortar. Nucleus and rudus mortar layers were composed of crushed brick aggregates and lime. Brick aggregates were pozzolanic and binders of mortar layers were hydraulic due to pozzolanic brick aggregates. The binders exhibited a uniform structure and the strong adherence between brick aggregates and lime.

Deterioration processes of the mosaics in Antandros Ancient city caused by destroyed original drainage systems, settlement in the mosaic floors, changes in temperature and humidity and biological colonization. Based on the results of this study, the recommendations are developed for the conservation works of the mosaics.

ÖZET

ANTANDROS ANTİK KENTİNİN ROMA MOZAİKLERİNİN MALZEME ÖZELLİKLERİ VE BOZULMA SORUNLARI

Roma Döneminde renkli taş, mermer, seramik ve cam tesseraların yatak harcı üzerine yerleştirilmesi ile etkileyici, renkli ve detaylı mozaikler üretilmiştir. Mozaiklerin korunması için; yapım teknikleri, malzeme özellikleri ve bozulma sorunlarının bilinmesi gereklidir.

Bu çalışmada Antandros Antik kentinde (Altınoluk, Balıkesir) bulunan Roma Dönemi mozaiklerinin malzeme özellikleri ve bozulma sorunları, korumada kullanılacak malzemelerin temel özelliklerini belirlemek üzere incelenmiştir. Mozaik harç tabakalarının ve tesseraların temel fiziksel özellikleri, ham madde kompozisyonları, mineralojik, kimyasal ve mikro yapısal özellikleri; renk ölçer, standart RILEM test yöntemleri, XRD, XRF, SEM-EDS ve TGA analizleri ile belirlenmiştir.

Analiz sonuçlarına göre mozaikler; tessera, yatak harcı, ince ve kaba harçtan oluşan çok katmanlı bir yapım sistemine sahiptir. Tesseralar küçük küpler şeklinde taş, seramik ve opak camlardan oluşmaktadır. Taş tesseralar kireç taşı ve dolomitlerden oluşmuştur. Seramik tesseralar yüksek sıcaklıklarda farklı kil kaynakları kullanılarak üretilmişlerdir. Cam tesseralar natron ile üretilen ve soda-kireçli, kurşunlu ve soda-kireç kurşunlu camlardır. Cam tesseralar Roma döneminde yaygın olarak kullanılan Ca ve Pb-antimonlar ile opaklaştırılmış ve geçiş elementleri ile renklendirilmişlerdir.

Tesseraların yerleştirildiği ince yatak harcı hidrolik olmayan kireç harcıdır. Bunun altındaki ince ve kaba harç tabakaları ise tuğla kırığı agregalardan ve kireç harcından oluşmaktadır. Harçlarda bulunan tuğla agregalar ve kireç birbirlerine iyi bağlanmışlardır.

Antandros Antik kentinde bulunan mozaiklerdeki bozulmalar; döşemelerdeki oturmalar, bozulmuş özgün drenaj sistemi, sıcaklık ve nem değişiklikleri ve biyolojik kolonizasyonlardan kaynaklanmaktadır.

Bu çalışma sonuçlarına dayalı olarak, mozaiklerin korunmasına yönelik öneriler geliştirilmiştir.

TABLE OF CONTENTS

LIST OF FIGURES

LIST OF TABLES

CHAPTER 1

INTRODUCTION

Mosaics were constructed on floors, walls, and ceilings as covering elements since 4000 BC in Mesopotamia. The decorative patterns of the mosaics were created by using natural stones, baked clays, ceramics, terracottas and glasses in different geometric forms and sizes.

The early floor mosaics examples called terrazo pavements were constructed with large stone pieces on a natural ground which were used in religious buildings in the Neolithic settlement of Çayönü in Diyarbakır at 7250-6750 BC (Figure 1. 1) (Braidwood and Çambel 1983).

Similar to the use of stone, colored baked clay cones were also used in ancient mosaics for decoration of temples on walls and columns in the beginning of the 3000 BC, in Sumer, Uruk, in southern Mesopotamia (Anthony 1968).

In 3100-2686 BC, walls, columns headings and artefacts were beginning to be decorated with colored glass fragments, lapis lazuli and other stones in Egypt.

Figure 1. 1. The terrazzo pavement of a religious building in Diyarbakır-Çayönü (Source: Erkan 2007)

In Ancient Greek (5^{th} - 4^{th} century BC) mosaics, small stone fragments and pebbles that were collected from river beds and sea shores with natural red, white, blue and green colors inserted in a thick coat of cement were used (Anthony 1968).

Figure 1. 2. Pebble mosaic pavement in polychrome house (Megaron 2), in Gordion (1956-57) (Source: Kaplan et. al. 2011)

The earliest examples of Roman mosaics which were dated to the 8th century BC were found in Gordion and Crete (Figure 1. 2) (Haswell 1973). The mosaics constructed in the Centaur Bath in Corinth (Olynthos, northern Greek) were the best pioneers of Roman mosaics in the last quarter of the 5th century BC (Dunbabin 1999, Özügül 1996, Tabanlı 2007).

Corinth, Sicyon and Eretria mosaics from Olynthus in northern Greece were constructed with natural pebbles in the beginning of the 4th century BC and 340 BC, at Late Classical period. In this period, private houses were decorated with mosaics in contrast to the Archaic Period mosaics that were commonly used in temples (Dunbabin 1999).

In the Early Hellenistic Period, about the last third of the 4th century BC, diversity of mosaics in forms, colors and materials were developed with the progress of stone cutting techniques (Dunbabin 1999). Small, square of stone tiles, marbles or baked clays called "tessera" (the plural form tesserae) were used with pebble mosaics since the 3rd century BC (Blake 1930, Üstüner 2002). Their use soon became widespread in Hellenistic and Roman Period from the center of Empire to the eastern and western states in the beginning of the 2nd century BC (Anthony 1968, Dunbabin 1999, Tabanlı 2007).

In Hellenistic Period (323 BC-31 BC), a panel that constructed with small scaled tesserae in mosaic workshops than applied in situ called "emblemata" were started to use in mosaic manufacture. In emblemata main scene in mosaic designs were created. (Anthony 1968).

Romans used stone, marble or baked clay tesserae in mosaics as in the Hellenistic Period. However, they developed materials and compositions of the floor mosaics. They constructed mosaics with chiefly black and white colored (monochrome) tesserae for designing geometric patterns and for depicting everyday life and animals. Emblemata were also used in Roman mosaics. Mosaics were constructed in private houses, public buildings and temples (Anthony 1968, Dunbabin 1999).

After 2nd century BC, glass was started to use in mosaics. In floor mosaics, glass tessera was used with stone tesserae when shiny blue or green colors were required. Therefore the patterns, figures and colors of the mosaics were diversified (Anthony 1968, Ödekan 1996). In the middle of the 1st century BC glass tesserae began to be used in wall and vault mosaics (Harden 1968, Van Saldern 1974, Davison 1989, Tait 1991).

Roman mosaics were classified into five categories according to compositions of mosaic and the material of the tesserae (stone, marble, ceramic and glass). They are opus tessellatum, opus vermiculatum, opus signinum, opus sectile and opus musivum (Strong 1929, Anthony 1968).

Opus tessellatum was the common mosaic-making technique applied on walls and floors in 2nd and 1st century BC in Rome (Gauckler 1897, Anthony 1968, Tabanlı 2007). In this technique, regularly cut and colored stones, marbles and ceramics were used as tesserae (Figure 1. 3) (Anthony 1968). The sizes of tesserae were larger than Hellenistic period mosaics. Tessellatum mosaics were often used in Roman baths (Dunbabin 1999, Genç 1984).

Figure 1. 3. Opus tesselatum mosaic from House of Ganymede at 3rd century BC in Morgantina, Sicily, (Italy) (Source: www.squinchpix.com)

Opus vermiculatum was similar to the tessellatum technique. In this technique, smaller and colorful tesserae such as lapis lazuli, cornelian, and alabaster were used. Red, yellow and turquoise colored glasses were also used when shiny and colored tesserae were required (Figure 1. 4). They were commonly used in baths, piscine's and fountains (Anthony 1986).

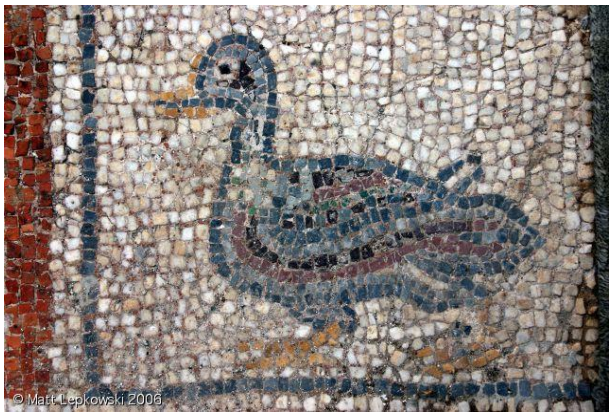

Figure 1. 4. Opus vermiculatum mosaic from Terrace houses in Ephesus, Selçuk, İzmir,(Turkey) (Source: http://www.travelsinparadise.com)

Opus signinum technique was executed by red colored brick-lime mortars (Cocciopesto) applied on walls and floors before covering them with marbles (Saltuk 1997, Dunbabin 1999), in this technique ceramic and marble fragments were mixed and randomly introduced into the mortars (Figure 1. 5) (Dunbabin 1999, Adam 1984). Opus signinum mosaics were commonly used in Italy from 2nd century BC to 2nd century AD.

This type of mosaics were used commonly in the atriums of the buildings, thresholds of the rooms, tricilinium (dining rooms) and cubiculum (rooms around the atrium) (Dunbabin 1999, Üstüner 2002).

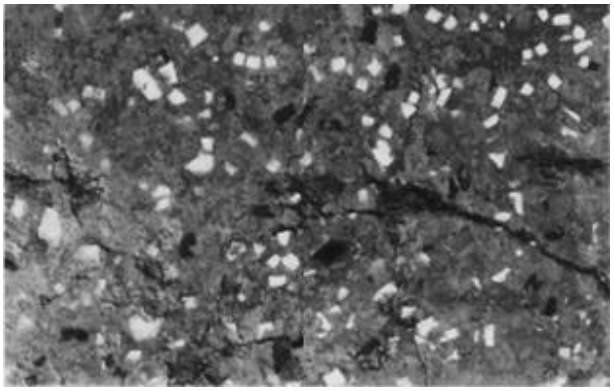

Figure 1. 5. Opus signinum mosaic of House of double cistern, in Morgantina, Sicily, (Italy) (3rd century BC–mid 1st century AD) (Source: Tsakirgis 1990)

Opus sectile mosaics were constructed with different colors tessera and large size marbles. Marbles were cut in the form of triangle, square or rectangle in accordance with mosaic pattern (Figure 1. 6) (Anthony 1968, Dunbabin 1999, Sözen 1999, Üstüner 2002). In general they were used in atriums, baths and triciliniums of buildings.

Figure 1. 6. Opus sectile mosaic of Hadrian's Villa (The Golden Court), Tivoli, Italy (2nd century AD) (Source: wikipedia.com.tr)

Opus musivum was a mosaic execution technique that glass tesserae were used as in the vermiculatum mosaics. It has similar properties with the other mosaic

techniques but it was more decorative. In general, they were applied on walls, vaults and domes of the buildings (Anthony 1968).

Figure 1. 7. Opus musivum mosaics in Herculaneum in Ercolano, Italy (6th century BC, 79 AD) (Source: wikipedia.com.tr)

In Byzantine period, mosaics were constructed with stone, glass and gold tesserae in brilliant colors. Sizes of tesserae were smaller (0.5cm-1cm) than Roman mosaics (1-1.5 cm). In mosaics, religious figures and mostly portraits were applied (Vance and Clarke 1994).

Byzantines were responsible for lifting mosaics from floor to walls and vaults from fifth to fifteenth centuries (Anthony 1968).

In the Renaissance, mosaics were not preferred due to the increased interest in wall paintings (Lovoos and Paramore 1969). However, mosaics were continued to the churches (Dierks 2004). In the 18th century, mosaics were became popular and miniature mosaics started to be produced.

Mosaics started to decorate civic buildings with colorful and stylized organic curves and shapes found in nature with the effects of Art Nouveau period during the 1890s and the early 1900s in Modernism (Vance and Clarke 1994, Efe 2009). In the 19th century pebble mosaics were just in the courtyards, stables, gardens and external wall coverings of buildings (Fawcett 1998).

1.1. Mosaics in Anatolia

In Anatolia many mosaics have been constructed since 4000 BC were found. However, mosaics have reached to the present in the archeological excavations are mostly floor mosaics. Many wall, vault and dome mosaics were disappeared since the architectural monuments have collapsed over time.

The early mosaic made with baked clay cones were found in Alacahöyük, Çorum (5000 BC), Alişar, Yozgat (4000 BC), and Yümüklütepe, Mersin (4500 BC) in inner Anatolia (Üstüner 2002). In Polychrome House, dated back to the end of the 8th century BC in Gordion, basic geometrical formed pebble mosaic pavements were also found (Young 1956, Kaplan et. al 2011, Ugur 2011).

In the Hellenistic Period, the mosaics of western Anatolia were constructed with pebbles. The only known early Hellenistic period mosaic pavement was found in Assos and dates back to end of the 4th century and the beginning of the 3rd century BC. This mosaic was constructed with black, white and colored pebbles (Işıklıkaya 2010).

In the 1st century BC in Rome, similar techniques were used with the Hellenistic mosaics as pebbles and tesserae. They were arranged to create geometric figures with black and white colors.

The common examples of this technique were found in ancient Roman cities such as Antandros (Altınoluk), Pergamum (Bergama), Ephesus (Selçuk) and Assos (Behramkale). The floor mosaics that were found in Assos were similar to 2nd century AD Roman mosaics with simple geometrical forms and black-white colors. Especially, Ephesus is the important city due to progressing of this technique in Late Antiquity (Campbell 1979, Jobst 1978).

Since the 3rd century AD softening the composition, increase in colors and figured patterns were used in mosaics. These types of mosaics were seen in Sardis (Manisa) and in Aphrodisias (Aydın) and they can be the common examples of 4th and 5th century AD mosaics (Işıklıkaya 2010). In Sardis, there were mosaics, which had complicated geometric patterns and the name of the donator's, dated back to the middle of the 4th century AD.

Antioch (Antakya) and Zeugma (Gaziantep) mosaics of southern Anatolia take place in Roman Imperial Period mosaics. Constantinople mosaics are reflecting the Palace style of the period (Brett 1942, Işıklıkaya 2010).

The mosaic technique that spread through the whole Anatolia in Roman Imperial Period continued to Late Antiquity was seen in Black Sea Region, Thrace and Central Anatolia in addition to the western and southern regions. The mosaics that were constructed with golden tesserae and the subjects of the mosaics were reflecting the modern and high quality styles of the Great Palace (Brett 1942).

Mosaics were disappeared when the Ottoman's conquered the East Roman Empire. Mosaics were destroyed or new decorations were constructed on them due to the conversion of buildings to mosques (Uğuryol 2005). A few wall and vault mosaics have reached the present are found in Medieval Churches which were restored in 13th and 14th centuries.

1.2. The Basic Construction Techniques and Materials of Roman Mosaics

Mosaics have a multilayered system composed of statumen, rudus, nucleus, bedding layer and tessellatum from the bottom to its surface (Figure 1. 8). In general mosaics were composed of two main layers; substrate (preparatory layers of mosaics) and tessellatum. Statumen, rudus, nucleus and bedding layers are the preparatory layers. Tesserae and filling mortar constitute the tessellatum layer (Getty Conservation Institute 2011).

1.2.1. Substrate of the Mosaic

Substrates of the mosaics were classified into four layers. They are listed below (Getty Conservation Institute 2003).

Statumen: it is a first preparatory layer which is constructed with large stones without mortar on ground that is rammed and leveled. This layer exists only when the mosaic are constructed on natural ground.

Rudus: is the second preparatory layer which is laid on statumen. It is consisted of coarse aggregates (sand, stone, and brick) and lime mortar. Rudus is constructed to prevent moisture migration from the interior to mosaic surface. Thickness of the rudus can vary according to the moisture content of the statumen and materials.

Nucleus: is the third preparatory layer which is laid on rudus. It consists of fine aggregates (sand, stone or brick) and lime mortar. Nucleus layer is thinner than the rudus layer.

Bedding Layer (Supranucleus/setting bed): It is the last preparatory layer consists of a lime rich mortar. It is applied thinly on nucleus and tesserae are inserted in it before the lime sets.

In mortars of the mosaic, where waterproofing was required, crushed brick was added to the mortar. Since, they have hydraulic properties due to the addition of pozzolanic materials to an air lime binder.

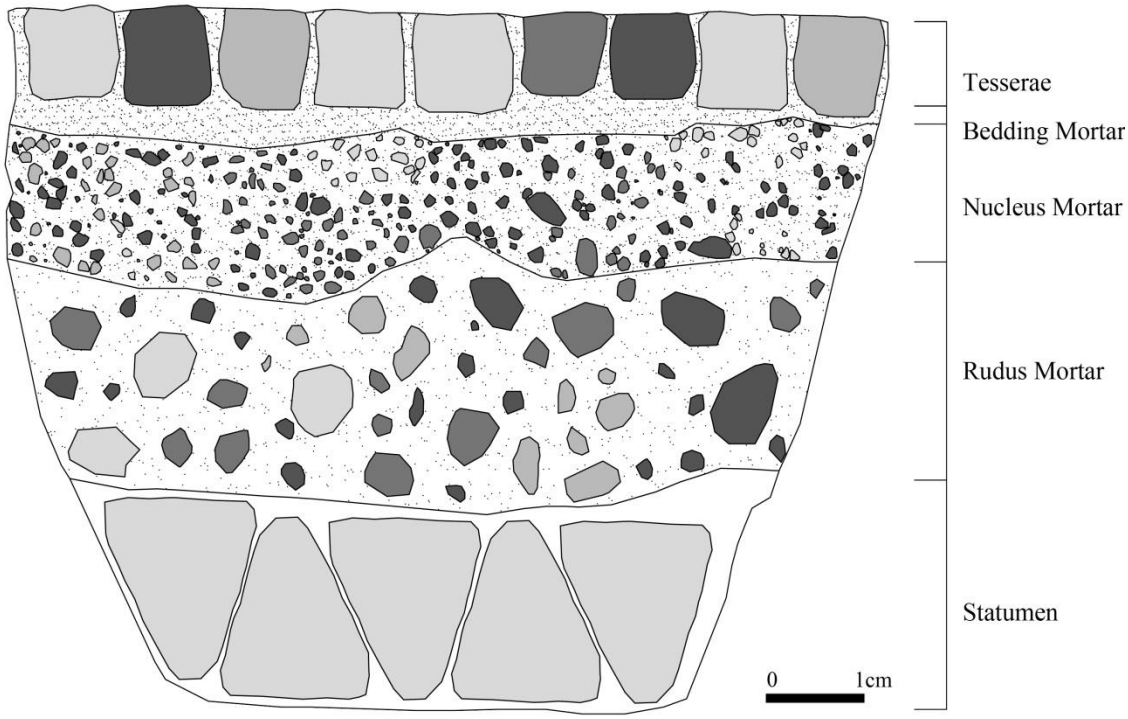

Figure 1. 8. Illustrative drawing of mosaic layers
(Drawing: Z. Karayazılı)

Vitruvius described construction techniques of mosaic layers in his book De Architectura (Vitruvius 1st BC);

Lay the bedding, composed of stones not smaller than can fill the hand. After the bedding is laid, mix the broken stone in the proportions, if it is new, of three parts to one of lime; if it is old material used again, five parts may answer to two in the mixture. Next, lay the mixture of broken stone, bring on your gangs, and beat it again and again

with wooden beetles into a solid mass, and let it be not less than three quarters of a foot in thickness when the beating is finished. On this lay the nucleus, consisting of pounded tile mixed with lime in the proportions of three parts to one, and forming a layer not less than six digits thick. On top of the nucleus, the floor, whether made of cut slips or of cubes, should be well and truly laid by rule and level.

After it is laid and set at the proper inclination, let it be rubbed down so that, if it consists of cut slips, the lozenges, or triangles, or squares, or hexagons may not stick up at different levels, but be all jointed together on the same plane with one another; if it is laid in cubes, so that all the edges may be level; for the rubbing down will not be properly finished unless all the edges are on the same level plane. The herring-bone pattern, made of Tibur burnt brick, must also be carefully finished, so as to be without gaps or ridges sticking up, but all flat and rubbed down to rule. When the rubbing down is completely finished by means of the smoothing and polishing processes, sift powdered.

Also Pliny described construction of pavements in detail in his book Naturalis Historia (Pliny 77 AD);

Open-air flooring was an invention of the Greeks, who roof their houses in this way, an easy method to use in regions with a warm climate, but unreliable wherever there is heavy rainfall and frost. It is essential that two sets of joists should be laid across each other, and that their ends should be nailed down to avoid warping. To fresh rubble should be added a third of its weight in pounded potsherds; and then the rubble, mixed with two-fifths of its weight in lime, should be rammed down to a thickness of one foot. After this, a final coat 4½ inches thick must be applied to the rubble and large square stones not less than 1½ inches thick laid on it. A fall of 1½ inches in 10 feet should be maintained and the surface carefully polished with grindstones. It is considered impracticable to lay the wood floor with oak planks, because they warp; and, furthermore, it is thought advisable to spread a layer of fern or straw below the rubble so that the worst effects of the quicklime may not reach the planks. It is essential also to lay a foundation of round pebbles under the rubble. Tiled floors with a herring-bone pattern are constructed in a similar fashion.

The layers, thicknesses and materials of the preparatory layers change according to physical conditions of sites and structures of buildings (Starinieri 2009).

In 4th century AD in the temple of the ancient town of Pitiunt, (Abkhazia), floor mosaic were constructed by seven preparatory layers composed of compacted clay and

coarse gravel and lime mixed with sand, crushed bricks and charcoal and also bedding layer with pure lime and tesserae (Todua 1975).

Although Pitiunt mosaics were constructed with seven layers, another 4th century AD floor mosaic from the Episcopal Palace at Aphrodisias, in Turkey was constructed by four preparatory layers. These layers are statumen, rudus, and nucleus and bedding layers. They were composed of coarse gravel, lime and gravel and pure lime mortar and then tesserae (Idil 1982).

In S. Severos Church and the archaeological area of Classe, in Ravenna (Italy), two floor mosaics were also found. Mosaics were constructed by three layers (rudus, nucleus and bedding mortar). Rudus and nucleus were composed of lime and brick aggregates while bedding mortar was composed of pure lime (Fiori et. al. 1987).

Similar with the Ravenna mosaics, another floor mosaic from 2nd century AD in the Roman city of Italia, in Spain called Tellus mosaic, was constructed with three mortar layers. Rudus and nucleus were composed of more lime and less brick aggregates with low density and porosity values. Bedding mortar was composed of less lime more aggregates (Puertas et. al. 1994a, b).

In addition, 6th century AD floor mosaics from Santa Eufemias Cathedral in Grado (Italy) were constructed by three mortar layers. Rudus and nucleus layers were composed of more lime and aggregates. Bedding mortar was composed of pure lime (Lopreato et. al. 2003).

In 2nd century AD floor mosaic from the archaeological area of Histonium in Vasto, Italy consisted of six mortar layers. They are statumen, rudus, and nucleus, bedding and two additional mortar layers between statumen and rudus. They were composed of lime and aggregates (brick, brick dust, sand and stone). Calcite fragments were also present in the mortars due to incomplete calcination of the stone used for the production of lime (Montanaro et. al. 1998).

In the Early Byzantine, nave mosaic in the basilica of Agios Lot (Jordan) were constructed by six mortar layers the same with Histonium mosaics. They are statumen, red sand layer, rubble hard core layer, rudus mortar, nucleus mortar and bedding mortar. Rudus and nucleus mortars were composed of grey lime and aggregates (sand, ceramic, brick, gravel, charcoal and tessera remains). Bedding mortar was composed of lime and fine aggregates (Chlouveraki et. al. 2003).

All mosaics have two mortar layers that have hydraulic properties by addition of pozzolanic materials (brick fragments and/or volcanic sand) to the lime. The thicknesses of this layer are variable due to usage of the room the type of surface (Starinieri 2009).

The Roman mosaics that were constructed on natural ground have rudus layers with high thickness and low porosity values to prevent uprising humidity (Alberti 1965). However, mosaics that were constructed on structures elevated above the ground especially in Roman baths and latrines, have two or three mortar layers, the thickness of mortars are variable according to room dimensions, marbles and tesserae that covered the surface of the mosaics especially bedding mortar (Starinieri 2009).

On the other hand, mosaics constructed either on natural levelled ground or on artificial backfilled ground, which did not contain special facilities or equipment, have complete preparatory layers when built on natural ground and a single preparatory layer when built on artificial backfilled ground (Starinieri 2009).

Bedding mortars should be constructed with high workability to give the mosaic the right inclination and sometimes it was mixed with aggregates to get the aesthetic harmonization with the color of the tesserae and sometimes it was painted for the same reasons (Starinieri 2009).

After all preparatory layers were constructed then tesserae were embedded to the upper mortar (bedding) layer.

In the following section, definition of tesselatum layer and embedding methods to the bedding mortar are given.

1.2.2. Tesselatum of the Mosaic

Tessellatum is the upper part of the mosaic consisted of tesserae and the bedding mortar layer that fills the joints or interstices between tesserae.

Tessera is small pieces of stone, glass, marble, baked clay, ceramic and terracotta that were cut and organized according to mosaic pattern to create a design or images.

Upon the preparatory layers, tesserae were inserted into bedding mortar to generate the mosaic. They were constructed with different methods listed in the below;

- Tesserae were directly introduced into mortar when it was wet.

- Tesserae were introduced into mortar after mosaic pattern was drawn with colors on the dry mortar.
- Tesserae were inserted after lead stripes introduced to the bedding mortar according to mosaic pattern.

In the following section stone, ceramic and glass tesserae are given.

1.2.2.1. Stone and Ceramic Tesserae

Stone and ceramic tesserae were the most common material of the mosaic manufacture. In the Classical Period mosaics (Greece) (510 BC-323 BC), pebbles were used as their natural forms and colors. They were collected from river beds and sea shores, and then classified as their sizes and colors. The colors are generally black and white until Late Classical Period (400 BC- 323 BC). After that period in addition with black and white colors, red, yellow and green were begun to use. The sizes of stones varied between 1 and 2 cm (Dunbabin 1999).

Since the Hellenistic period (323 BC-146 BC) with developments in stone cutting techniques, irregular stone fragments and cut stones (tesserae) were used together in mosaics (Dunbabin 1999).

In Roman Period (509 BC-330 AD), in the production of stone tesserae, in addition to lime stones (white, grey, and blue), sandstone were used (Fawcett 1998). Stones were quarried and then cut to the required sizes and forms for the tesserae, however, generally mosaic makers got their materials from builders and sculptors remains.

Bricks, terracottas and pots were used as red stones when suitable red color could not be found (Dunbabin 1999).

1.2.2.2. Glass Tesserae

Glass is the common an ideal material for tesserae since it provides a wide range of colors and patterns to create a mosaic.

Glass was produced in Mesopotamia prior to 2500 BC and developed during the Roman period. Glass was made by melting a mixture of quartz sand (SiO_2), alkaline

flux (Na_2O, K_2O) and a stabilizer (CaO, MgO) at 1000°C in a furnace (Newton and Davison 1989). An alkaline flux obtained from natron (Na_2CO_3) or plant ash which decreases the melting temperature of the batch. A stabilizer obtained from lime or magnesia which makes the glass water resistant.

Silica minerals are composed of silicon-oxygen tetrahedrons that have four oxygen atoms and one silicon atom (Figure 1. 9). Its melting temperature is about 1700°C. At the melting temperature, most of the silicon-oxygen bond breaks and the material becomes a paste then a viscous liquid when the temperature is further increased (Figure 1. 10) (Torraca 2009). When an alkaline flux is added to the silica, the melting temperature decreases (1000°C) and monovalent alkaline cations loosely hold by oxygen atoms in silicon-oxygen tetrahedrons. The formed product during this process is water soluble. A stabilizer, such as lime (CaO) or magnesia (MgO), is needed to make the glass water insoluble. CaO or MgO is doubly charged so is held oxygen atoms more tightly than the monovalent Na or K ion. The glass produced by silica, alkaline and lime contains about 60-70 % silica, 12-16% sodium oxide, 5-12% calcium oxide, 2-5% magnesium oxide and low amounts of aluminum, iron and potassium oxides.

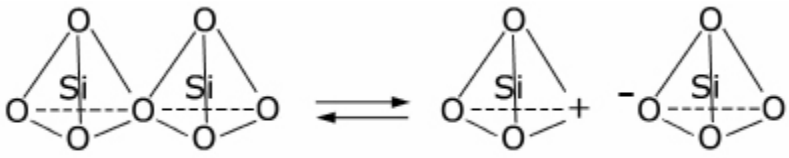

Figure 1. 9. Breaking of silicon-oxygen bonds at the melting temperature
(Source: Torraca 2009)

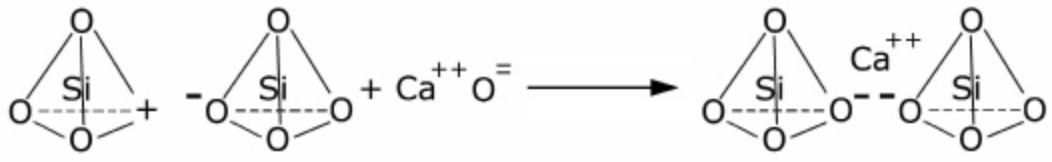

Figure 1. 10. Stabilization of silicon-oxygen bonds by Ca ions
(Source: Torraca 2009)

In Roman times and until eleventh to twelfth centuries, the glass batch consisted of natron and sand. Natron (Na_2CO_3), a natural mineral consisting mainly of sodium

carbonate, was obtained from salt lakes. Natron was mined in Egypt (Wadi Natrun, North-West of Cairo) and used in glass-production during the Roman period (Henderson 1988, Lemke 1998, Werf et. al. 2009). Sand contains silica and calcium carbonate in optimal ratios for glassmaking. Calcium carbonate was a basic compound that was added with raw materials. Calcium carbonate bearing sand was chosen and brought from rivers (Brill 1988, Newton and Davison 1989, Verita 2000).

In addition, lead oxide (PbO) was used as raw materials in glass making to lower the melting point of the glass. Also lead oxide increases the resistance of glass and decrease the hardness of the glass. Lead oxides (between 10 and 50%) were introduced to glass in the form of minium or galena, and the resulting glass was known as lead glasses. (Verita 2000, Costagliola et. al. 2000).

Glasses can be classified into three major types according to the PbO% to SiO_2%, Na_2O% and CaO% content (Formula 1.1). They are soda lime, lead and soda lime lead glasses (Shortland 2002).

	<0,01 soda-lime glass	
PbO% / (SiO_2% + Na_2O%+CaO%)	0,01 -0,1 soda-lime-lead	Formula 1. 1
	>0,1 leaded glass	

In the formula, if the ratio is less than 0.01 glasses are classified as soda-lime glasses; if the ratio is between 0.01-0.1 then glasses are classified as soda-lime-lead glasses and if the ratio is higher than 0.1, than the glasses are classified as lead glasses (Fiori et. al. 2003, Vandini et. al. 2006, Silvestri et. al. 2012).

Soda-lime silica glasses can also be classified into two groups based on their potassium, sodium and magnesium content. They are sodic glasses (natron based) and potassic glasses (plant ash based) (Sayre and Smith 1961, Brill 1976, Henderson 1991).

Sodic glasses are produced with the natron ($Na_2CO_3 \cdot NaHCO_3 \cdot 2H_2O$) that contains low amounts of K_2O and MgO (lower than 1.5%) (Brill 1976, Croveri et. al. 2010, Silvestri et. al. 2012). Glasses belonging to this group were produced in Roman period (1^{st}-4^{th} century AD) (Brill 1976, Vandini et. al. 2006). However potassic glasses were produced with plant ash that contains high amounts of K_2O and MgO compared to the sodic glasses (Sayre and Smith 1961, Brill 1968, Hartmann 1994, Shortland et. al. 2006a, Werf et. al. 2009, Arletti et. al. 2010).

Soda-lime glasses can also be classified according to their potassium and sodium content (Costaglia et. al. 2000, Arletti et. al. 2010). If the glass contains high amount of Na_2O (12-19%) and low amounts of K_2O (1-4%), it can be classified as sodic glasses.

In some cases plant ash was added to natron based glasses in the production of glass. This hypothesis was verified with studies of Roman and Late Ancient Period opaque red and transparent green glass tesserae (Brill and Cahill 1988, Brun et. al. 1991, Henderson 1988, 1991, Lemke 1998, Ruffini et. al. 1999 a, b, and Gratuse 2002, Triscari et. al. 2005, Boschetti et. al. 2007, Santagostina Barbone et. al. 2008, Verita et. al. 2008, Arletti et. al. 2010).

The base glass was opacified and colored with minerals in another manufacturing process and furnace called secondary manufacture of glass.

1.2.2.2.1. Opacifiers

Glass was opacified with air bubbles and intentionally added minerals to the raw materials of glass or glass melt in the secondary manufacture. Air bubbles were produced due to low temperatures in the furnaces. Intentionally added minerals were antimonies, tin oxide and phosphorous compounds.

The antimonies used to opacify glass had been used since Ancient Egypt (2^{nd} millennium BC) (Lahlil et. al. 2008). During the Ancient Period natural stibnite Sb_2O_3 or roasted stibnite (Sb_2O_3, Sb_2O_4) and metal antimony were used as antimony sources (Turner et. al. 1959, Mass et. al. 2001, Shortland 2002, Lahlil et. al. 2010, b). Basic opacifiers were ca and Pb-antimony ($CaSb_2O_6$, $Ca_2Sb_2O_7$, $Pb_2Sb_2O_7$) in Roman Period (Lahlil 2008, Schibille et. al. 2012, Silvestri et. al. 2012). Opacified glass was produced in two different methods as ex situ and in situ crystallizations.

The addition of natural or previously synthesized opacifiers to a transparent glass which lead to ex situ crystallization and this is called primary opacifier.

The introduction of opacifiers which lead to in situ crystallization of opacifying agents through separation from the glass melt and called secondary opacifier (Verita 2000, Lahlil 2010b, Silvestri et. al. 2012).

However, due to the shortage of antimony sources (late 5^{th} century AD) glass makers started to use semi-opaque glasses or tin oxide and lead-tin oxides (SnO_2, $PbSnO_3$, $PbSnO_4$, $Pb_2Sn_2O_6$) as opacifiers from 4^{th} century and from East Mediterranean to the Northern Europe until Renaissance (Sayre 1963, Turner and Rookby 1959, Ubaldi and Verita 2003, Fiori 2004, Tite 2008, Lahlil et. al. 2008, 2010a, 2011, Tite 2008, Schibille et. al. 2012, Silvestri et. al. 2012, Janssens 2013). On the other hand tin

exists in crystals and play a role at the crystallization of antimony; the low amount of tin is due to the low solubility of tin in the glassy matrix than antimony. Tin was also added to the glass melt with tin bronze as source of copper as a chromophore in ancient period. (Lahlil et. al. 2008).

In addition to tin, in some regions calcium phosphate [$3Ca_3$ $(PO_4)_2CaF_2$] was used in the beginning of the 14th century AD and since the end of the 17th century lead arsenates [$3Pb_3$ (As_2O_4) PbO] were used as opacifier in glass manufacture (Janssens 2013). Presence of opacifiers in the glass composition provides historical information about the glass tesserae (Table 1. 1).

Table 1. 1. Chronological order of opacifiers

Opacifier	**Period**
Ca-and pb antimonies ($CaSb_2O_6$, $CaSb_2O_7$, $Pb_2Sb_2O_7$)	18th BC-limited use after 5th century BC
Tin oxide (cassiterite) and lead-tin oxide (SnO_2, $PbSnO_3$, Pb_2SnO_4, $Pb_2Sn_2O_6$)	4th century AD
Calcium Phosphate [$3Ca3(PO_4)_2CaF_2$]	14th century AD
Lead arsenates [$3Pb_3(As_2O_4)PbO$]	17th century AD

Pb-antimony

Pb-antimonate (bindheimite ($Pb_2Sb_2O_7$)) was manufactured previously from the proper mixing and heating of galena (PbS) or minium (Pb_3O_4) with stibnite (Sb_2S_3) at temperatures ranging between 730° C and 1000° C (Reactions 1.1 -1.4) (Silvestri et. al. 2012, Mass et. al. 1998, Mass et. al. 2002, Shortland 2002, Galli et. al. 2004, Schibille et. al. 2012, Paytner and Kearns 2011,).

Galena contains high levels of zinc (Zn) compounds than minium and hence it can be differentiated from minium by Zn content of the glass (Verita 2000, Shortland 2002).

$$2\ Pb_3O_4 \longrightarrow 6PbO + O_2 \quad 1.1$$

$$2\ PbS + 3O_2 \longrightarrow 2PbO + 2SO_2 \quad 1.2$$

$$2\ Sb_2S_3 + 11O_2 \longrightarrow 2Sb_2O_5 + 6SO_2 \quad 1.3$$

$$2\ PbO + Sb_2O_5 \longrightarrow 2Pb_2Sb_2O_7 \quad 1.4$$

Opaque green and yellow tesserae were produced by adding previously synthesized Pb-antimony to the glass melt (Arletti et. al. 2010). Pseudo-rhombohedral Pb-antimony crystals were produced with partially crystallized and recrystallization of antimony. Tin was identified with Pb-antimony crystals and aggregates as an impurity (Lahlil et. al. 2008, Santagostina Barbore et. al. 2008, and Arletti et. al. 2010).

Ca-antimony

Calcium antimonate ($Ca_2Sb_2O_7$ and $CaSb_2O_6$) does not occur naturally as a mineral. Calcium antimonate glasses were produced with two methods either by adding roasted stibnite (Sb_2O_4-Sb_2O_5) to the raw materials of glass or by adding roasted stibnite to the melted glass (Shortland 2002). Calcium antimonates are found to be as $CaSb_2O_6$ (hexagonal structure) and $Ca_2Sb_2O_7$ (orthorhombic structure) phases in the glass. These crystals have homogeneous geometry and they are scattered around and inside the air bubbles. Also they are found in different forms and sizes as aggregates (Silvestri et. al. 2012). Their ratio of the Ca-antimony phases may give the manufacturing temperature of the glass. Calcium antimonies ($Ca_2Sb_2O_7$, $CaSb_2O_6$) are formed at temperatures of 927°C and 1094°C respectively. If roasted stibnite was added to glass melt (ex situ), euhedral Ca-antimonate crystals are formed whereas roasted stibnite added to the raw materials of the glass and then melted (in situ), they have amorphous structure. (Lahlil et. al. 2008, 2010, a, Schibille et. al. 2012).

1.2.2.2.2. Colorants

Ancient glasses were colored with transition metals (chromophores) by adding them as powders to the glass melt in the secondary glass production. They were in varying combinations and oxidation states within the glassy matrix and different amounts of transition metal oxides provide different hues to the glass (Newton et. al. 1989, Newton and Davison 1999, Costagliola et. al. 2000, Shortland 2002, Mirti 2002, Croveri et. al. 2009, Schibille et. al. 2012, Silvestri et. al. 2012).

The color has been related to the base glass composition, amount of chromophore elements, the temperature that can be reached at the furnace and the duration of the heating (Newton 1980, Vandini et. al. 2006, Arletti et. al. 2006). Therefore, chromophore elements (colorants) provide information about technology (Newton et. al. 1989) of glass manufacture and also the origin of the tesserae (Costagliola et. al. 2000).

In general, four colorants were identified in ancient glass tesserae; iron, manganese, cobalt and copper (Newton and Davison 1999, Mirti 2002). Iron is a natural contaminant of the raw materials of glass also it was added to obtain yellow, green, red, black and blue colors. Manganese was used to obtain brown color and used together with iron and cobalt to produce black. Cobalt was added to the glass to obtain blue color and copper was used for green and also red color. On the other hand cobalt and copper were used together to produce dark green glasses. (Davison 1989) (Table 1. 2).

Table 1. 2. Colorants of glass tesserae

Colorant	Color
Iron oxide	Yellow, green, black, red
Manganese oxide	Brown, purple
Copper oxide	Green, blue, red
Cobalt oxide	Blue, violet
Lead oxide	Green
Pb-antimony	Yellow
Ca-antimony	White

Yellow tesserae that lead glasses were colored with Fe^{+3} ions together with Pb-antimony and low amounts of copper oxide (CuO <0.2%) (Vandini et. al. 2006, Croveri et al 2010, Silvestri et. al. 2012).

Green tesserae that were lead and unleaded glasses were colored with lead oxide (PbO) and copper oxide (CuO_2) (Davison 1989). The Cu^{+2} ion gives rise to a bright green color in glassy matrix in presence of significant amounts of lead (Croveri et. al. 2009).

The bright red tesserae were lead glasses whereas dark red tesserae were unlead glasses. Red colors of the tesserae were produced with copper and iron and they contain high amounts of iron (Davison 1989, Costagliola et. al. 2000, Barber et. al. 2009, Ricciardi et. al. 2009). In dark red tesserae, Copper oxide ($CuO_{2)}$ contents are lower while MnO is higher than bright red tesserae (Vandini et. al. 2006). ‘‘Low-lead and low-copper’’ contained red tesserae were common in Roman period.

Blue tesserae were unleaded glasses (Vandini et. al. 2006) that were colored with cobalt, copper and iron oxides. The light blue colors of the tesserae were due to the presence of low amounts of copper (Croveri et. al. 2009). The deep blue colors in glasses were due to cobalt, often present in low concentrations (0.05% CoO is enough for a strong blue tint). (Croveri et. al. 2009). Also Romans used Fe^{+2} (ferrous iron) in addition to Cu and Co to produce dark blue color (Davison 1989).

White tesserae that unlead glasses were produced with Ca-antimony ($Ca_2Sb_2O_6$) minerals (Vandini et. al. 2006). In addition, absence of transition metals in white tesserae gives its white color.

These colorants were used in glass production to provide different colors since Ancient times.

1.3. Aim of the Study

Construction techniques, materials and designs of mosaic are represent history, culture, economy and the art of their periods. Hence, they should be preserved with their technologic, historic and aesthetic values.

Despite the importance of mosaics there was a general lack of interest in their conservation. This was outlined by International Committee for the Conservation of Mosaics (ICCM) that established in 1977. Conservators, archaeologists and art historians were attended to the Committee as volunteers. The objectives of Committee include the preservation of mosaics through the promotion of studies on the technology of mosaics and practices of their conservation, maintenance and presentation.

The ICCM international conferences are organized once every three years and since 1977, eleven International Conferences were organized and at the end of each conference, a series of recommendations and evaluations are made.

The first recommendation of the Committee was the in situ conservation of mosaics, as opposed to lifting, which was became a rule in mosaic conservation. The Committee has also emphasizing the essential role of preventive conservation and maintenance in the preservation of mosaics. Recommendations can be summarized as follows;

- Excavations of mosaics should not be performed if immediate conservation in is not required;
- Basic documentation of mosaics is required to identify condition and risk assessment;
- Reburial should be considered if the mosaics cannot be actively maintained;
- Improve training of professions in mosaic conservation and management of ancient sites and officials and the public should be informed about the importance of mosaics and their and rapid loss;
- Further researches should be undertaken into the causes of deterioration and the conservation methods.

All these points require diagnostic methods to evaluate restorations of mosaics.

In Turkey, mosaics are generally exposed to environmental conditions after excavations and they were rapidly deteriorated and in danger of extinction. They lie into ruins or maintain for exhibition and also they are carried to the museums. These are deprive both mosaics and archaeological sites values.

There are limited number of studies about material characteristics and deterioration problems of mosaics in Turkey (Archambeault 2004, Efe 2009, Erkan 2010, and Uğur 2011).

Excavated mosaic that have been exposed to the environmental conditions in an archeological site, inadequate and insufficient restorations and also carrying mosaics to the museums have caused loss of architectural and historical values of mosaics and archeological sites.

In this scope, this study aims to determine the material characteristics and deterioration problems of Roman mosaics of Antandros Ancient city in order to define main characteristics of the intervention materials, which will be used in the conservation works of the mosaics. Based on the results of the analysis, proper recommendations can be made in the conservation of the mosaics.

CHAPTER 2

HISTORY OF ANTANDROS

Antandros Ancient city is located in Altınoluk, Balıkesir. The site was used from 5th century BC to 7th century AD. During the archeological excavations a Roman Villa with a bath was found on a hillside of the site facing the sea. The Villa dated back to 4th century AD. Floors of the Villa and bath were covered with Roman mosaics. Excavations that started in 1991 are ongoing.

2.1. Location of Antandros

Antandros was located on top and west hillsides of Kaletaşı Hill, which is at an altitude of 215 m, descending steeply down to the Adramyttion (Edremit) Gulf. It is also to the south of the İda (Kaz) Mountain and north coast of the Adramyttion (Edremit) Gulf in Altınoluk, Balıkesir (Figure 2. 1).

2.2. History of Antandros

At Antandros, there was a settlement from 5th century BC to 7th century AD according to excavations (Polat and Polat 2005).

Many ancient writers gave different information about the origins of Antandros. According to Herodotus; Antandros was originally Pelasg establishment (Herodotus 1991), and Thucydides mentioned that Antandros was an Aiol establishment and Vergilius mentioned Leleg with Antandros in his book Aenias (Vergilius 1998). Also Vergilius indicated that Demetrios from Skepsis noted that Antandros originated from Cilicia (Strabon 2005). According to Stephanos Byzantinos, Antandros had names like Edonis and Kimmeris (Herodotus 1991). Aristoteles said that Antandros got the name of Hedonis, due to Thracian Hedones was settled down in Antandros and got the name Kimmeris due to Kimmeris invasion (Kaletsch 1958).

In 652, BC Kimmeris settled down to Antandros and establish domination for 100 years. However, the Lydians put an end to Kimmeris domination in 570 BC. The city entered Persians rule in 508 BC.

Figure 2. 1. Location of Antandros

Figure 2. 2. Location of Roman Villa and Necropolis

Antandros was a member of Delian League in 425-421 BC when the city was under the rule of Athens (425 BC) (Thukydides 1976).

Antandros was again under Persian Empire rule in 410 BC, until Alexander the Great conquered Anatolia in 4th century BC. After the Magnesian war in 189 BC, Apameia peace treaty was signed in 188 BC, with the peace treaty Antandros was given to Pergamum (Malay 1992). Than Romans came to Anatolia in 190 BC and city came under the Roman Empire. The city was moved to the hill known as Şahin Kalesi to be protected from Arab invasions in 6^{th} -7^{th} centuries AD and at 10^{th} -11^{th} centuries a new settlement was established in Antandros and city became a Bishopric Center (Quien 1958). Consequently in 14^{th} century, it was completely abandoned.

Strabo mentioned that the coast from Lekton to Kanai was called Adramyttion Gulf (Edremit Gulf), and also he said that Gargara (Küçükkuyu) was located at the cape of the Adramyttion Gulf and at the inlands, at the upper part of Antandros, there was Aleksandreia Mountain. He also mentioned that Aspaneus was located here where timbers that were derived from Ida Mountain, were merchandise. After Aleksandreia Mountain, Adramyttion City was located (Figure 2. 3) (Strabon 2005).

Figure 2. 3. Location of Antandros
(Source: H.Kiepert 1890)

Thucydides also mentioned Antandros in his book Peloponnese Wars between Athens and Spartians (431-404 BC) (Thukydides). Vergilius said that Antandros was a timber-rich city and these timbers were used in ship construction in his book Aeneas (Vergilius 1998). The city coined money (sikke) in the early 4th century BC (Thukydides 1976).

In 1842, H.Kiepert discovered Antandros at Dervent hill (Kaletaşı Tepesi) (Figure 2. 3) (Kiepert 1889). In 1881, H. Schliemann also discovered an ancient city with the dimensions of 1000m×1000m at Dervent Hill. In 1911, Leaf also discovered the necropolis at west hillside (Leaf 1923, Sekban 2007).

In 1989, Kaletaşı hill was zoned for housing, graves (Necropolis) were found and salvage excavations were started in 1991 (Figure 2. 2) (Yalman 1992). In 2000, survey was conducted with a team directed by Assoc.Prof.Dr. Gürcan Polat from Ege University, Faculty of Letters, Department of Archaeology, and Department of Classical Archeology (Sekban 2007) and in 2001 excavations were started at Kaletaşı Hill (Polat 2002).

According to excavations there was a settlement at that hillside from 8th century BC to 6th century AD and at the west side of the hill there was a settlement from 6th century BC to Byzantine Period. Also a Roman Villa was found with its bath complex on the hillside of the Kaletaşı Hill (Figure 2. 2) (Polat 2002, Polat and Polat 2005).

The excavations are continued by a team under the direction of Assoc. Prof. Dr. Gürcan Polat and Balıkesir Museum Directorate.

2.3. Architectural Characteristics of Roman Villa

The Roman Villa (terrace house) was located at the south-west hillside of Kaletaşı hill and towards the sea. It was located at 1100 m^2. The house and the bath complex was constructed in the late 3rd century AD and inhabited to the 6th century AD (Polat 2002). Until 2012 excavation season, nineteen spaces were found in the villa and bath.

In Roman Villa there was a portico and kriptoportico (upper portico) and at one side of the portico there were rows of spaces; two tricilinium used in summer and winter (welcoming spaces), four rooms and a latrine (toilet).

The spaces of bath are; an apodyterium (dressing room), a tepidarium (warm space), two piscine's (pool), caldarium (hot space), preafurnium (furnace) and a hall. At the east of the bath a street was found (Figure 2.3).

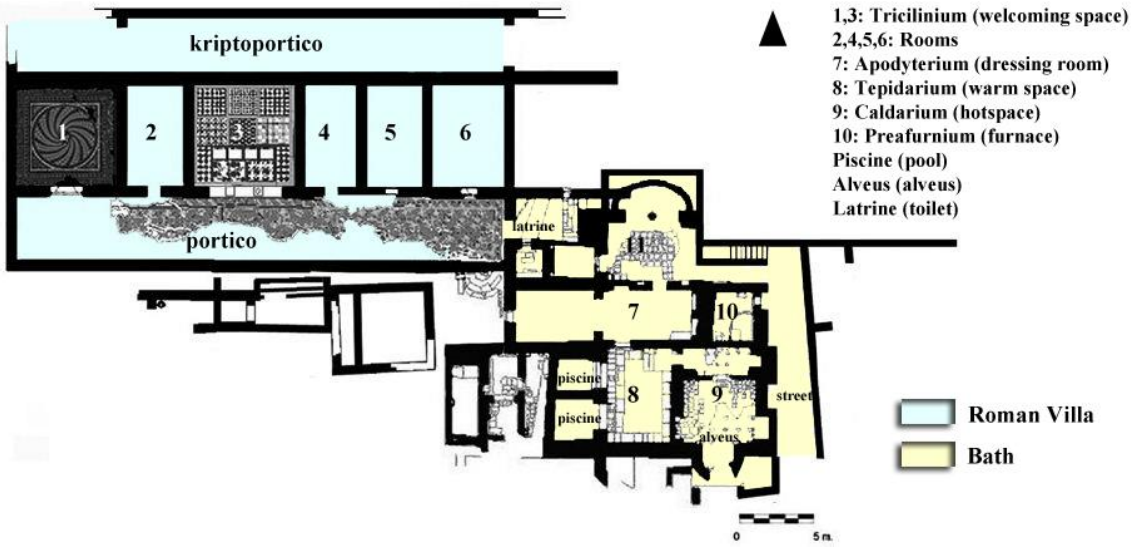

Figure 2. 4. Plan of the Roman Villa (terrace house)
(Source: Polat et. al. 2009)

The Villa was similar to Roman Terraced House typology due to its rows of spaces at one side of the portico (Smith 1997). Portico was located at the sea side of the house. Portico situated from east to west direction has rectangular form with 32.90×4.30 m dimensions and its floor was covered with mosaics (Figure 2. 5) (Polat and Polat 2005). There were six spaces at the north and a latrine at the east of the portico.

The spaces numbered 1 and 3 shown in the plan (Figure 2. 4), were tricilinium used for welcoming. The space 1 was used in winter while space 3 was in summer. Function of the other 4 spaces were not identified (Sekban 2007).

The space 1 is situated in the first row from west to east direction, has square form with 6.80×6.80 m dimensions and its floor was covered with mosaics. There were wall paintings that reached to the present at the bottoms of the walls (Polat and Polat 2003). Glass mosaic fragments were found in this space during the excavations (Polat 2002). Space 3 had same form and dimensions with space 1, however, there were remains of two pillars (Polat and Polat 2003). Remains of the mosaics on the floor were observed in space 3, mortar traces of marble coverings were also observed.

The space 4, situated at the east of space 3, has rectangular form with 3.80×6.80 m dimensions and its floor was covered with mosaics but they were not completely excavated. The walls were covered with plaster (Polat and Polat 2003).

Space 2 with 3×7 dimensions, space 5 with 3.90×6.80 m dimensions and space 6 with 5×6.80 m dimensions were rectangular in form (Polat and Polat 2003). Walls were covered with plaster but there were no mosaics and wall paintings in these spaces.

On the upper level of the six spaces there was a kriptoportico situated from east to west direction with rectangular form 4.5×33 m length (Polat et.al. 2011).

Under the latrine there was a sewerage system 1.2 m in depth. This sewerage system was 15 m at south direction whereas 8m at the north direction (Polat and Polat 2003).

Figure 2. 5. Portico of the Villa and floor mosaic with shelter

Figure 2. 6. Space 1, Tricilinium of the Villa (welcoming space used in winter) and floor mosaic

Figure 2. 7. Space 3, Tricilinium of the Villa (welcoming space used in summer) and opus sectile mosaic traces

2.4. Architectural Characteristics of Bath Complex

Bath was located at the south east and at the lower level of the villa. There was a stair reaching to the bath with circular steps on the south east of the portico. Spatial characteristics of the bath were altered due to usage changes and deformations in the past (Polat et. al. 2006).

Space 7, situated at the entrance of the bath, has rectangular form with 11.63×3.40 m dimensions and it was apodyterium (dressing room) of the bath (Polat and Polat 2005). Its floor was covered with mosaics and the on walls there are remains of wall paintings. There were three niches in the apodyterium; one niche on the northern wall, two niches on the eastern wall. A platform 1 m in length was located on the east of the southern wall.

Figure 2. 8. Space 7, Apodyterium of the Bath (dressing room) and floor mosaic

Space 8, situated at the south of space 7 and south west of the bath, has rectangular form with 6.20×4.15 m dimensions and it was tepidarium (warm space) of bath (Polat and Polat 2005). Connection between space 8 and 7 was provided with an opening on the northern wall of space 7.

Mortar traces of mosaics were observed on the floor and it was thought that there were wall paintings similar to the apodyterium according to excavation meeting

reports (Polat and Polat 2005). Two piscine's (pool) situated at the west of space 8 had square form with 2×2.30 m (Polat and Polat 2005).

Figure 2. 9. Space 8, Tepidarium of the Bath (warm space) and mortar traces of floor mosaic

Space 9, situated at the east of space 8 and south east of the bath, has rectangular form with 3.5×4.15 m dimensions and it was caldarium (hot space) of the bath. There were steps connecting space 9 and 8. The space with an apse at the south of the caldarium was thought as alveus (hot water pool). It was thought that there were wall paintings similar to the apodyterium and tepidarium according to excavation meeting reports (Polat and Polat 2005).

The hypocaust system of the caldarium was filled and a new hypocaust system was constructed above this filling so the level of the floor was elevated.

Space 10, situated at the north of the space 7 (caldarium), had nearly square form with 1.95×2.90 m dimensions and it was preafurnium (furnace) of the bath. However, later it was converted to a furnace (Polat et. al. 2006).

Space 11, situated at the north of the bath and east of the roman villa, had rectangular form with 5.30 m width (Polat et. al. 2006). There was a street at the east of the bath reaching to space 11. Also the space was connected with a vaulted corridor 3.50 m in length on the south-east corner of the space to the street (Polat et. al. 2007). Two niches were observed at the south of the space. There were partially conserved

brick tiles on the floor. Plaster traces were observed on the walls (Polat et. al. 2007). Also it was thought that there was an opening that connected space 15 and 7 (Polat et. al. 2007).

CHAPTER 3

EXPERIMENTAL STUDY

In this study, material characteristics of the mosaics' substrate, found at the excavations of Antandros Ancient city in Altınoluk (Balıkesir), were investigated. Basic physical properties, raw material compositions, mineralogical and chemical compositions, and microstructural characteristics of preparatory mortars and tesserae were determined with standard RILEM test methods, color spectrometer, X-ray diffactrometer (XRD), Scanning Electron Microscope (SEM) equipped with X-Ray Energy Dispersive System (EDS), X-Ray fluorescence spectrometer (XRF) and Thermogravimetry (TGA).

3.1. Sampling

Nine mosaic samples were provided by the head of archaeological excavation team of Antandros. All the samples consisted of preparatory mortars and tessellatum. Preparatory mortars consisted of rudus, nucleus and bedding layers (Figure 3. 1). The thicknesses of the rudus and nucleus layers varied from 2 to 2.5 cm. Bedding layer which tesserae were inserted was about 0.5 cm thick. Tessellatum were composed of cubes of stone (1-1.5 cm), ceramic (1 cm) and glass (0.5-1 cm) tesserae in different colors. Mosaic samples were labeled by the abbreviated name of Mosaics (M) and numbered.

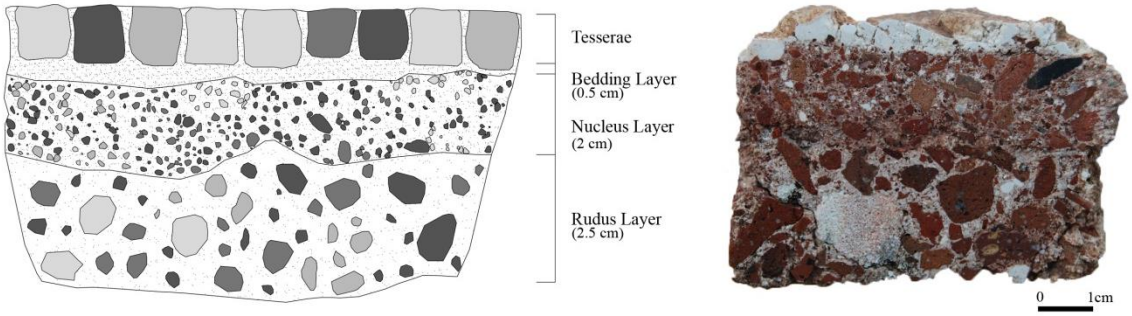

Figure 3. 1. Illustrative drawing of mosaic stratigraphy and a section of mosaic

3.1.1. Preparatory Mortars

The mosaics preparatory layers consisted of statumen, rudus, nucleus and bedding layer. In the collected samples, statumen layer did not exist (Table 3. 1). Rudus and nucleus layers were both seen in four mosaic samples (M1, M2, M4, and M5). In three samples only rudus layer existed (M3, M6, M7), while in two samples only nucleus layer were seen (M8, M9). Rudus layer was composed of coarse brick aggregates and lime, whereas nucleus layer was composed of fine brick aggregates and lime. Bedding mortars were composed of lime-rich mortar.

Table 3. 1. Preparatory mortar layers of mosaics

Name	Definition	Sample
M1-(R)	Rudus Layer: consisting of coarse brick aggregates and lime	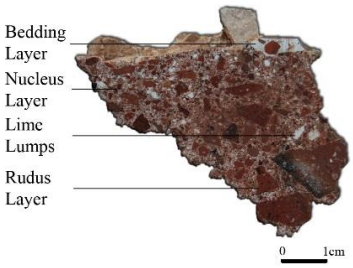
M1-(N)	Nucleus Layer: consisting of fine brick aggregates and lime	
M1-(B)	Bedding Layer: composed of lime rich mortar	
M1-LL	Lime Lumps	
M2-(R)	Rudus Layer: consisting of coarse brick aggregates and lime	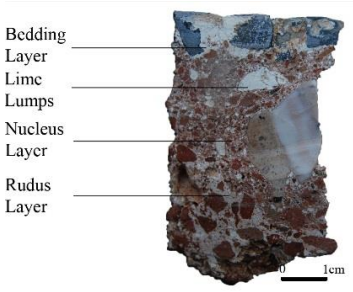
M2-(N)	Nucleus Layer: consisting of fine brick aggregates and lime	
M2-(B)	Bedding Layer: composed of lime rich mortar	
M2-LL	Lime Lumps	
M3-(R)	Rudus Layer: consisting of coarse brick aggregates and lime	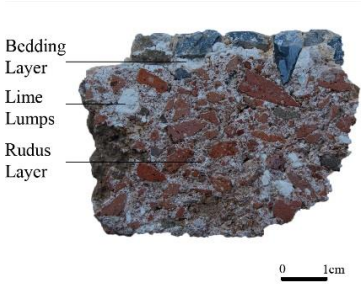
M3-(B)	Bedding Layer: composed of lime rich mortar	
M3-LL	Lime Lumps	
M4-(R)	Rudus Layer: consisting of coarse brick aggregates and lime	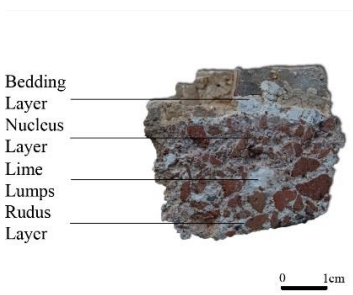
M4-(N)	Nucleus Layer: consisting of fine brick aggregates and lime	
M4-(B)	Bedding Layer: composed of lime rich mortar	
M4-LL	Lime Lumps	
M5-(R)	Rudus Layer: consisting of coarse brick aggregates and lime	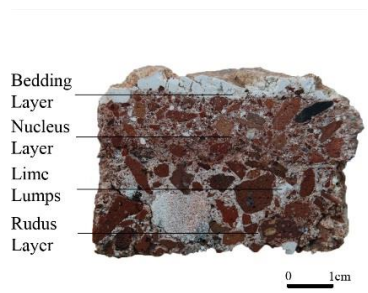
M5-(N)	Nucleus Layer: consisting of fine brick aggregates and lime	
M5-(B)	Bedding Layer: composed of lime rich mortar	
M5-LL	Lime Lumps	

(cont. on next page)

Table 3. 1. (cont.).

M6-(R)	Rudus Layer: consisting of coarse brick aggregates and lime	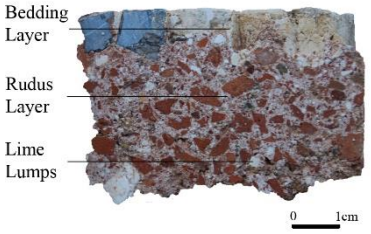
M6-(B)	Bedding Layer: composed of lime rich mortar	
M6-LL	Lime Lumps	
M7-(R)	Rudus Layer: consisting of coarse brick aggregates and lime	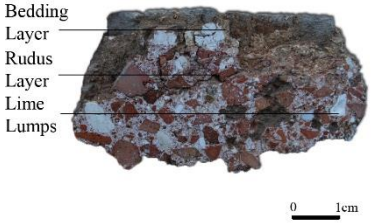
M7-(B)	Bedding Layer: composed of lime rich mortar	
M7-LL	Lime Lumps	
M8-(N)	Nucleus Layer: consisting of fine brick aggregates and lime	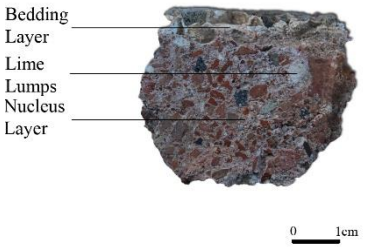
M8-(B)	Bedding Layer: composed of lime rich mortar	
M8-LL	Lime Lumps	
M9-(N)	Nucleus Layer: consisting of fine brick aggregates and lime	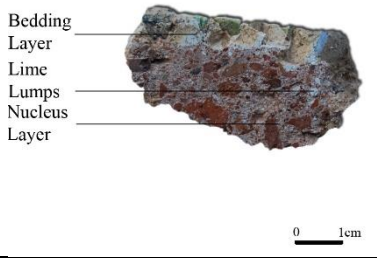
M9-(B)	Bedding Layer: composed of lime rich mortar	
M9-LL	Lime Lumps	

3.1.2. Tesserae

The 25 tessera samples were separated from mosaic samples. Nineteen of them were glass, 4 of them were stone and 2 of them were ceramic tessera.

The colors of the glass tessera were white, yellow, different hues of green and blue, turquoise, light brown, dark red and black. All the samples were identified as opaque glasses except one blue and white tessera which were semi-opaque glasses. The

colors of the stone tessera were white, beige, yellow, grey and colors of ceramic tesserae were red and pink. They were labeled considering their type and the color.

Table 3. 2. Glass tesserae samples

Name	Color	Transparency	Sample
Glass white tessera (G-Wt)	White	Semi-Opaque	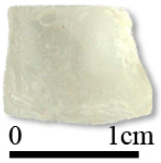
Glass yellow tessera (G-Yt)	Yellow	Opaque	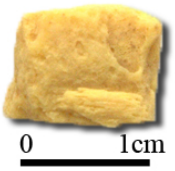
Glass light brown tessera (G-Lbrt)	Light brown	Opaque	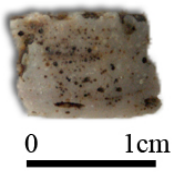
Glass dark red tessera (G-Drt)	Dark red	Opaque	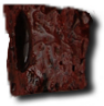

(cont. on next page)

Table 3. 2. (cont.).

Name	Color	Transparency	Photo	Name	Color	Transparency	Sample
Glass black tessera (G-Bt)	Black	Opaque		Glass blue violet tessera 2 (G-Bvt2)	Blue violet	Semi-Opaque	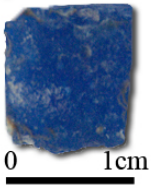
Glass light blue tessera 1 (G-Lbt1)	Light Blue	Opaque		Glass turquoise tessera 1 (G-Tt1)	Turquoise	Opaque	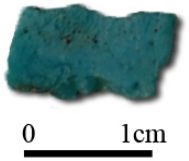
Glass light blue tessera 2 (G-Lbt2)	Light Blue	Opaque		Glass turquoise tessera 2 (G-Tt2)	Turquoise	Opaque	
Glass blue violet tessera 1 (G-Bvt1)	Blue violet	Opaque	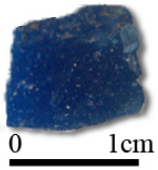	Glass dark turquoise tessera (G-Dtt)	Dark Turquoise	Opaque	

(cont. on next page)

Table 3. 2. (cont.).

Name	Color	Transparency	Photo	Name	Color	Transparency	Sample
Glass light green tessera (G-Lgt)	Light Green	Opaque		Glass dark green tessera 1 (G-Dgt1)	Dark Green	Opaque	
Glass green tessera 1 (G-Gt1)	Green	Opaque		Glass dark green tessera 2 (G-Dgt2)	Dark Green	Opaque	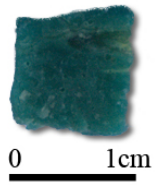
Glass green tessera 2 (G-Gt2)	Green	Opaque	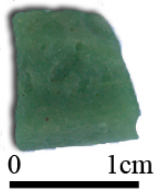	Glass cyan tessera 2 (G-Ct2)	Cyan	Opaque	
Glass cyan tessera 1 (G-Ct1)	Cyan	Opaque	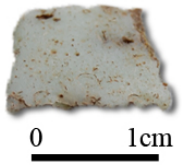				

Table 3. 3. Stone tesserae samples

Name	Color	Sample
Stone white tessera (St-Wt)	White	
Stone beige tessera (St-Bt)	Beige	
Stone yellow tessera (St-Yt)	Yellow	
Stone grey tessera (St-Gt)	Grey	

Table 3. 4. Ceramic tesserae samples

Name	Color	Sample
Ceramic red tessera (Cr-Rt)	Red	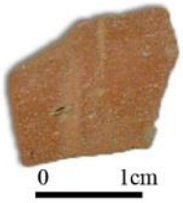
Stone pink tessera (Cr-Pt)	Pink	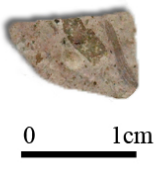

3.2. Experimental Methods

In order to identify the material characteristics of mosaic mortars and glass, stone and ceramic tessera series of laboratory tests were carried out in order to determine;

- the colors of the tessera,
- the basic physical properties of mosaic mortar layers and tessera,
- raw material compositions of mortar layers,
- soluble salt contents of mortar layers and tesserae,
- pozzolanic activities of aggregates,
- hydraulic properties of mortars,
- mineralogical compositions of mortars, aggregates and tesserae,
- chemical compositions and microstructural properties of mortars and glass with standard RILEM test methods, electrical conductivity measurements, color spectrometer, SEM-EDS, XRD, XRF and TGA (Table 3. 5).

Table 3. 5. The methods used for the characterization of the samples

Sample	**Characterization**	**Methods**
Tessera	Colors	Color spectrometer
Mortars (Rudus, nucleus) Tessera	Basic physical (Density &Porosity)	Standard RILEM tests (RILEM 1980)
Mortar (Rudus, nucleus)	Raw material	Standard RILEM tests (RILEM 1980)
Mortar layers, tesserae	Soluble salts	Electrical conductivity measurements Spot tests
Mortars	Hydraulicity	Thermogravimetric Analysis (TGA)
Aggregates	Pozzolanicity	Electrical conductivity measurements
Bedding mortars Aggregates Lime lumps Tessera	Mineralogical	X-ray Diffactrometer (XRD)
Tesserae	Chemical	X-ray fluorescence (XRF) spectrometer
Bedding mortars Lime lumps		Scanning Electron Microscope (SEM - EDS)
Mortars Lime lumps Tessera	Microstructural	Scanning Electron Microscope (SEM)

3.2.1. Determination of Colors of the Tessera

Colors of the cleaned and dried tessera were identified by using a colorimeter (Avantes) and expressed by colorimetric coordinates in the CIEL*a*b* color space system. CIEL*a*b* system was prepared to determine standard colors by the Commission Internationale de l'Eclairage (CIE). In this system colors were expressed in 3D sphere with color coordinates (Formula 3.1). In formula, L indicates the lightness (ranging from black to white). A and b, were the chromatic coordinates (ranging from a: greenness to redness and b: blueness to yellowness). Hunter L, a, and b values were averaged from three readings across for each sample. The total color difference ΔE can be calculated by the following formula:

$$\Delta E = \sqrt{(\Delta L)^2 + (\Delta a)^2 + (\Delta b)^2} \qquad \text{(Formula 3. 1)}$$

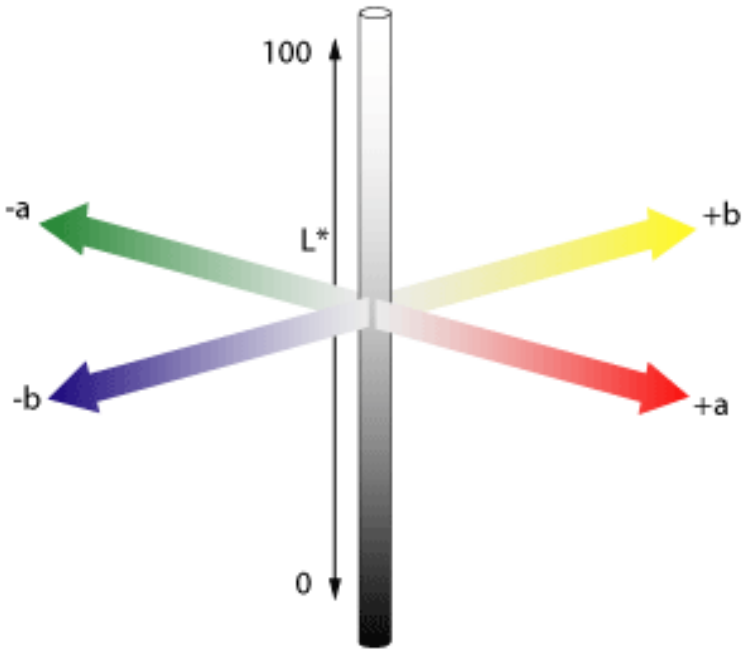

Figure 3. 2. CIEL*a*b* Color Coordinates
(Source: http://www.specialchem4coatings.com)

L, a, b, C, h, X, Y, Z values were obtained from color analysis. L*, a* and b* values were converted into RGB values with an online "Color Calculator" program (http://www.easyrgBCom/index.php?X=CALC). The RGB values were expressed on

the coordinate system and CIELAB (L*a*b*) color sphere with Microsoft Office Excel 2012 and Adobe Photoshop CS4 programs.

3.2.2. Determination of Basic Physical Properties of Preparatory Mortar Layers and Tessera of Mosaics

Bulk density and porosity of the mortars were determined with standard RILEM test methods (RILEM 1980). Bulk density is the ratio of the mass to its bulk volume and expressed with grams per cubic centimeters (g/cm3) (Formula 3.2). Porosity is the ratio of pore volume to the bulk volume of the sample and expressed in percent (%) (Formula 3.3).

In the analysis, mortars and tessera were dried in oven at low temperature (60° C) at least 24 hours and then weighed with a precision balance (AND HF-3000G). Subsequently, they were entirely saturated with distilled water in a vacuum oven (Lab-Line 3608-6CE Vacuum Oven). Saturated weights (Msat) and Archimedes weights (March) of the samples were determined.

Bulk density (D) and porosity (P) values of samples were calculated using the dry, saturated and hydrostatic weights.

$$\text{Density (gr/cm)} = M_{dry} / (M_{sat} - M_{arch}) \quad \text{(Formula 3. 2)}$$

$$\text{Porosity (\%)} = [(M_{sat} - M_{dry}) / (M_{sat} - M_{arch})] \times 100 \quad \text{(Formula 3. 3)}$$

M_{dry} = Dry weight (g)

M_{sat} = Saturated weight (g)

M_{arch} = Archimedes weight (g)

$M_{sat}-M_{dry}$ = Pore volume (g)

$M_{sat}- M_{arch}$ = Bulk volume (g)

3.2.3. Determination of Soluble Salts of Preparatory Mortar Layers and Tesserae of Mosaics

Soluble salts in mortars and tesserae were determined by an electrical conductivity meter (WTW MultiLine P3 pH/LF) (Black 1965). In the analysis, 1.00 g of powdered mortars and tesserae were mixed with 50 ml distilled water. The solutions

were stirred and then they were filtered. Conductivity of the filtered solution was measured by the electrical conductivity meter. Percentage of soluble salts within the sample was calculated using the following formula:

Soluble Salts (%) = [(A x Vsol) / 1000] x [100 / Msam] where;

A = Salt concentration (mg/lt) = 640 x EC

EC = Electrical conductivity measured by electrical conductivity meter

(mS/cm = mmho/cm)

640 = Constant

Vsol = Volume of the solution (ml)

Msam = Weight of the sample (mg)

After conductivity tests, anion parts of the soluble salts were determined by spot test (Black 1965, Arnold 1983, Teutonico 1988). Principle anions such as sulphate (SO_4^{-2}), chloride (Cl^-), nitrate (NO_3^-), carbonate (CO_3^{-2}) and phosphate (PO_4^{-3}) in the solutions were determined.

3.2.4. Determination of Raw Material Compositions of Preparatory Mortar Layers

Raw material compositions analyses were carried out for mosaic mortars in order to determine their acid soluble/aggregate ratios and the particle size distributions of aggregates. Ratio of lime and aggregate used in mortar layers were determined by dissolving of calcium carbonate ($CaCO_3$) from acid insoluble aggregates in dilute hydrochloric acid (5%) solution (Jedrzejevska 1981). Acid soluble and insoluble parts were calculated with the following formulas:

Insoluble % = [(Msam – Magg) / (Msam)] × 100 (Formula 3. 4)

Acid Soluble % = 100 – Insoluble % (Formula 3. 5)

Msam = Dry weight of the sample (g)

Magg = Dry weight of the aggregates (g)

Acid soluble ratio does not give the lime ($Ca(OH)_2$) ratio of the mortars, it gives the dissolved carbonated lime ($CaCO_3$). Lime reacts with CO_2 in the atmosphere and converts into $CaCO_3$. In order to calculate the lime, the conversion of calcium carbonate to calcium hydroxide was achieved by using the molecular weights of $CaCO_3$ (100 g/mol) and $Ca(OH)_2$ (74 g/mol) (Reaction 3.1, Formula 3.6).

$Ca(OH)_2 + CO_2 \longrightarrow CaCO_3 + H_2O$ (Reaction 3.1)

(74g) (44 g) (100g) (Molecular weights)

According to the formula 100 gr carbonated lime derives from 74 gr lime and acid soluble/aggregate ratio was calculated as following:

Aggregate %= (100 × Insoluble)/ [(Acid soluble % × $M.W._{Ca(OH)2}$)/$M.W._{CaCO3}$)+ Insoluble %] (Formula 3.6)

Lime % = 100 – Aggregate %

$M.W.CaCO_3$ = Molecular weight of $CaCO_3$ which is 100.

M.W. $Ca(OH)_2$ = Molecular weight of $Ca(OH)_2$ which is 74.

In the analysis two samples were prepared from each mosaic mortar and dried in an oven then weighed (Msam). Dried samples were put in a dilute hydrochloric acid solution (5%) until the carbonated lime ($CaCO_3$) dissolved. Insoluble parts that consist of aggregates were filtered and washed with distilled water, then dried in an oven and weighed by a precision balance (Magg). Aggregates that remained on filter paper were used for the particle size distribution analysis of aggregates.

Particle size distributions of aggregates were determined by analytical sieve shaker (Retsch AS200) with a series of sieves 53µm, 125µm, 250µm, 500µm and 1180µm. Particles remaining on each sieve surface were weighed by a precision balance and their percentages were calculated.

3.2.5. Determination of Pozzolanic Activities of Aggregates

Pozzolanic activities of crushed bricks used as aggregates were determined by electrical conductivity measurements. Pozzolanic activities of fine brick aggregates (less than 53µm) were determined by mixing them with saturated calcium hydroxide solution [$Ca(OH)_2$] with the ratio of 0.5g/20 ml. First, electrical conductivity of the saturated calcium hydroxide solution was measured. Then solution was mixed with powdered bricks and stirred for 2 minutes. After 2 minutes, electrical conductivity of calcium hydroxide brick powder suspension was measured.

Difference between two values (ΔEC in mS/cm) is expressed the pozzolanic activities of crushed brick aggregates. It was suggested that if the ΔEC is higher than 1.2 mS/cm the aggregates has good pozzolanicity (Luxan et. al. 1989).

3.2.6. Determination of Hydraulicity of Preparatory Mortar Layers of Mosaics

The hydraulic properties of mortar composed of fine aggregates and carbonated lime (binder) were determined with thermogravimetric analysis (TG/DGT), by using Shimadzu TGA-21. Thermogravimetric analysis was carried out in static nitrogen atmosphere at a temperature range 30-1000 ºC with the heating rate of 10ºC/min. The weight losses at 200º-600ºC and 600-900 ºC were measured. Weight loss at 200ºC is due to the loss of hygroscopic (absorbed) water and at 200º-600ºC weight loss is due to the loss of chemical bound (H_2O) water of hydraulic products. Weight loss over 600ºC is mainly due to the decomposition of calcium carbonates. If the CO_2/H_2O ratio is between 1 and 10, the mortars can be accepted as hydraulic (Bakolas et. al. 1998, Moropoulou et. al. 2000a).

3.2.7. Determination of Mineralogical Compositions of Preparatory Mortar Layers and Tesserae of Mosaics

Mineralogical compositions of binder of mortars, lime lumps, aggregates and tesserae were determined with Philips X-Pert Pro X-ray diffactrometer. The analyses were carried out by using powdered samples with less than 53 μm size. XRD spectrum was evaluated by using Philips X-Pert Pro program to identify the crystal phases of samples.

3.2.8. Determination of Chemical Compositions of Binders and Lime lumps of Preparatory Mortar Layers

The binders of the mortars were composed of carbonated lime and small grain sized aggregates. Lime lumps or white lumps represent the binding material used in the mortars.

Their chemical compositions were determined with SEM-EDS analysis by a Philips XL 30S-FEG Scanning Electron Microscope (SEM). Analyses were carried out on pellets prepared by pressing powder samples under 10 tons/cm2 pressure. Results were taken from three different areas of samples and the averages of them were used to determine the chemical compositions.

3.2.9. Determination of Chemical Compositions of Tesserae

Major, minor and trace element compositions of stone, ceramics and glass tesserae were determined by X-ray fluorescence spectroscopy (XRF). XRF analyses were carried out by a Spectro IQ II on melt tablets of powdered samples < 53 μm. Glass samples were diluted with lithium tetraborat. The weight losses of the tesserae between 200ºC - 600ºC due to loss of chemically bound waters and between 600ºC and 900ºC due to loss of CO_2 were determined by TGA analysis.

3.2.10. Determination of Microstructural Properties of Preparatory Mortar Layers and Tesserae of Mosaics

Microstructural properties of mortar layers and tesserae were determined with Philips XL 30S-FEG Scanning Electron Microscope (SEM) equipped with X-Ray Energy Dispersive System (EDS).

Proper sizes of samples were prepared and dried in oven (60° C) for at least 24 hours for the analysis. In the SEM analysis, tessera samples were not coated with gold.

CHAPTER 4

RESULTS AND DISCUSSION

This chapter includes the results of material characteristics of the mosaics mortars and tesserae of Roman mosaics found in Antandros Ancient city. Colors of tesserae, raw material compositions and hydraulicty of mosaic mortars, pozzolanic activities of brick aggregates, basic physical properties, mineralogical and chemical compositions of tessera and mosaics mortars, microstructural characteristics of tesserae were given and discussed.

4.1. Colors of Tessera

Colors of tessera determined by color spectrometer were expressed with colorimetric coordinates (L*, a*, b*, C*, h, X, Y, Z) in the CIEL*a*b* color space system (Table 4. 1). The a*b* values were converted into coordinates by Microsoft Office Excel 2013 program and expressed on CIELa*, b* color plane. Then colorimetric coordinates of tessera were used to determine RGB (Red, Green, and Blue) colors by converting L, a, b, C and h values into R, G, and B by an online color calculator program. Colors were expressed symbolically on the same coordinate system with Adobe Photoshop CS4 program according to CIELa*, b* colors (Figure 4. 1). The colors of the tessera indicated by colors spectrometer matches with the ones determined by naked eyes.

Table 4. 1. Colors and color coordinates of the tesserae determined by colorimetry

Sample	Type	Naked Eye Color	Cielab Color	Color Coordinates							
				L*	a*	b*	C*	h	X	Y	Z
St-Wt	Stone	White	Brown light	80.21	1.69	8.25	8.42	78.46	54.88	57.05	53.29
St-Gt		Grey	Grey	30.32	1.64	1.87	2.48	48.84	6.2	6.37	6.46
St-Bt		Beige	Earth yellow	72.44	5.81	18.91	19.78	72.91	44.08	44.32	32.44
St-Yt		Yellow	Yellow orange	65.58	8.68	32.49	33.63	75.04	35.57	34.78	17.22
Cr-Pt	Ceramic	Pink	Violet red light	53.58	6.56	2.79	7.13	23.08	21.89	21.58	21.89
Cr-Rt		Red	Orange red	57.11	16.81	25.63	30.65	56.74	27.81	25.04	13.78
G-Yt	Glass	Yellow	Yellow	64.73	2.6	50.21	50.28	87.03	32.76	33.71	9.59
G-Lgt		Light green	Yellow green	57.95	-11.69	23.03	25.83	116.92	22.01	25.9	15.51
G-Gt1		Green 1	Green 1	43.57	-21.19	16.54	26.88	142.03	9.94	13.55	8.71
G-Gt2		Green 2	Green 2	43.73	-16.81	15.71	10.59	136.93	10.59	13.65	9.04
G-Dgt1		Dark green 1	Blue green-light	37.03	-15.01	5.63	16.04	159.43	7.41	9.56	8.6
G-Dgt2		Dark green 2	Blue green dark	35.49	-9.95	0.06	9.95	179.65	7.24	8.75	9.5
G-Ct1		Cyan 1	Blue green 1	59.89	-5.32	3.34	6.28	147.92	25.34	28	28.21
G-Ct2		Cyan 2	Blue green 2	62.45	-3.74	-1.1	3.9	196.47	28.43	30.93	34.51
G-Tt1		Turquoise 1	Turquoise 1	51.13	-9.5	-4.18	10.38	203.77	16.66	19.38	23.47
G-Tt2		Turquoise 2	Turquoise 2	60.12	-10.77	-6.69	12.68	211.86	24.30	28.26	35.72
G-Dt3		Dark turquoise	Turquoise dark	29.76	-4.79	-8.26	9.55	239.91	5.42	6.14	9.01
G-Lbt1		Light Blue 1	Blue light 1	54.16	-0.81	-1.71	1.89	244.57	20.86	22.12	25.12
G-Lbt2		Light blue 2	Blue light 2	53.02	-0.89	-9	9.04	264.34	19.84	21.06	28.53
G-Bvt1		Dark blue 1	Blue violet	23.47	2.36	-9.68	9.96	283.72	3.9	3.94	6.39
G-Bvt2		Dark blue 2	Blue violet	17.64	6.21	-16.46	17.59	290.66	2.63	2.44	5.62
G-Drt		Dark red	Violet red	35.77	10.81	7.18	12.97	33.6	9.74	8.89	7.53
G-Lbrt		Light brown	Brown light	57.34	2.9	2.72	3.98	43.2	24.69	25.28	25.78
G-Bt		Black	Black	30.32	1.64	1.87	2.48	48.84	6.2	6.37	6.46

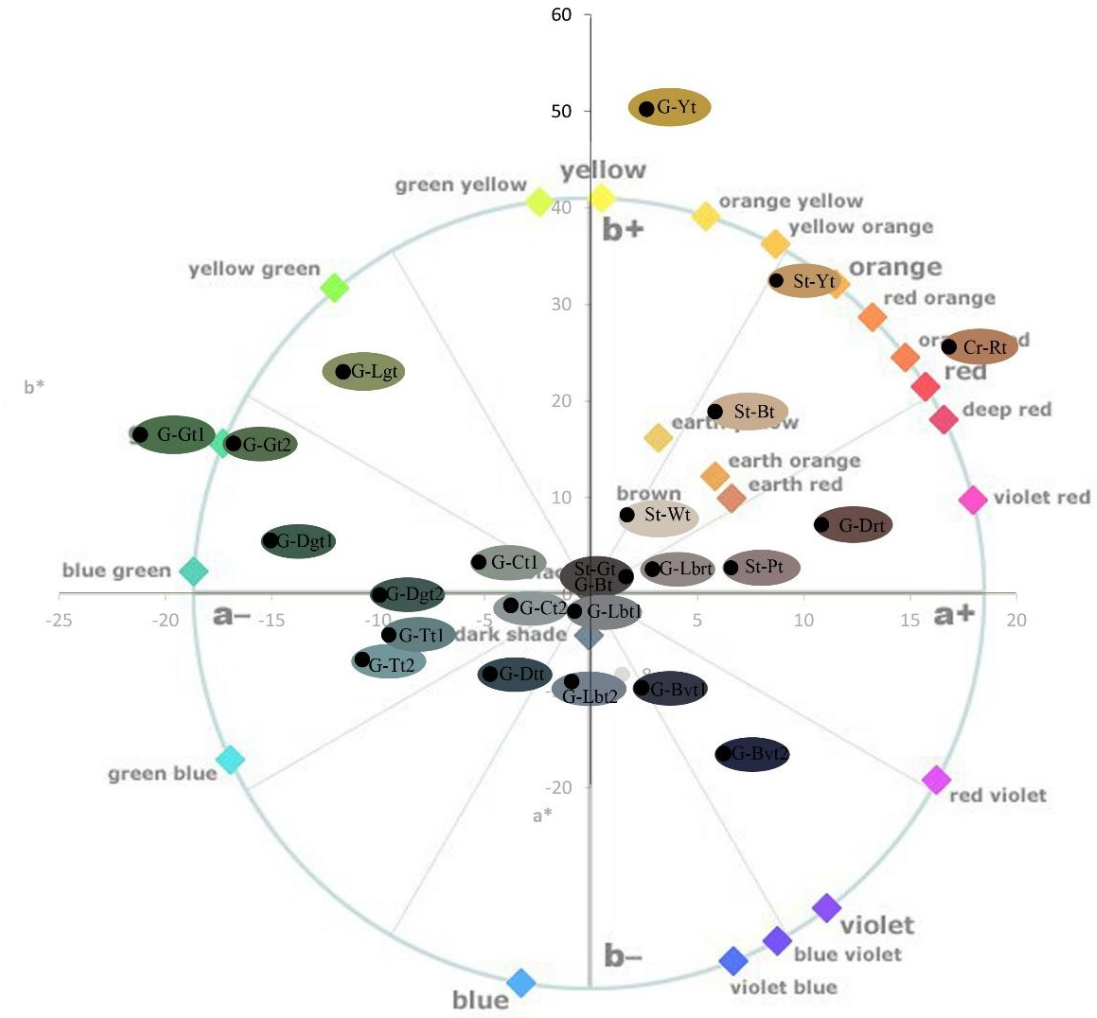

Figure 4. 1 CIELa*b* color plane, points are expressing color chromaticity (lighting values (L*) are changing 17-80).

4.2. Basic Physical Properties of Preparatory Mortar Layers and Tesserae of Mosaics

Basic physical properties of preparatory mortar layers of mosaics and tesserae were defined as density and porosity values. In this section, their density and porosity values are given.

4.2.1. Preparatory Mortar Layers

Density and porosity values of rudus and nucleus layers were given in (Table 4. 2). Density values of rudus and nucleus layers were in the range of 1.5 - 1.6 gr/cm^3 and porosity values were in the range of 38 - 42.3 % by volume in the samples. However, nucleus layers were slightly denser and porous than those of rudus layers due to small grain size of brick aggregates in their compositions (Figure 4. 2).

Table 4. 2. Density and porosity values of preparatory mortars (rudus and nucleus)

	Density(g/cm3)	Porosity(%volume)
M1-N	1.5	41.4
M2-N	1.6	39.9
M4-N	1.6	38.5
M5-N	1.6	38.4
M8-N	1.6	41.3
M1-R	1.5	42.3
M2-R	1.5	40.9
M3-R	1.5	42.8
M4-R	1.6	38.0
M5-R	1.6	41.2
M6-R	1.5	41.0
M7-R	1.6	39.4

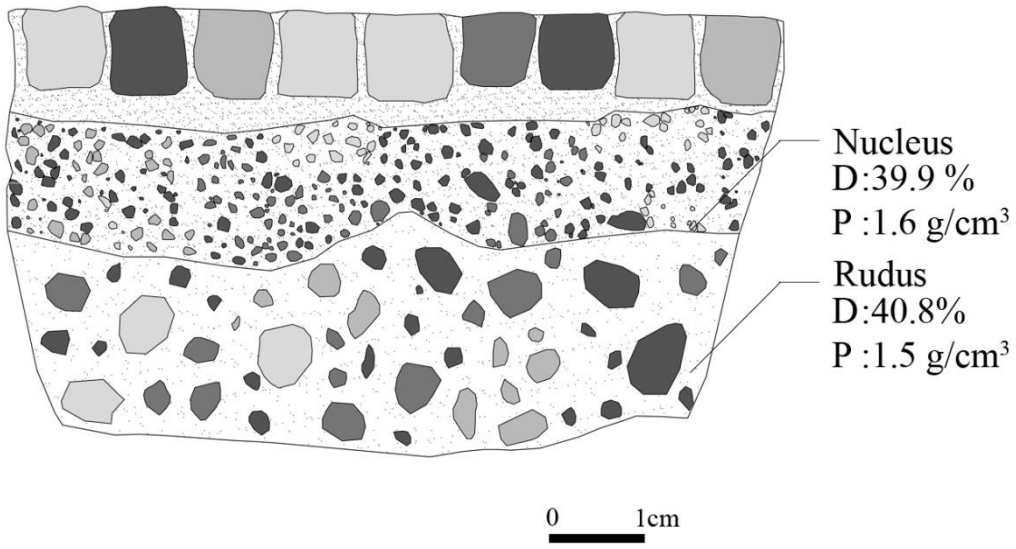

Figure 4. 2. Density and porosity values of nucleus and rudus mortar layers

Density and porosity values of mosaic mortars were nearly same as the ones found in some Roman period buildings (Marcehese and Garzillo 1982, Moropoulou et. al. 2000a, Uğurlu 2005, Starinieri 2009, Kramar et. al. 2011).

4.2.2. Tesserae

Density and porosity values of stone, ceramic and glass tessera are given in Table 4. 3. The density and porosity values of stone and ceramic tessera were between 1.45 gr/cm3 and 2.39 gr/cm3 and 1.99- 18.68% by volume respectively.

The glass tesserae had porous spongy microstructure that originated from micro cracks and air bubbles determined by SEM analyses (Figure 4. 3). Their average porosity values were between 2.95 - 17.26 % by volume. The high porosity values of glasses may be explained by presence of tiny bubbles of air due to low temperature of furnace that could not reach melting point of the glass, dispersed opacifier in glass matrix and deterioration process of tessera during burial and after excavation (Verita 2009).

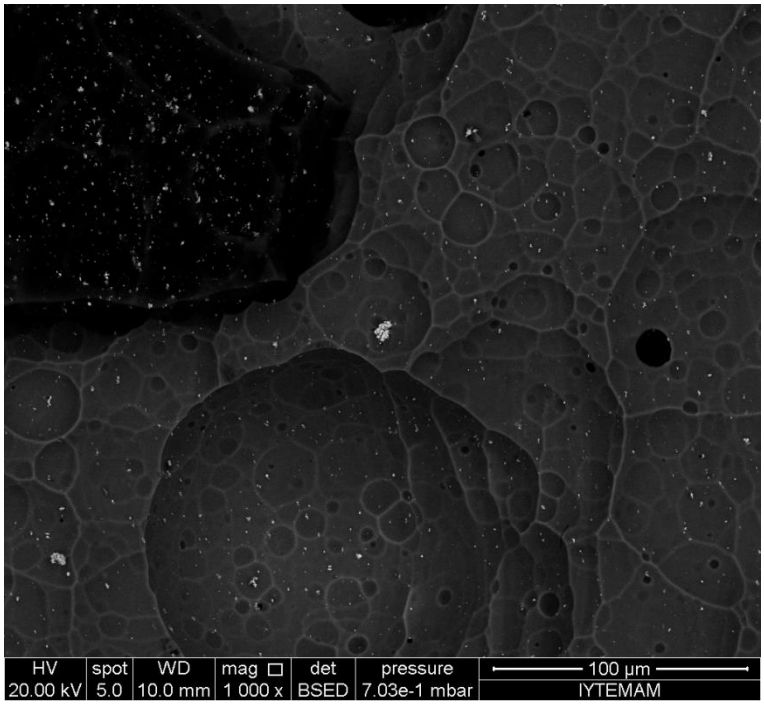

Figure 4. 3. SEM image of yellow tesserae with its spongy microstructure

Table 4. 3. Density and porosity values of stone, ceramic and glass tesserae

Sample	Porosity(%volume)	Density (g/cm3)
St-Wt	8.40	2.12
St-Bt	11.97	1.76
St-Yt	18.66	1.55
St-Gt	1.99	2.39
Cr-Pt	16.86	1.98
Cr-Rt	18.68	1.45
G-Yt	14.13	1.93
G-Lgt	7.28	2.06
G-Gt1	4.58	2.37
G-Dgt2	9.61	2.12
G-Ct1	17.26	1.75
G-Tt1	2.95	1.55
G-Tt2	3.67	3.01
G-Dtt	7.68	1.92
G-Bvt1	4.48	2.23
G-Bvt2	5.47	2.15
G-Drt	16.20	2.37
G-Bt	13.83	1.75

4.3. Raw Material Compositions of Preparatory Mortar Layers

In this study, the raw materials of mosaic mortar layers (rudus and nucleus) used in the construction of mosaics were determined as to whether they are hydraulic or not.

Lime/aggregate ratios of rudus and nucleus layers were in the range of 1:1 by weight (Figure 4. 4). These ratios were nearly same with some floor mosaic mortars used in some Roman period buildings (Puertas et. al. 1994 a, b, Montanaro et. al. 1998, Lopreato et. al. 2003, Starinieri 2009, Kramar et. al. 2011).

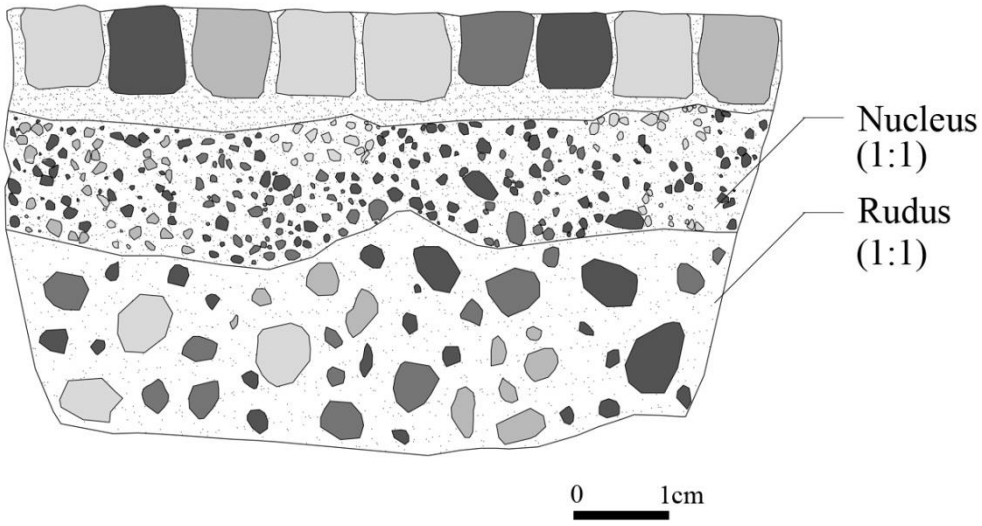

Figure 4. 4. Lime/aggregate ratios of rudus and nucleus mortar layers

The aggregates were mainly composed of crushed bricks. The rudus layer aggregates with particle sizes greater than 4.75 mm were composed the largest fraction of the total aggregates this was between 44.9 % and 69.2 % by weight (Figure 4. 5).

On the other hand, the fine aggregates of the nucleus mortars (<1180 micrometer) composed the main fraction of the total aggregates (Figure 4. 6).

These results showed that although rudus and nucleus layer mortars were composed of nearly same aggregate/lime ratios, the manufacturing of mortars were not same when considering the particle size distribution of the brick aggregates in the mortars.

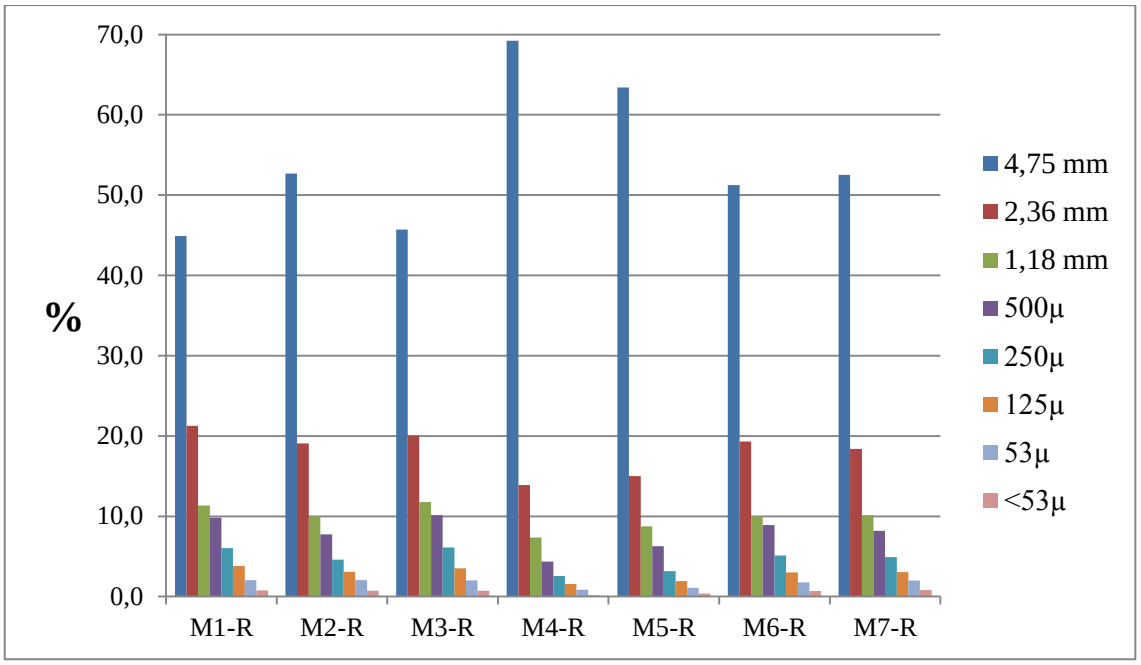

Figure 4. 5. Particle size distributions of aggregates of rudus mortar layers

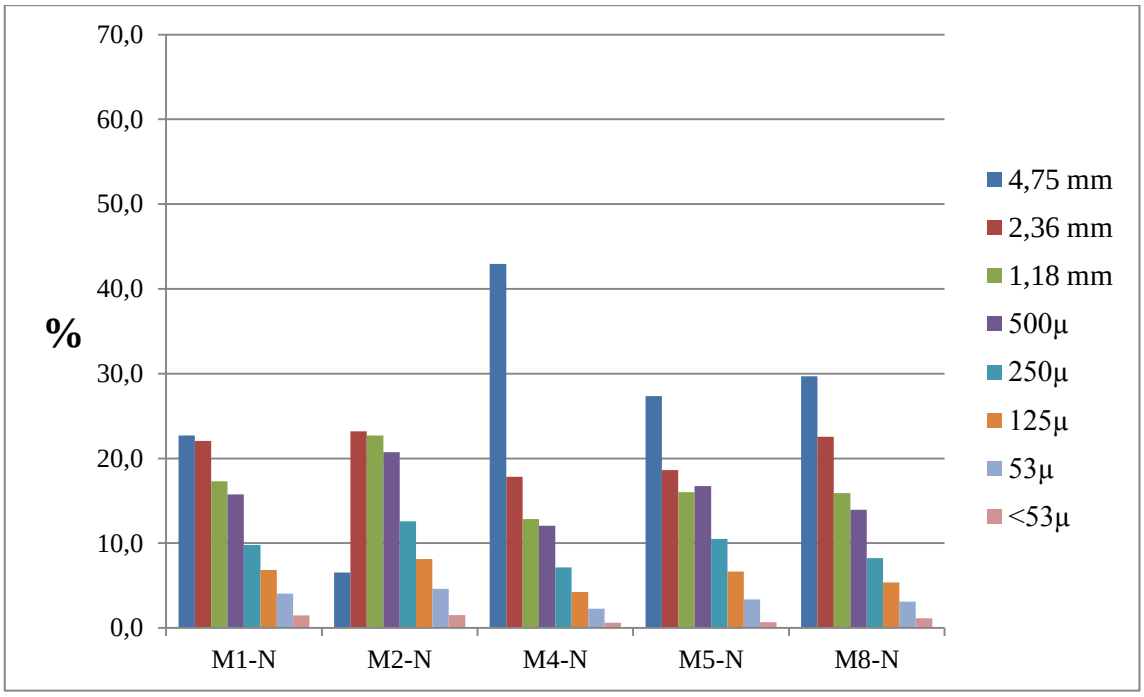

Figure 4. 6. Particle size distributions of aggregates of nucleus mortar layers

4.4. Pozzolanic Activity of Brick Aggregates

Hydraulic lime mortars were manufactured by mixing lime with natural and artificial pozzolanas (crushed brick) in Roman times (Vitruvius, 70 AD). If mortars manufactured by mixing lime with crushed bricks, it was called Cocciopesto in Roman times. Cocciopesto was generally used in humid places such as foundations, baths, cisterns, etc. due to their water proof properties.

In this study, the pozzolanacity of the brick aggregates used in rudus and nucleus mortars were determined whether to know they were pozzolanic or not.

Pozzolanic activities of the brick aggregates used in mortars were found to be about 4 mS/cm (Figure 4. 7). This value shows that the brick aggregates were pozzolanic (Luxan et. al. 1989) that acquires a hydraulic character of the mortars.

Similar results were obtained for crushed bricks used as aggregate in lime mortars (Cocciopesto) and in some wall of the Roman buildings and mosaics (Uğurlu 2005, Özkaya and Böke 2009, Kramar et. al. 2011).

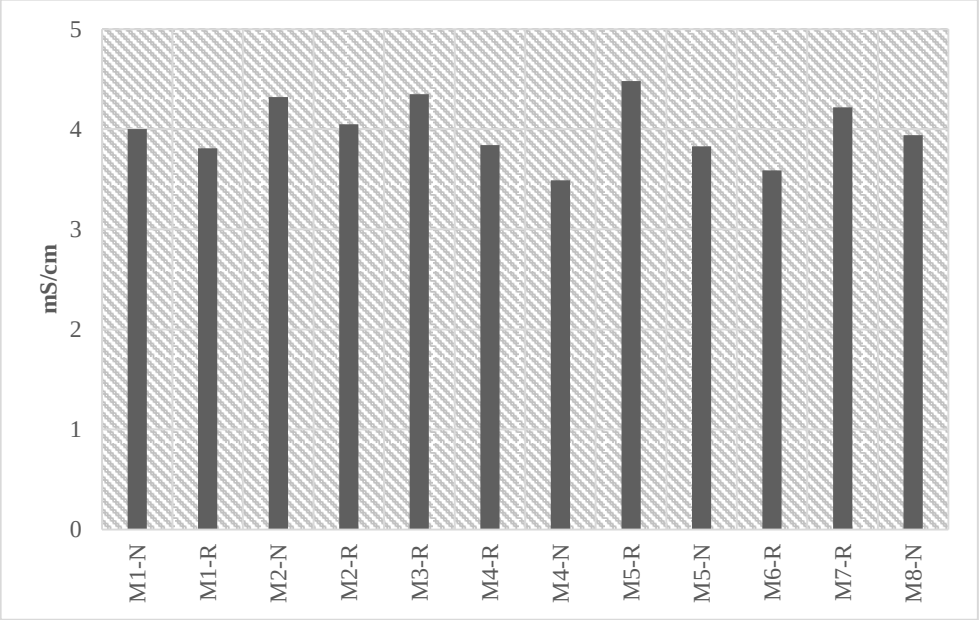

Figure 4. 7. Electrical conductivity (mS/cm) differences of brick aggregates of rudus and nucleus mortar layers

4.5. Hydraulicity of Preparatory Mortars

Hydraulic properties of binders of the rudus, nucleus and bedding mortars were determined with TGA analysis. In this analysis, percentages of weight loss of the mortars samples at temperatures between 200 ºC and 600 ºC due to the loss of structurally bound water of hydraulic compounds, and temperatures over 600 ºC due to loss of carbon dioxide gas from carbonated lime were determined. If the ratio of CO_2/H_2O is between 1 and 10, mortars can be accepted as hydraulic (Bakolas et. al. 1998, Moropoulou et. al. 2000a).

In this study, the CO_2/H_2O ratios of the binders of rudus and nucleus mortars were nearly 7 (Figure 4. 8, Table 4. 4). This value indicates that all binders of the mortars were hydraulic. However, the CO_2/H_2O ratios of the bedding mortars under the tessera were much more than 10 that can be accepted as non-hydraulic mortars (Figure 4. 9, Table 4. 4).

In some of the previous studies, similar CO_2/H_2O values were also indicated for crushed brick lime mortars used in some Roman buildings in Turkey (Uğurlu 2005, Özkaya and Böke 2009).

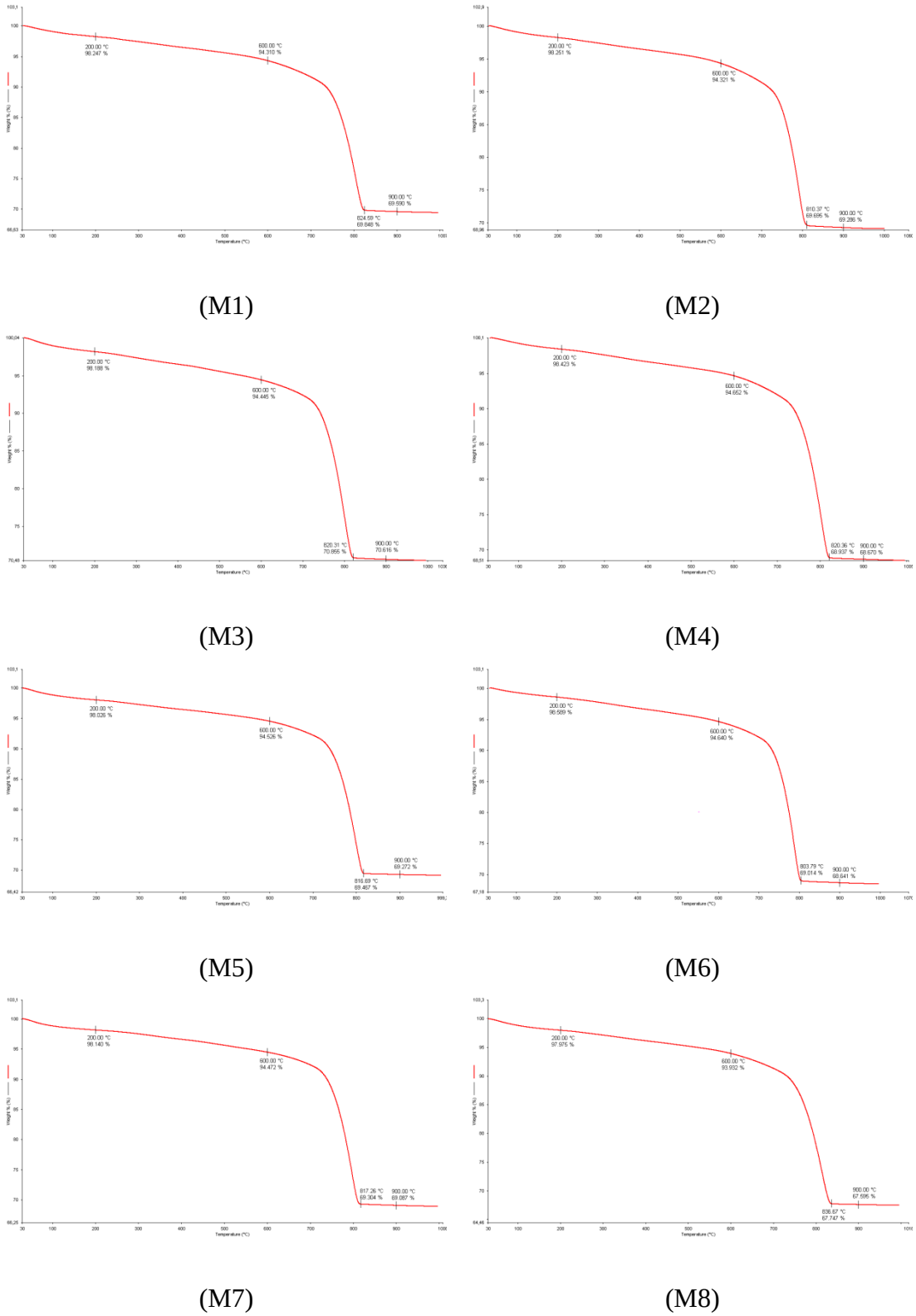

Figure 4. 8. TGA graphs of binders of nucleus and rudus mortars

(cont. on next page)

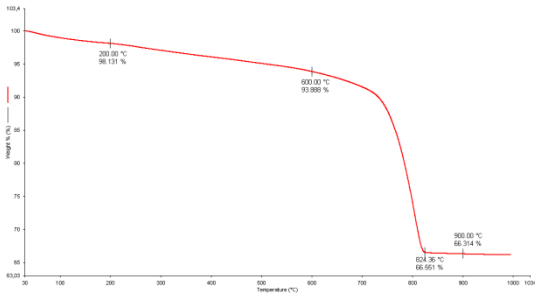

(M9)

Figure 4.8. (cont.).

Table 4. 4. Chemically bound water (H_2O %) and CO_2% amounts and CO_2/H_2O ratios of binders of rudus and nucleus mortars

Binders	**H_2O**	**CO_2**	**CO_2/H_2O**
M1	3.94	24.72	6.28
M2	3.93	25.03	6.37
M3	3.74	23.83	6.36
M4	3.77	25.98	6.89
M5	3.50	25.25	7.21
M6	3.95	26.00	6.59
M7	3.67	25.38	6.91
M8	4.04	26.34	6.52
M9	4.24	27.57	6.50

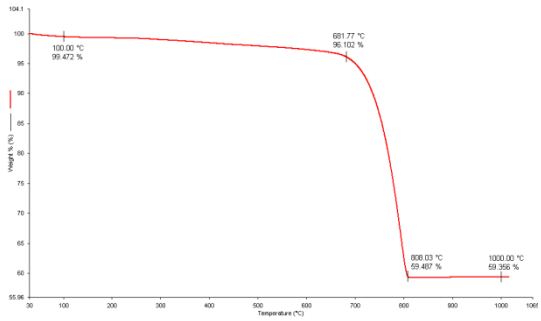

(M1)

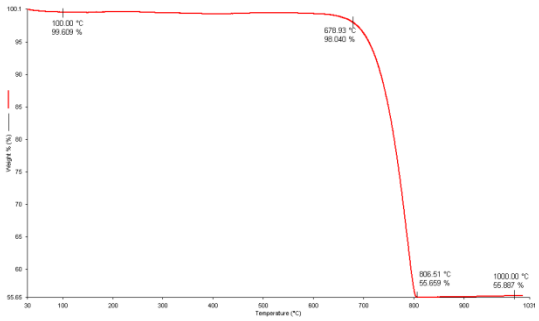

(M2)

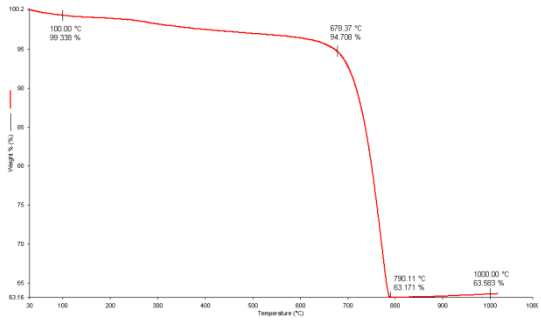

(M3)

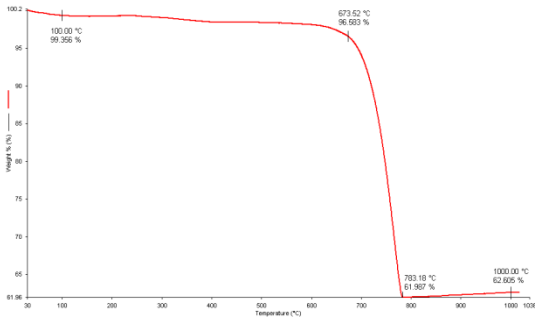

(M4)

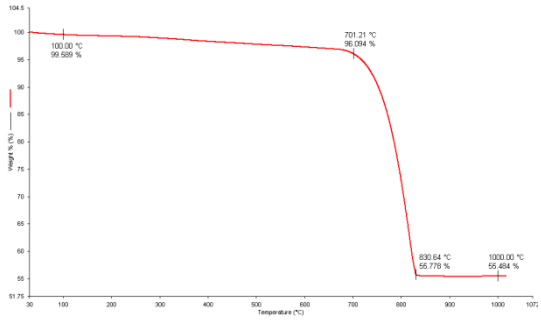

(M5)

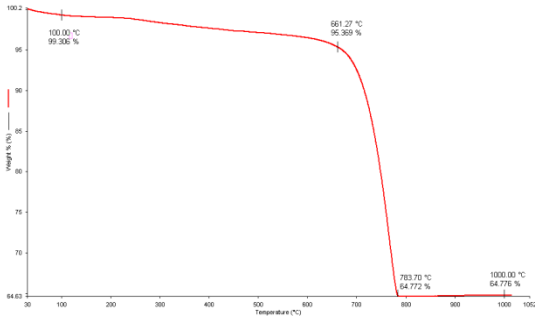

(M6)

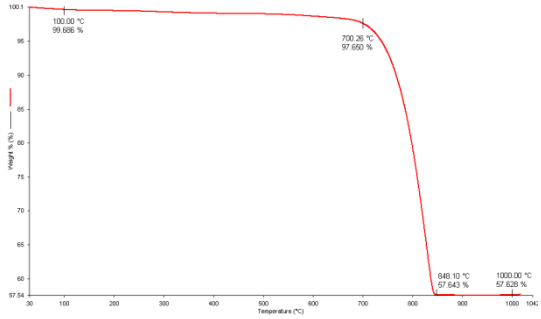

(M7)

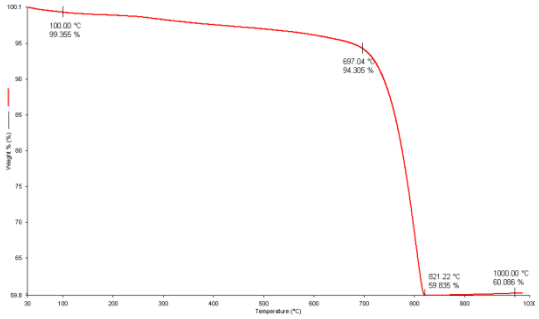

(M8)

Figure 4. 9. TGA graphs of bedding mortars

(cont. on next page)

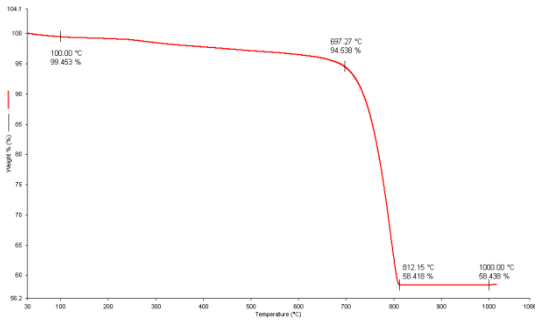

(M9)

Figure 4.9. (cont.).

Table 4. 5. Chemically bound water (H_2O %) and CO_2% amounts and CO_2/H_2O ratios of bedding mortars

Bedding Mortar	H_2O	CO_2	CO_2/H_2O
M1B	1.97	38.00	19.27
M2B	0.28	43.63	155.22
M3B	2.51	33.12	13.18
M4B	1.15	35.85	31.26
M5B	2.00	41.91	20.93
M6B	2.50	31.81	12.72
M7B	0.83	41.15	49.79
M8B	2.77	36.27	13.09
M9B	2.65	38.10	14.37

4.6. Mineralogical, Chemical and Microstructural Characterization of Preparatory Mortars of Mosaics

Mineralogical, chemical and microstructural characteristics of preparatory mortars were determined by using XRD and SEM-EDS analysis. Their characteristics were given in the following sections

Mineralogical and chemical compositions of mortars were determined by XRD and SEM-EDS analysis.

Chemical compositions of white lumps of all preparatory mortars representing the binding material used in the mortars were determined by SEM-EDS analysis. The results of the analysis were given in the following sections.

4.6.1. Rudus and Nucleus Mortars

In the XRD patterns of the binders of the rudus and nucleus mortars calcite and quartz peaks were identified (Figure 4. 10, Table 4. 6). Calcite originated from carbonated lime and quartz from brick aggregates. Although the brick aggregates were found to be pozzolanic, the peaks of hydraulic reaction products such as calcium silicate hydrates and calcium aluminate hydrate were not observed due to amorphous characters of hydraulic products that cannot be indicated in the XRD analysis (Haga et. al. 2002).

The similar characteristics of the crushed brick-lime, mortars and plasters used in several historic buildings were also indicated (Moropoulou et. al. 1995, Uğurlu 2005, Böke et. al. 2006, Uğurlu and Böke 2009,)

Chemical composition analysis of binders indicated that they are composed of mainly high amounts of CaO (49.32-62.54%), SiO_2 (22.36-28.69%) and Al_2O_3 (9.33-12.69%) (Table 4. 6). Calcium oxide was originated from carbonated lime, and SiO_2 and Al_2O_3 from brick powders. Less amounts of MgO, FeO, K_2O and P_2O_5 could be derived from the raw materials of lime and brick (Uğurlu 2005, Kramar et. al. 2011).

Microstructural analysis of rudus and nucleus mortars indicated that the adherence between brick aggregates and lime was diffused and strong (Figure 4. 11). This shows that mortars were prepared by through mixing of lime with aggregates. In rudus and nucleus mortar matrices small, white, round and soft white lumps or lime lumps representing the binding material used in the mortars were observed (Figure 4. 12). They were composed of micritic calcite crystals contained high amounts of CaO (96.21 %) (Table 4. 7).

Table 4. 6. Mineralogical and chemical compositions of binders determined by XRD, SEM-EDS

	Crystals	CaO	SiO_2	Al_2O_3	MgO	FeO	K_2O	P_2O_5
M1-Bi	Calcite, Quartz, Albite	53.88 ± 2.88	26.45 ± 1.73	11.68 ± 1.21	4.03 ± 0.69	2.35 ± 0.26	1.06 ± 0.06	0.53 ± 0.47
M2-Bi	Calcite, quartz	53.25 ± 0.34	26.55 ± 0.17	11.77 ± 0.08	4.13 ± 0.22	2.45 ± 0.14	1.10 ± 0.06	0.74 ± 0.70
M3-Bi	Calcite, quartz	49.32 ± 1.95	28.69 ± 0.91	12.69 ± 1.02	3.48 ± 0.12	3.11 ± 0.50	1.52 ± 0.08	1.18 ± 0.37
M4-Bi	Calcite, quartz	56.15 ± 2.2	25.76 ± 0.77	10.70 ± 0.77	3.77 ± 0.34	2.33 ± 0.24	1 ± 0.03	0.28 ± 0.49
M5-Bi	Calcite, quartz	52.83 ± 1.92	27.06 ± 1.55	11.54 ± 0.71	3.97 ± 0.18	2.78 ± 0.16	1.25 ± 0.07	0.58 ± 0.51
M6-Bi	Calcite, quartz	53.15 ± 0.55	26.77 ± 0.48	11.85 ± 0.03	3.8 ± 0.04	2.28 ± 0.11	1.13 ± 0.06	1.03 ± 0.07
M7-Bi	Calcite, quartz	50.76 ± 2.16	28.07 ± 1.54	12.36 ± 0.86	3.94 ± 0.12	2.5 ± 0.4	1.43 ±0.15	0.95 ± 0.16
M8-Bi	Calcite, quartz	61.29 ± 1.73	23.96 ± 0.27	9.33 ± 0.59	3.5 ± 0.27	1.1 ± 1.91	0.82 ± 0.74	-
M9-Bi	Calcite, quartz	62.54 ± 1.45	22.36 ± 0.21	10.05 ± 0.51	3.48 ± 0.02	1.17 ± 2.02	0.39 ± 0.68	-

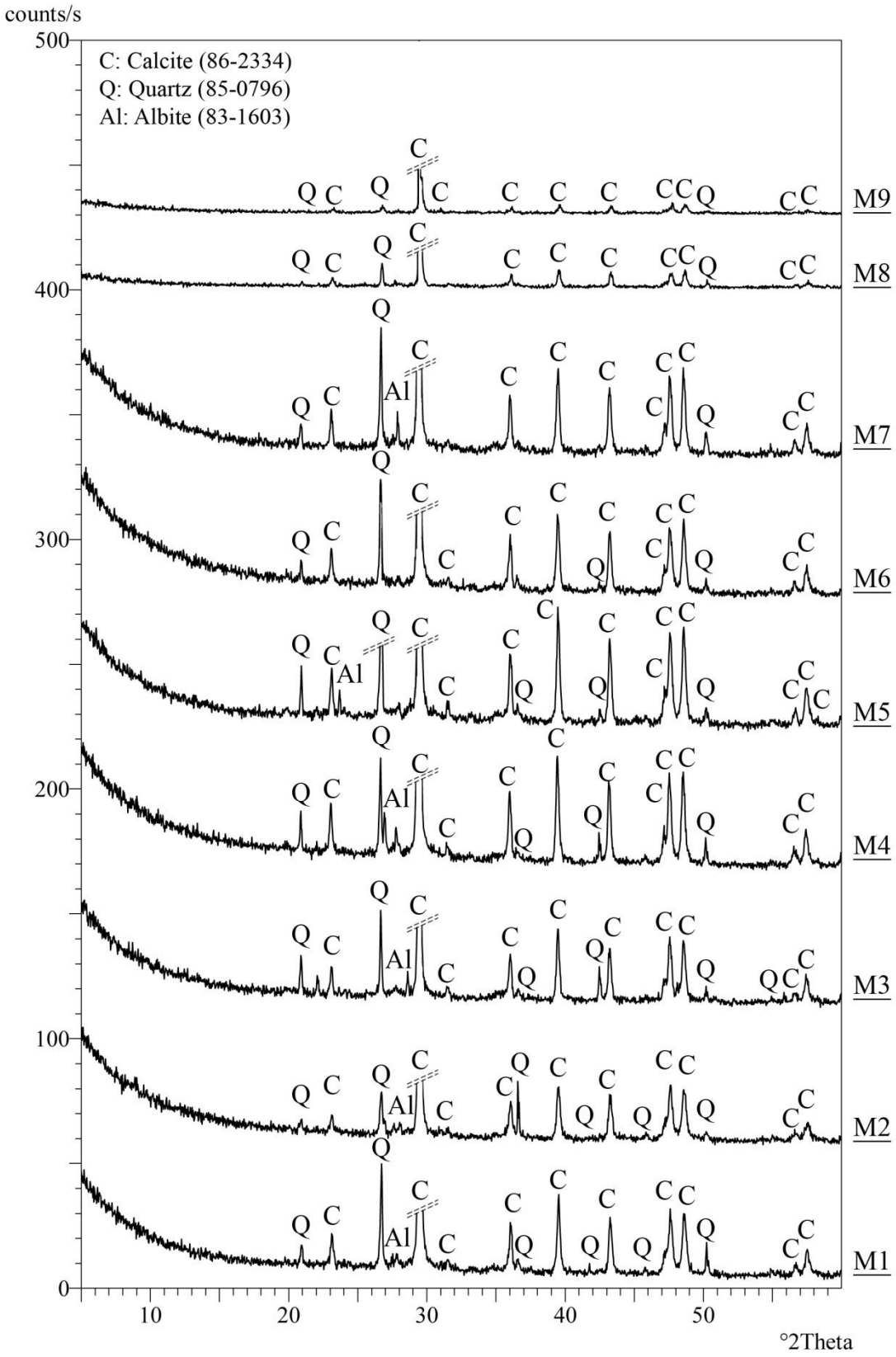

Figure 4. 10. XRD patterns of binders of rudus and nucleus mortars layers mosaics

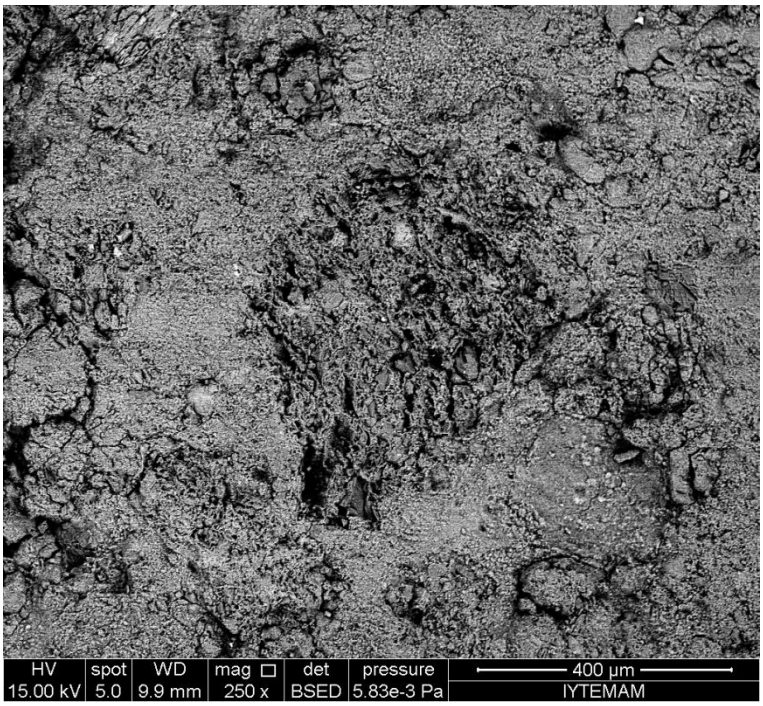

Figure 4. 11. SEM image of brick aggregate within the rudus and nucleus mortar matrix

Table 4. 7. Chemical compositions of lime (white) lumps determined by SEM-EDS

Lime Lumps	CaO	SiO_2	Al_2O_3	MgO
LL1	99.7±0.4	0.3±0.4	nd	nd
LL2	93.5±3.2	3.3±2.1	1.4±1.1	1.8±0
LL3	86.2±1.7	11.2±1.2	2.6±0.6	nd
LL4	93.8±0.6	3.9±0.4	1.7±0.1	0.6±0.1
LL5	89.6±1.2	6±0.2	0.7±1	3.7±0
LL6	98.8±0.8	1.2±0.8	nd	nd
LL7	97.1±0.6	1.2±0.9	0.4±0.5	1.2±0.6
LL8	97.8±0.4	0.8±0.1	nd	nd
LL9	98.6±0.4	0.4±0.5	0.9±0.7	nd

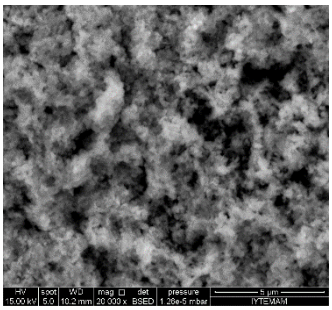
(M1-LL)

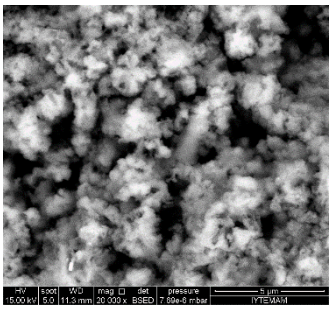
(M2-LL)

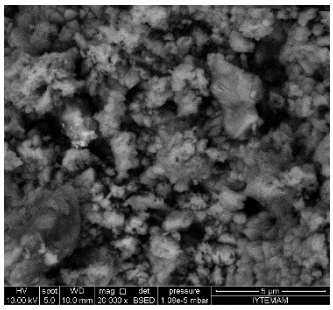
(M3-LL)

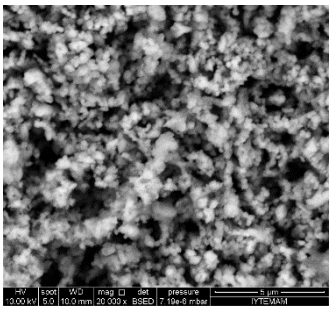
(M4-LL)

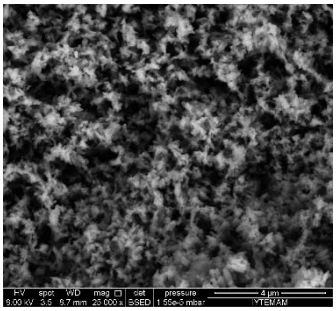
(M5-LL)

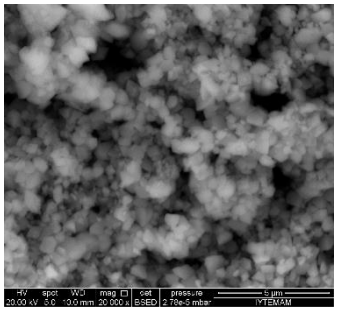
(M6-LL)

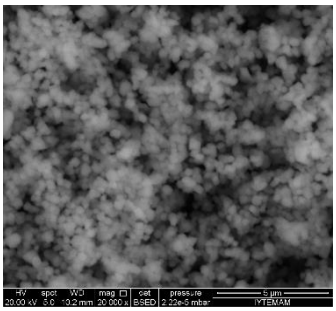
(M7-LL)

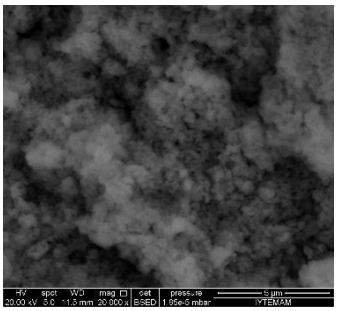
(M8-LL)

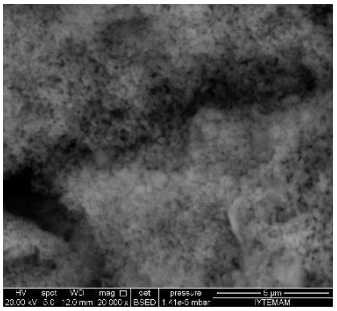
(M9-LL)

Figure 4. 12. SEM images of lime (white) lumps consisted of micritic calcite crystals

4.6.2. Bedding Mortars

In the XRD patterns of bedding mortars, high intense peaks of calcite (C: $CaCO_3$) and low intense peaks of quartz (Q: SiO_2) were observed (Figure 4. 13). Calcite was derived from carbonated lime and quartz from the fine aggregates. In the chemical compositions analysis of the mortars carried out by SEM-EDS analysis, high amounts of CaO and low amounts of SiO_2 were indicated (Table 4. 8). SEM analysis indicated that mortars were composed of small sized calcite crystals (Figure 4. 14). The results of the XRD and SEM-EDS analysis show that bedding layers were produced by using lime rich mortars.

Table 4. 8. Mineralogical and chemical compositions of bedding mortars determined by XRD, SEM-EDS

	Minerals	**CaO**	**SiO_2**	**Al_2O_3**	**MgO**	**FeO**
M1B	Calcite, quartz	93.7±0.3	3.89±0.3	1.2±0.1	1.2±0.1	-
M2B	Calcite, quartz	96.2±0.5	0.2±0.4	3.6±0.3	-	-
M3B	Calcite, quartz	84.2±0.9	9.6±0.1	2.5±2.2	2.1±0.2	-
M4B	Calcite, quartz	91.7±1.1	5±0.6	1.9±0.3	1.4±0.2	0.4±0.6
M5B	Calcite, quartz	94.6±0.4	2.7±0.2	1.2±0.3	1.6±0.2	-
M6B	Calcite, quartz	80.8±0.7	11.8±0.5	4.1±0.3	1.7±0.1	-
M7B	Calcite, quartz	91.7±1.6	4.8±0.9	2.1±0.7	1.4±0	1.6±0.2
M8B	Calcite, quartz	84.2±0.6	9.5±0.4	3.4±0.3	2.6±0.1	-
M9B	Calcite, quartz	90.8±2.7	4.4±1.3	1.9±0.8	2.9±0.6	0.3±0.5

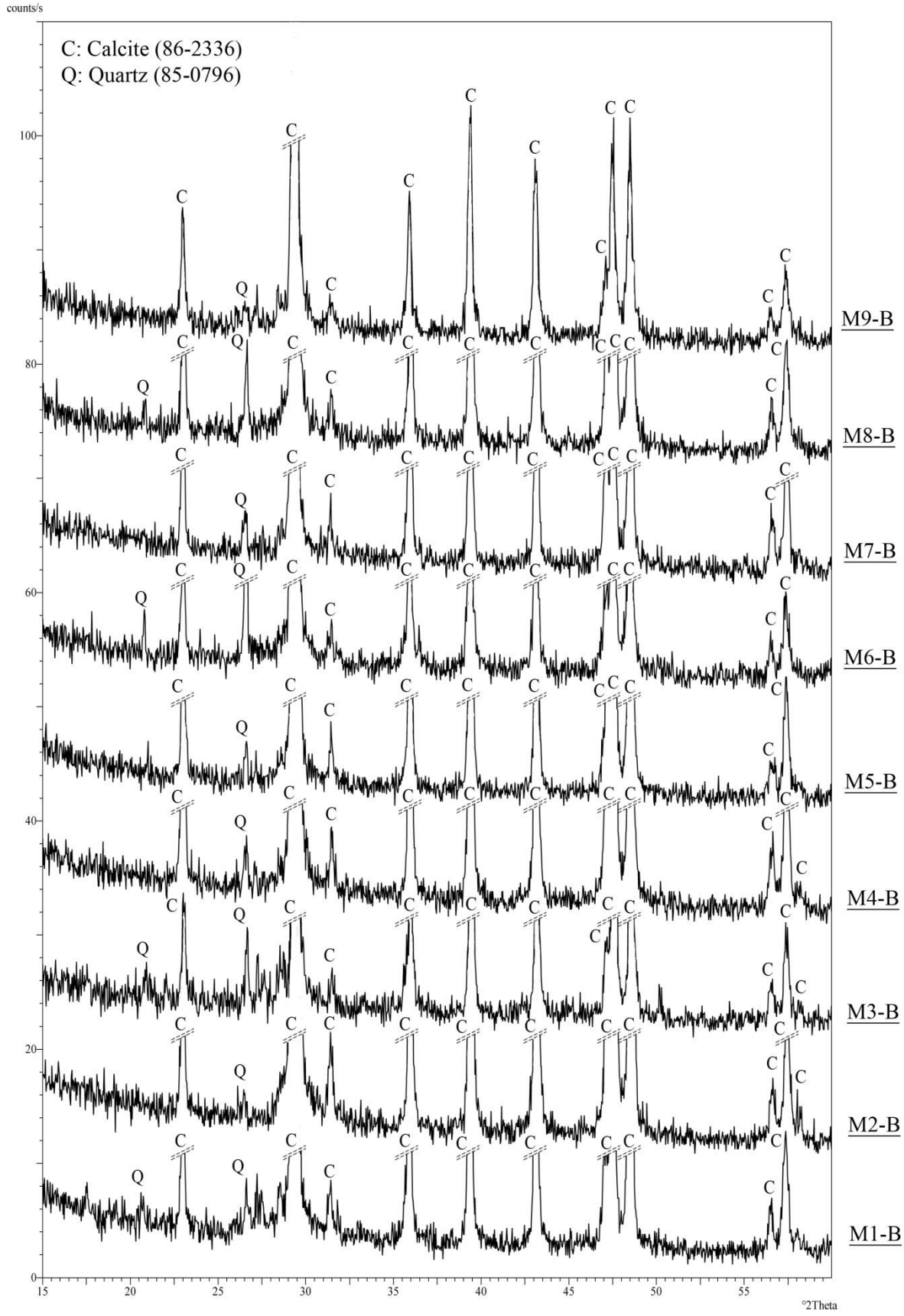

Figure 4. 13. XRD patterns of bedding mortars of mosaics

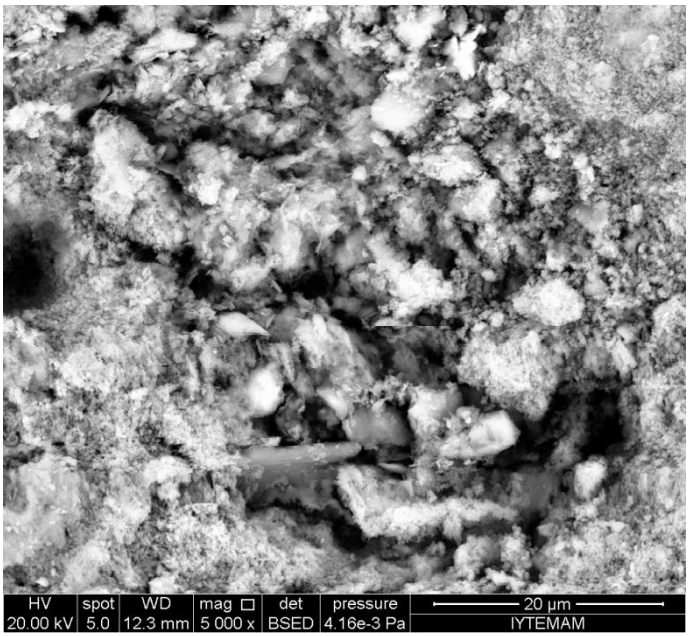

Figure 4. 14. SEM image of calcite crystals in bedding mortars

4.6.3. Mineralogical Compositions of Brick Aggregates of Rudus and Nucleus Mortar Layers

Bricks are manufactured by using natural clays containing quartz, and feldspars. Natural clays are mixed with water, shaped, dried and heated. When the heating temperature is between 450 ^{o}C and 800 ^{o}C, pozzolanic amorphous substances like metakaolin are formed. At temperatures over 800 °C, pozzolanicity of the substances are lost and high temperature mineral phases such as mullite and cristobalite were formed.

In the XRD patterns of bricks aggregate, quartz (SiO_2), albite ($NaAlSi_3O_8$), muscovite [$KAl_2(AlSi_3O_{10})(F,OH)_2$] and hematite peaks were observed (Figure 4. 15). In the XRD patterns of the bricks, a diffuse band between 20-30 degrees 2θ was also observed. This band shows the presence of amorphous substances derived from the high amounts of heated clay minerals. The pozzolanic activity measurements also confirmed the presence of high amounts of pozzolanic amorphous substances that give the hydraulic character of the mortars. These results showed that the brick aggregates used in the mortars were manufactured by using raw materials containing high amounts of clay minerals.

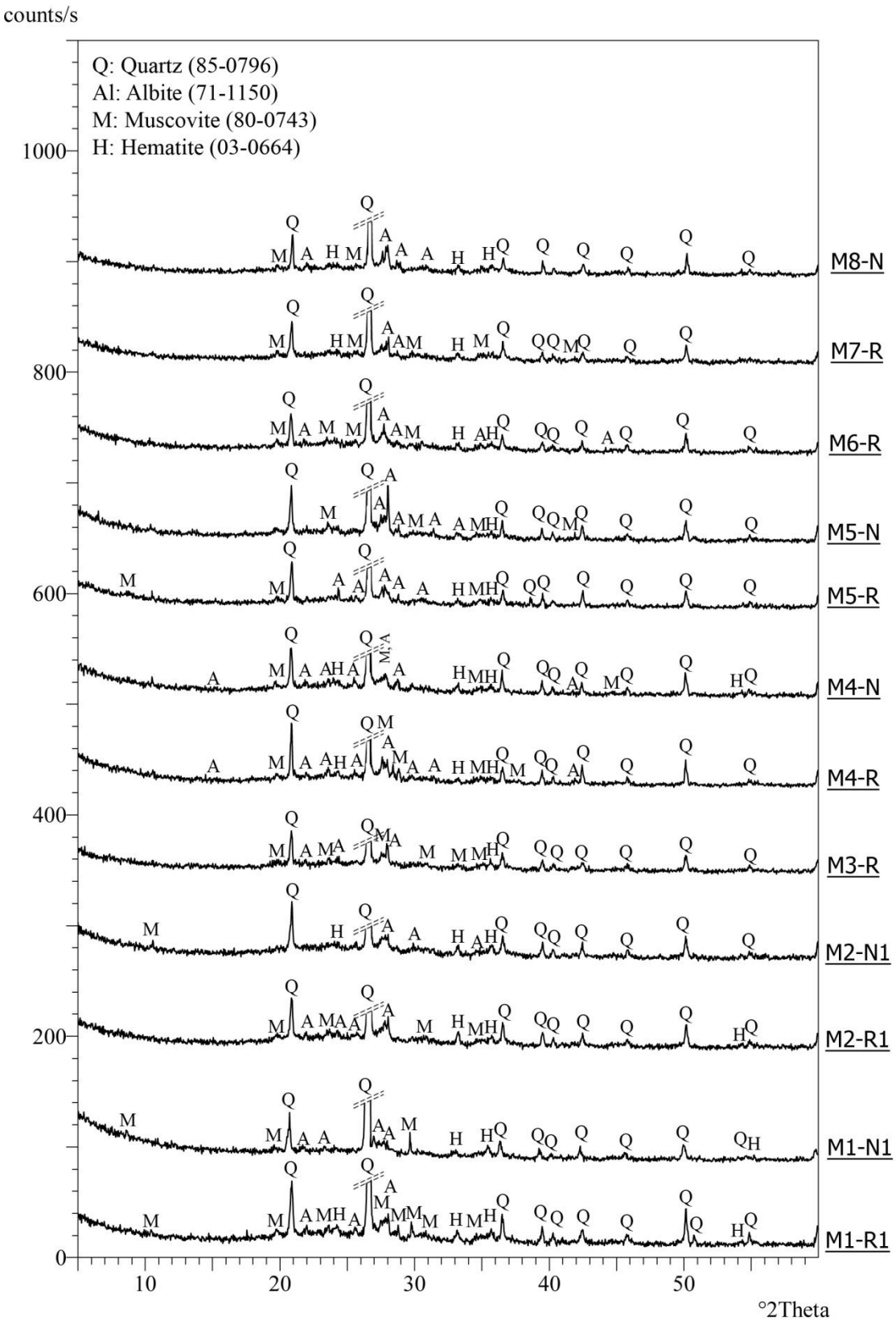

Figure 4. 15. XRD pattern of brick aggregates of rudus and nucleus mortars

4.7. Mineralogical, Chemical and Microstructural Characterization of Tesserae

Mineralogical, chemical and microstructural characterizations of tesserae were conducted using XRD, XRF and SEM-EDS analysis. They are given in the following sections.

4.7.1. Stone Tesserae

The colors of the stone tesserae used in the mosaics were beige, yellow, white and grey. Beige and yellow stone tesserae were mainly composed of dolomite and tridymite. The calcination temperature of beige and yellow stones was nearly 650 ºC and 709 ºC. The weight losses of the samples at temperatures over 700 ºC due to loss of carbon dioxide gas from dolomite crystals were 15.2 % for beige and 34.3 % for yellow stones. White and grey stone tesserae were composed of only calcite minerals (Figure 4. 17). Their calcination temperatures were between 640 ºC and 680 ºC. The weight losses of the tesserae at temperatures over 650 ºC due to loss of carbon dioxide gas from calcite were 43.2 % for white and 42.2 % for grey stones.

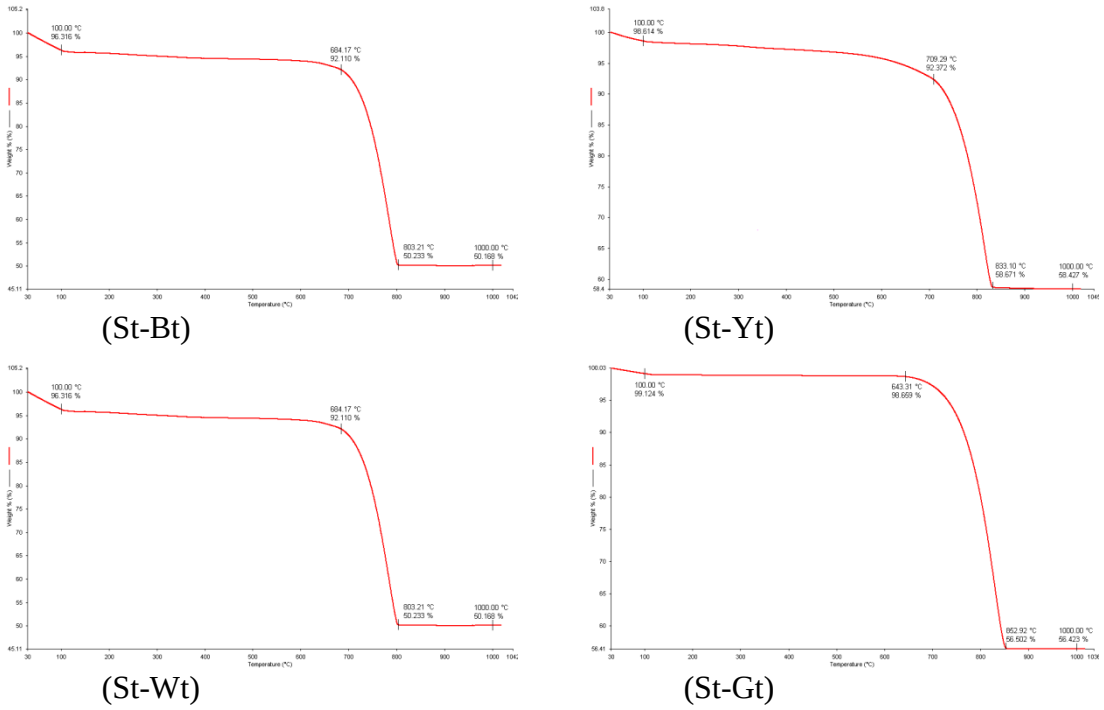

Figure 4. 16. TGA graphs of stone tesserae

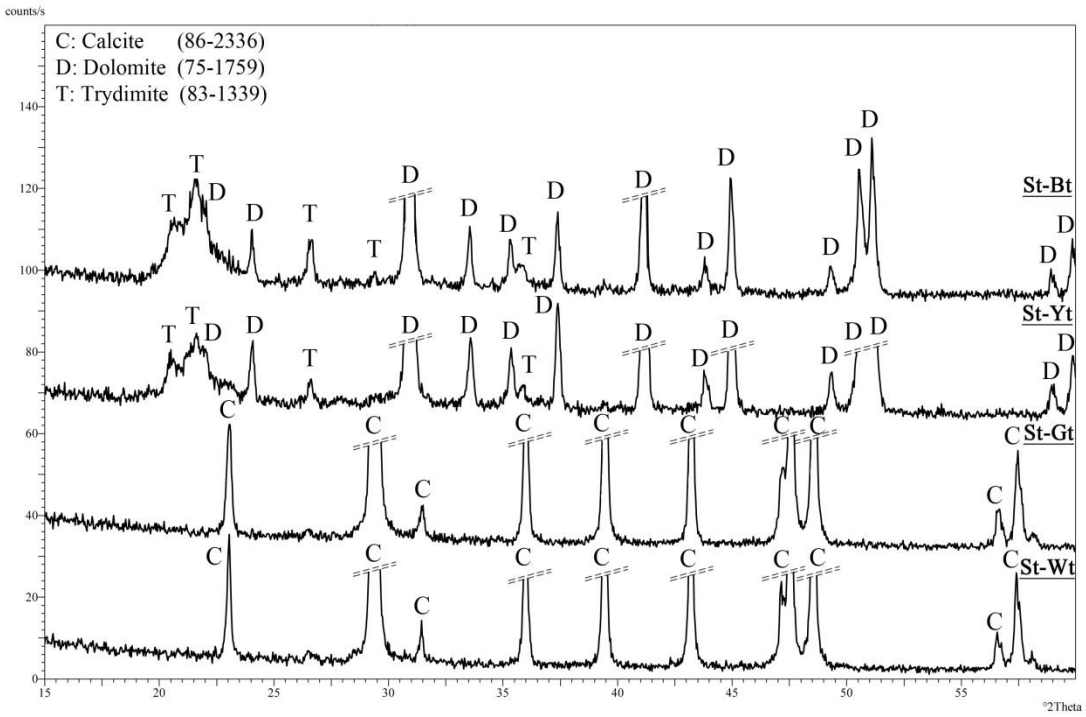

Figure 4. 17. XRD patterns of stone tesserae

Major, minor and trace elements in tesserae were determined by XRF analysis (Table 4. 9, Table 4. 10). XRF analysis indicated that white and grey stone tesserae were composed of mainly CaO. However, yellow and beige ones were composed of CaO, SiO_2 and MgO. The minor oxides found in the stone tesserae were Na_2O, Al_2O_3 and Fe_2O_3.

Table 4. 9. Major and minor elements in stone tesserae (%)

	Minerals	**SiO_2**	**CaO**	**Na_2O**	**Al_2O_3**	**MgO**	**Fe_2O_3**	**P_2O_5**	**K_2O**	**TiO_2**
St-Gt	calcite	-	54.99	0.52	0.11	0.42	-	0.02	0.05	-
St-Wt		0.62	48.11	0.49	0.33	0.32	0.04	0.03	0.06	-
St-Yt	dolomite	15.51	21.98	1.10	0.74	17.80	0.90	0.05	0.04	0.02
St-Bt	tridymite	28.92	18.37	1.00	0.86	15.06	0.42	0.06	0.05	0.01

Table 4. 10. Trace elements in stone tessera (%)

	Cl	**V_2O_5**	**SrO**	**Cd**	**ZrO_2**	**Mo**	**SO_3**	**Y**	**Ba**	**In**	**MnO**
St-Pt	0.07	0.01	0.03	0.01	0.04	0.01	0.10	0.01	0.11	-	-
St-Wt	0.04	-	0.03	0.01	-	0.01	0.07	-	-	0.01	-
St-Yt	0.06	0.01	0.08	-	-	0.01	0.05	-	-	0.03	0.06
St-Bt	0.06	-	0.07	-	-	-	0.04	-	-	-	0.01

The microstructural analysis of white and grey limestone indicates that they were composed of mainly fine-grained calcite crystals (Figure 4. 18, Figure 4. 19). Different from the white and grey limestone samples, yellow and beige dolomite contain high amounts of tridymite crystals composed of a high-temperature polymorph of quartz minerals (Figure 4. 20, Figure 4. 21).

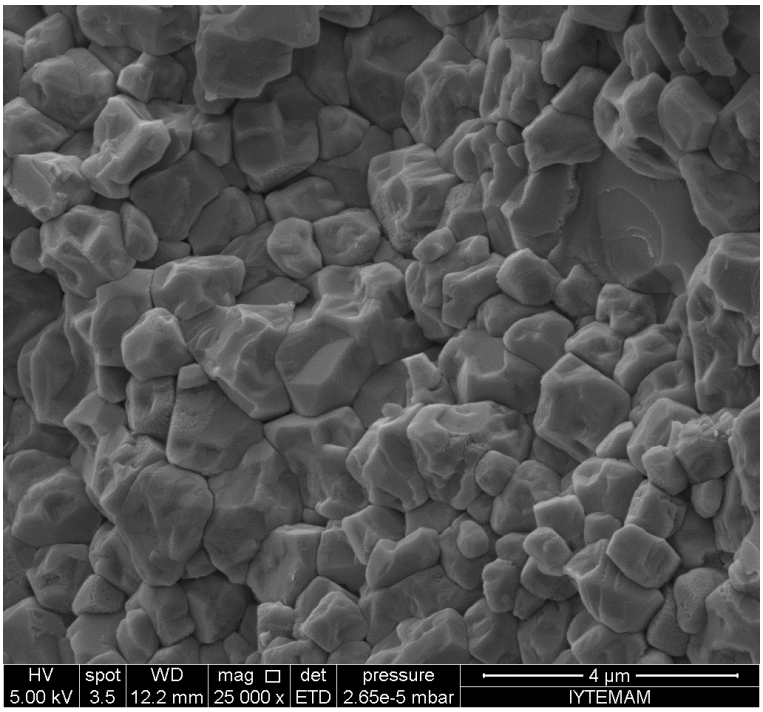

Figure 4. 18. SEM images of micritic calcite crystals (25000x) in white stone tesserae

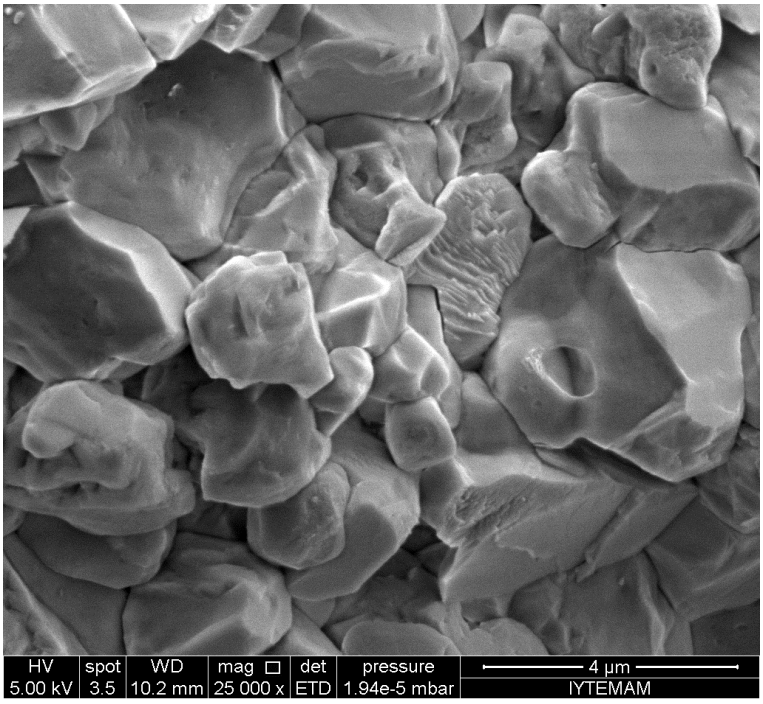

Figure 4. 19. SEM images micritic calcite crystals (25000x) in grey stone tesserae

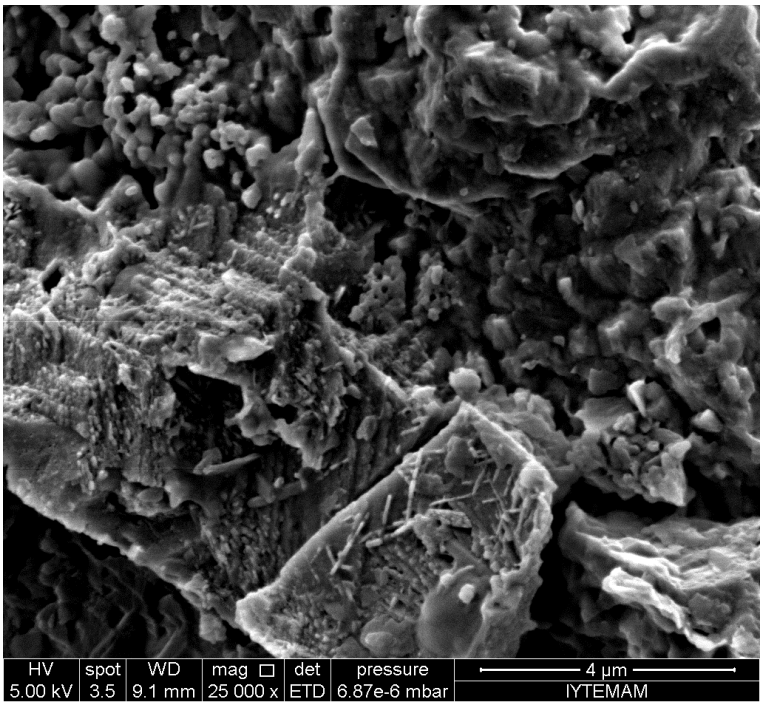

Figure 4. 20. SEM images of amorphous crystals (25000x) in beige stone tesserae

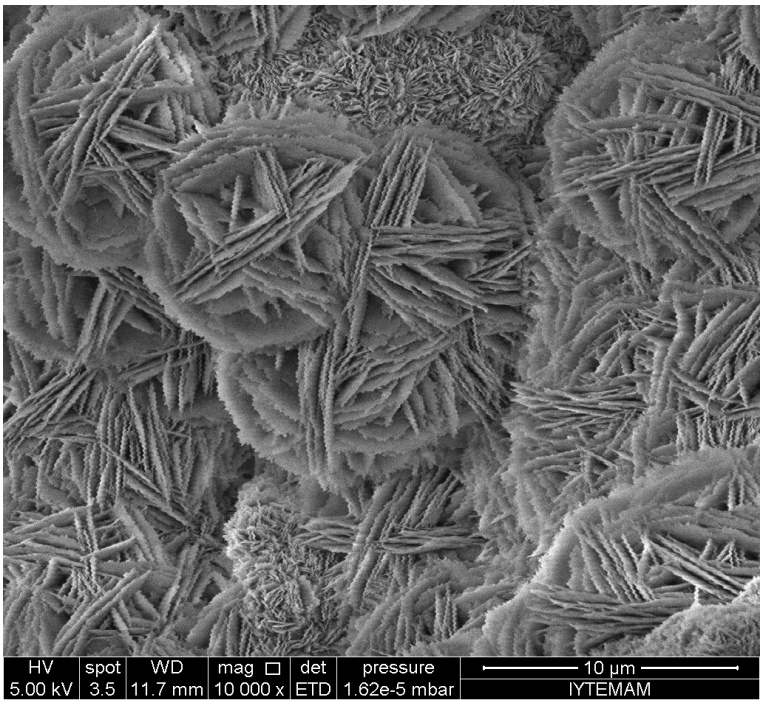

Figure 4. 21. SEM images of small size of tridymite crystals (10000x) in yellow stone tesserae

4.7.2. Ceramic Tesserae

Pink and red colors of the ceramic tesserae used in the mosaics were primarily consisted of quartz, calcite, albite and muscovite minerals (Figure 4. 23).

Major and minor oxide and trace-element compositions of the ceramic tesserae were given in tables they were mainly consisted of quartz, calcite, albite and muscovite minerals. They contained high amounts of SiO_2 and Al_2O_3, and low amounts of MgO, CaO, Fe_2O_3, Na_2O and K_2O (Table 4.11, Table 4.12). Red ceramics contained higher CaO and Fe_2O_3 than pink. TGA analysis indicated that the weight losses of the ceramics observed in the range of 100-600 ºC were negligible (Figure 4. 22). This indicates that clay minerals found in the composition of bricks were dehydroxylated during firing.

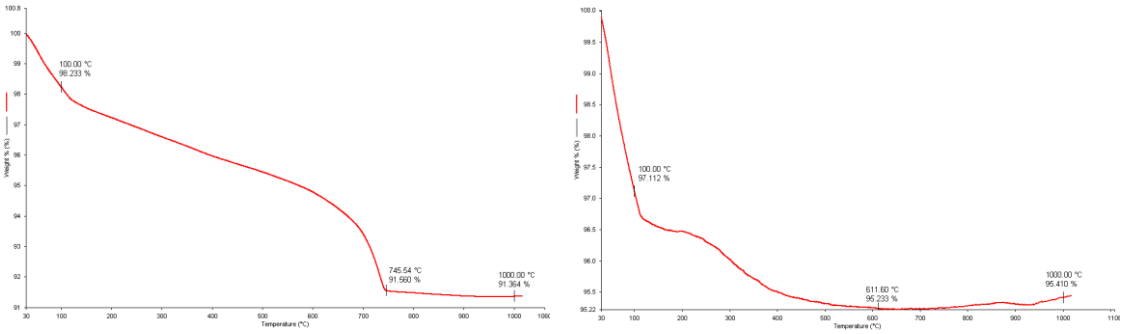

(Cr-Rt) (Cr-Pt)

Figure 4. 22. TGA graphs of ceramic tesserae

Table 4. 11. Mineralogical compositions and major elements of ceramic tesserae determined by XRD, XRF (%)

	Minerals	**SiO_2**	**CaO**	**Na_2O**	**Al_2O_3**	**MgO**	**Fe_2O_3**	**P_2O_5**	**K_2O**	**TiO_2**
Cr-Pt	quartz calcite	67.44	1.13	3.17	14.14	2.24	1.52	0.06	5.10	0.23
Cr-Rt	albite muscovite	50.63	8.55	1.43	16.33	6.57	4.06	0.31	2.48	0.63

Table 4. 12. Trace elements of ceramic tesserae determined by XRF (%)

	Cl	V_2O_5	SrO	Cd	ZrO_2	Mo	SO_3	Y	Ba	In	MnO
Cr-Pt	0.04	0.03	-	0.01	-	-	0.07	-	-	0.16	-
Cr-Rt	0.11	0.02	0.03	-	0.02	0.01	-	0.01	0.03	-	0.08

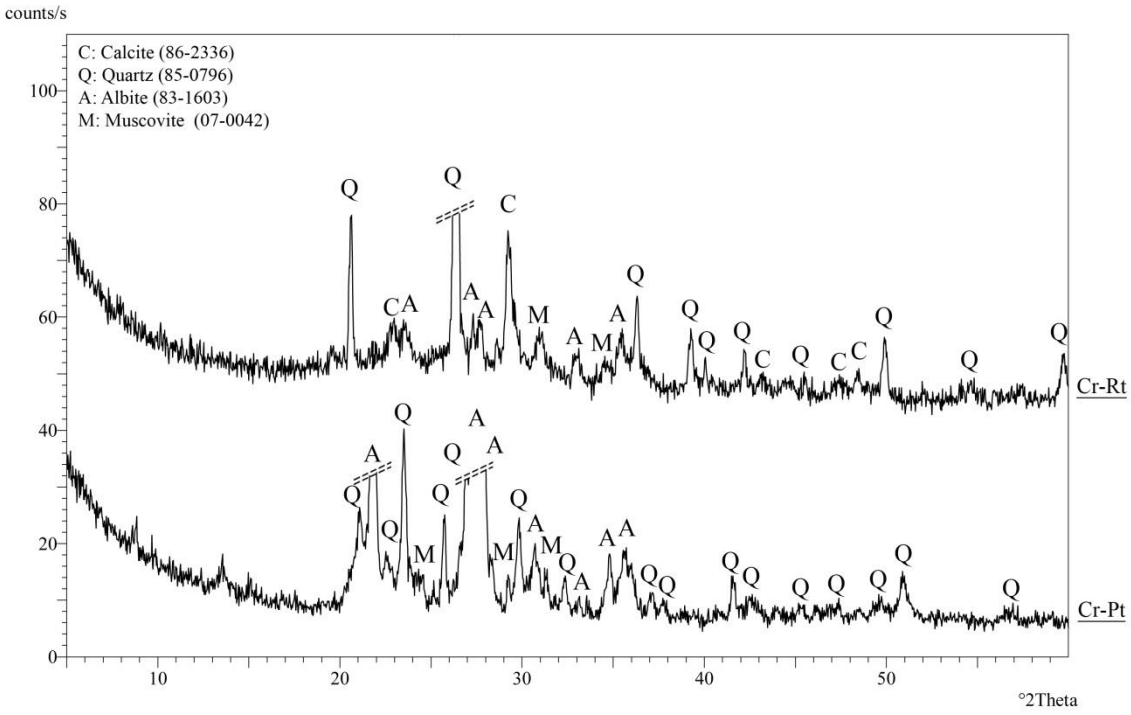

Figure 4. 23. XRD patterns of ceramic tesserae

Microstructural analyses of bricks indicated that red and pink ones mainly consisted of feldspar, quartz and glassy phase (Figure 4. 24, Figure 4. 25). Presence of glassy phase in the compositions of bricks suggests a high heating temperature of clay.

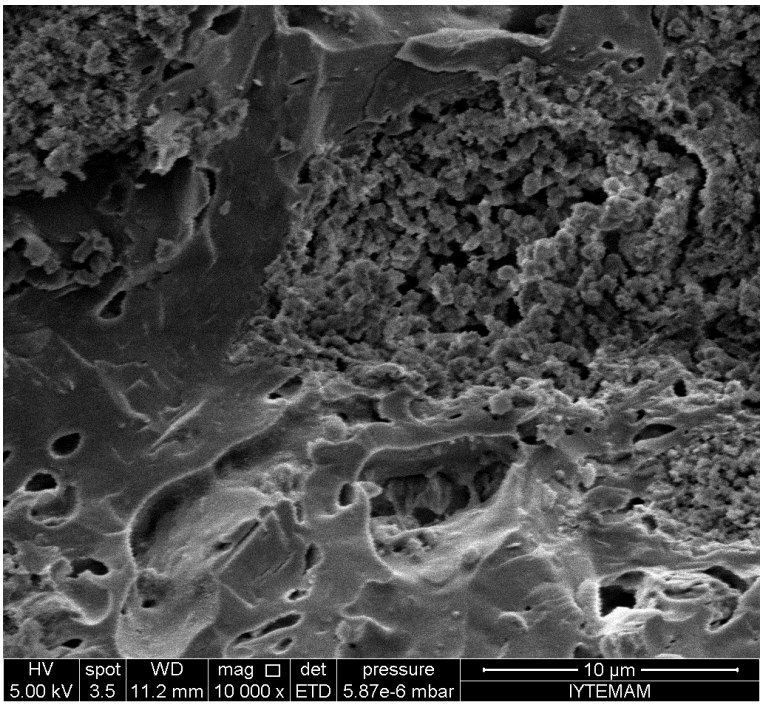

Figure 4. 24. SEM images of glassy phase quartz crystals (25000x) in pink ceramic tessera

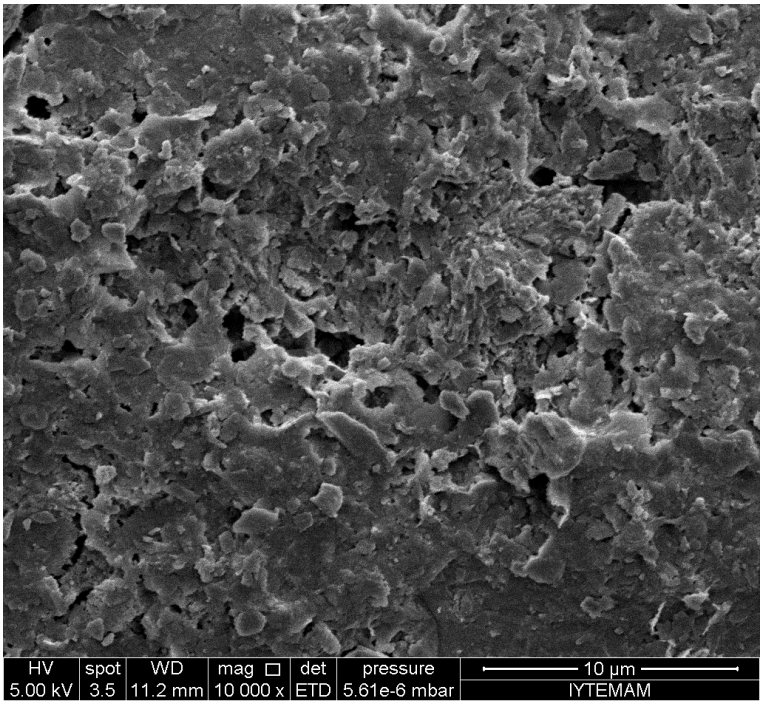

Figure 4. 25. SEM images of glassy phase quartz crystals (10000x) in red ceramic tessera

4.7.3. Glass Tesserae

Assos (Behramköy) was important glass producing site in western Anatolia in Roman Period (Figure 4. 26) (Atik 2004, Lauwers et. al. 2007). The glass tesserae that collected from the archeological site of Antandros (Altınoluk, Balıkesir) near Assos could be provided in this area. In this section, mineralogical and chemical compositions and microstructural properties of glass tesserae collected from Antandros were given and described.

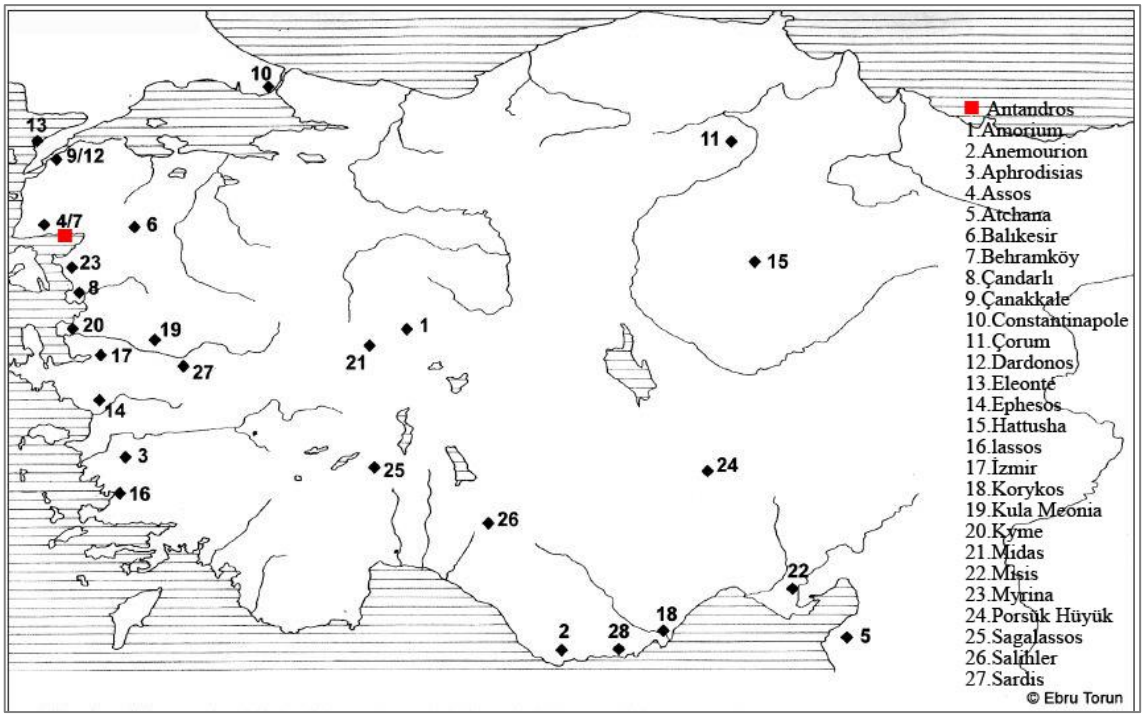

Figure 4. 26. Glass production sites in Anatolia
(Source: Torun E.)

Mineralogical Compositions of Glass Tessera

XRD analysis results indicate that all glass tesserae were primarily composed of amorphous silica (diffuse band between 15-40 degrees in the XRD pattern) and crystalline form of Ca-antimonate ($CaSb_2O_6$) and Pb-antimonate ($Pb_2Sb_2O_6$-$Pb_2Sb_2O_7$). $CaSb_2O_6$ crystals in white, turquoise, blue and cyan glass tesserae and $Pb_2Sb_2O_6$-$Pb_2Sb_2O_7$ crystals in yellow and green glasses were indicated (Table 4. 13).

Amorphous silica was a major constituent and Ca and Pb-antimonates were the common opacifiers used for the production of Roman mosaic glass tesserae (Butler et. al. 1950, Mass 1997, Shortland 2002, Lahlil et. al. 2010a, 2008, Werf et. al. 2009, Silvestri et. al. 2012, Schibille et. al. 2012).

Tesserae opacified with Pb-antimonate and Ca-antimonate were produced by chemical reactions between lead (Reactions 1.1-1.4) and calcium with antimony.

Table 4. 13. Types, opacifiers and colorants of glass tesserae

Sample	**Glass Type**	**Opacifier**	**Colorant**
Yellow Glass (G-Yt)	Lead	Pb-antimony ($Pb_2Sb_2O_6$, $Pb_2Sb_2O_7$)	Pb-antimony
Green Glass (G-Gt)	Lead	Pb-antimony ($Pb_2Sb_2O_6$, $Pb_2Sb_2O_7$)	PbO+CuO
White Glass (G-Wt)	Soda Lime	Ca-antimony ($CaSb_2O_6$)	Ca-antimony
Turquoise Glass (G-Tt)	Soda Lime	Ca-antimony ($CaSb_2O_6$)	CuO
Blue Glass (G-Lbt)	Soda Lime	Ca-antimony ($CaSb_2O_6$)	CuO, CoO
Cyan Glass (G-Ct)	Soda Lime	Ca-antimony ($CaSb_2O_6$)	CuO
Dark Red Glass (G-Drt)	Soda Lime Lead	Iron oxides, copper oxides	CuO, Fe_2O_3
Black Glass (G-Bt)	Soda Lime	Ca-antimony ($CaSb_2O_6$)	Fe_2O_3

Table 4. 14. Major elements of glass tesserae determined by XRF (%)

	SiO_2	Al_2O_3	Na_2O	K_2O	CaO	MgO	Fe_2O_3	TiO_2	CuO	ZnO	PbO	MnO	CoO	SnO_2	P_2O_5	Sb_2O_5	Ta_2O_5	SrO
G-Yt	59.18	2.31	6.27	0.33	6.81	0.99	0.85	0.10	0.49	0.03	19.31	0.40	0.01	0.08	0.48	1.02	0.47	0.12
G-Lgt	56.05	2.14	5.90	0.26	6.73	0.98	1.02	0.11	0.88	0.03	22.66	0.42	0.11	0.12	0.51	0.83	0.50	0.08
G-Dgt1	66.27	2.57	6.70	0.57	9.17	1.11	0.80	0.12	2.65	0.38	6.61	0.73	_	0.04	0.34	0.64	_	0.07
G-Dgt2	60.78	2.26	6.25	0.37	7.38	1.01	0.71	0.12	1.80	0.04	16.27	0.46	_	0.20	0.42	0.58	0.44	0.13
G-Gt1	58.37	2.21	5.67	0.30	6.69	0.94	0.85	0.11	2.39	0.03	18.95	0.50	0.07	0.20	0.46	0.86	_	0.07
G-Gt2	59.29	2.30	6.18	0.35	7.51	0.99	0.82	0.13	1.70	0.03	17.48	0.48	0.01	0.12	0.43	0.77	0.46	0.10
G-Tt1	69.08	2.56	6.83	0.62	8.76	1.12	0.69	0.14	3.25	0.03	0.06	0.50	0.01	0.39	0.23	3.46	_	0.08
G-Tt2	71.95	2.41	7.75	0.56	7.96	1.15	0.49	0.12	0.74	0.02	0.09	0.39	0.02	0.09	0.23	3.44	0.23	0.09
G-Dtt	71.57	2.50	7.49	0.59	8.92	1.15	0.57	0.12	2.56	0.02	0.13	0.49	_	0.44	0.23	1.41	_	0.09
G-Ct1	69.99	2.76	7.39	0.62	8.22	1.25	0.79	0.13	0.35	0.01	0.29	0.49	_	0.07	0.27	4.07	_	0.11
G-Ct2	70.22	2.49	7.61	0.57	7.97	1.19	0.75	0.11	0.30	_	0.35	0.50	0.01	0.07	0.26	4.22	0.45	0.12
G-Lbt1	68.71	3.09	11.61	0.52	7.29	2.29	0.42	0.09	_	_	_	0.22	0.02	_	0.14	_	_	0.08
G-Lbt2	72.05	2.38	8.08	0.84	7.61	1.17	0.59	0.09	0.07	_	0.27	0.46	_	0.03	0.25	3.26	0.43	0.12
G-Bvt1	69.78	2.77	6.98	0.51	9.59	1.17	1.11	0.12	0.16	_	0.18	0.36	_	0.02	0.23	4.27	0.35	0.07
G-Bvt2	72.51	2.45	8.50	0.69	8.64	1.17	0.85	0.14	0.10	_	0.04	0.41	0.01	_	0.24	2.03	0.36	0.12
G-Lbrt	69.90	2.51	7.66	0.67	9.05	1.18	0.54	0.12	0.04	_	0.05	2.38	_	0.02	0.28	3.10	0.33	0.08
G-Bt	65.96	3.13	10.51	0.49	7.39	2.22	5.61	0.08	_	_	_	0.05	_	_	0.16	_	_	0.05
G-Drt	68.55	2.81	7.07	0.64	9.06	1.20	3.81	0.14	1.07	0.02	2.00	0.65	_	0.10	0.31	0.59	_	0.10
G-Wt	76.21	2.14	8.35	0.43	6.92	1.13	0.44	0.12	0.02	0.01	0.19	0.07	_	_	0.17	1.68	0.30	0.05

Table 4. 15. Trace elements of glass tesserae determined by XRF (%)

	Cl	**Ba**	**SO_3**	**Te**	**Mo**	**V_2O_5**	**I**	**Br**	**Nb_2O_5**
G-Yt	0.69	0.02	_	_	0.01	_	0.01	0.02	0.01
G-Lgt	0.65	0.01	_	_	0.01	_	0.01	0.02	0.02
G-Dgt1	0.85	0.01	0.28	_	_	0.01	_	0.01	0.01
G-Dgt2	0.75	_	_	_	0.01	_	_	0.02	0.01
G-Gt1	0.64	0.03	_	_	0.01	_	_	0.01	0.01
G-Gt2	0.77	_	_	_	0.01	_	0.01	0.02	0.01
G-Tt1	0.98	0.04	0.98	0.19	0.00	0.01	_	_	_
G-Tt2	1.03	0.06	0.97	0.24	_	0.01	_	_	_
G-Dtt	1.09	0.09	0.47	0.05	_	0.01	_	_	_
G-Ct1	0.99	0.06	1.22	0.31	_	0.01	0.01	_	_
G-Ct2	0.98	0.07	1.17	0.36	_	0.01	0.01	_	_
G-Lbt1	1.01	0.01	0.52	_	0.01	_	0.00	_	_
G-Lbt2	1.04	0.08	0.92	0.26	_	0.01	0.02	_	_
G-Bvt1	0.74	0.04	1.05	0.36	_	0.01	0.01	_	_
G-Bvt2	0.95	0.02	0.65	0.08	_	0.01	_	_	_
G-Lbrt	0.99	0.08	0.75	0.22	_	0.02	_	_	_
G-Bt	0.55	_	0.23	_	0.01	0.01	_	_	_
G-Drt	0.97	0.07	0.37	_	_	0.01	_	_	_
G-Wt	1.11	0.05	0.50	0.09	_	0.01	0.00	_	_

Chemical Compositions of Glass Tessera

Elemental composition analysis indicated that glass tesserae were composed mostly of SiO_2, Na_2O, CaO and PbO. When the formula 1.1 was taking into account, glass tesserae can be classified into three main groups which were; soda-lime glasses, soda-lime-lead glasses and lead glasses (Table 4. 13).

Soda-lime glasses were turquoise, dark turquoise, cyan, light blue, blue, light brown and black tesserae. Soda-lime-lead glasses were dark green and red tesserae and lead glasses were yellow, light green and dark green tesserae (Figure 4. 12).

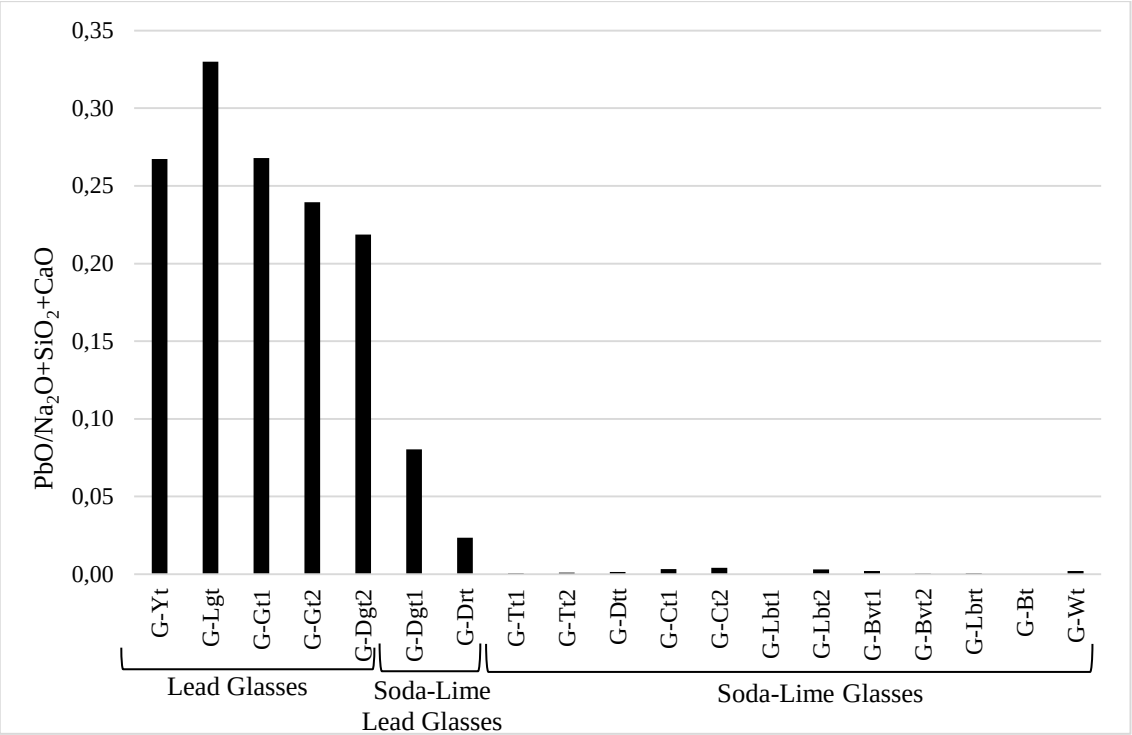

Figure 4. 27. Classification of glass tesserae based on the percent ratio of PbO/ (SiO_2+Na_2O+CaO) ratio

In K_2O% versus MgO% diagram glass tesserae can also be classified as sodic glasses due to low amounts of K2O and MgO contents (less than 1.5 wt %), except black and light brown tesserae (Figure 4. 28). Black and light brown tesserae were not included in these groups due to their high amounts of MgO and low amounts of K_2O. In Na_2O% versus K_2O% diagram glass tesserae can be classified as sodic glasses (Figure 4. 29). Based on this knowledge it can be suggested that glass tesserae were produced from natron based glasses. Natron was mined in Egypt (Wadi Natrun, North-West of Cairo) and used in glass-production during the Roman period (Henderson 1988, Lemke 1998, Werf et. al. 2009). Natron was traded from Egypt to local glass workshops (Pliny 77 AD, Jacoby 1991, 1993, James 2006).

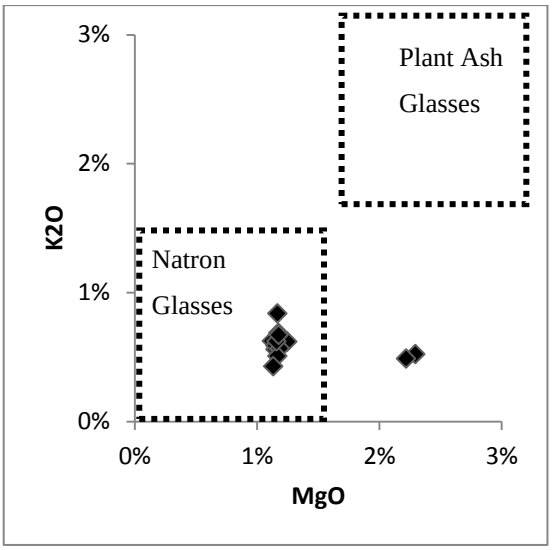

Figure 4. 28. K_2O% versus MgO% diagram of glass tesserae

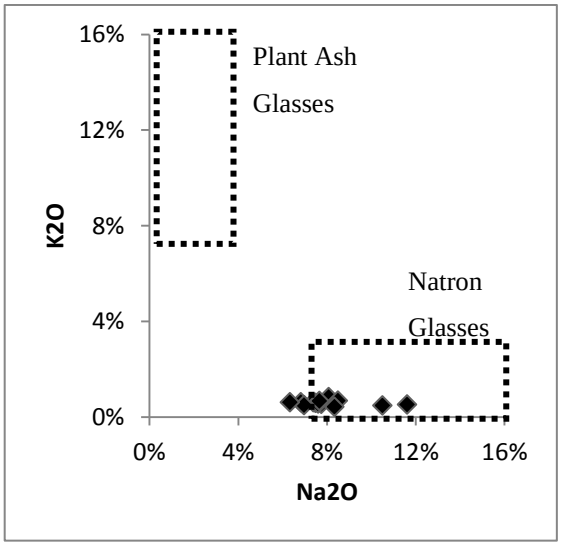

Figure 4. 29. K_2O% versus Na_2O% diagram of glass tesserae

Sand (quartz) is the main raw material of glass that contains inorganic impurities such as TiO_2, FeO and MnO which do not exceed 1%. If glass tesserae contain a high percentage of these oxides, they were intentionally used for producing colored tessera (Arletti et. al. 2006). The high percentage of oxide found in the tesserae related to their color was discussed in more detail.

The chemical analysis of glass tesserae provided evidence about the origin of the sand sources. Different sand sources can be differentiated by CaO, Al_2O_3, TiO_2, Zr and

Sr analysis. The comparison of TiO_2% content of glass tesserae may be a reliable indicator to differentiate their sand sources. The glass tesserae contain nearly same TiO_2% content that may show the use of similar silica sources (Vandini et. al. 2006, Arletti et. al. 2006, 2010, Schibille et. al. 2012, and Silvestri et. al. 2012).

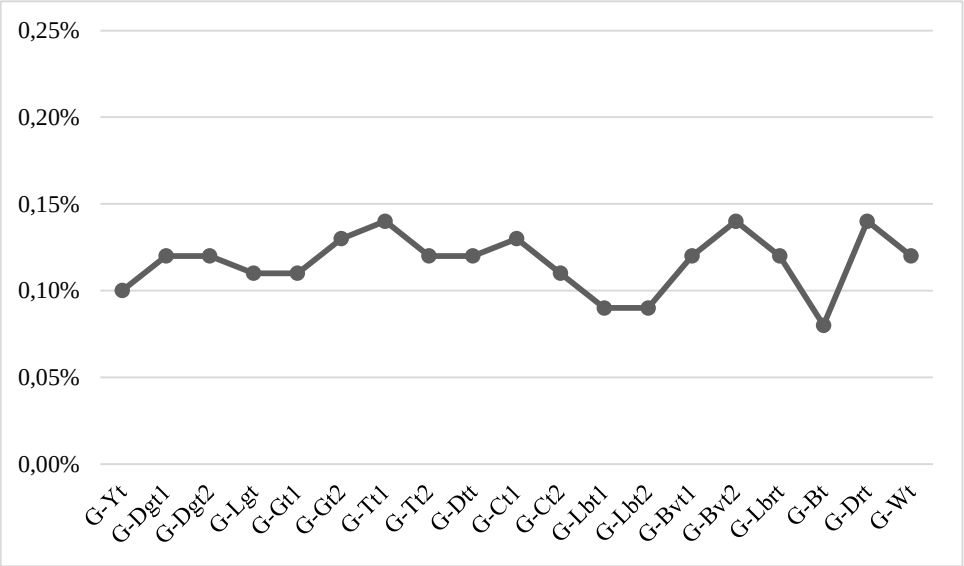

Figure 4. 30. TiO_2% contents in the composition of glass tesserae

The presence of considerable amounts of antimony oxide in the compositions of glass tesserae (0.6 - 4.3%) indicated the use of lead antimonate (yellow and green) and calcium antimonate (white, turquoise, blue, cyan and brown tesserae) as opacifying agents. The Ca-antimonate glasses (G-Tt1, G-Tt2, G-Dtt, G-Ct1, G-Ct2, G-Lbt1, G-Lbt2, G-Bvt1, G-Bvt2, G-Lbrt) contained high amounts of Sb_2O_5 than Pb-antimonate ones (G-Yt, G-Dgt1, G-Dgt2, G-Lgt, G-Gt1, G-Gt2). Hence they can be differentiated from their Sb_2O_5 content (Schibielle et. al. 2012).

In the following sections, microstructural, mineralogical and chemical compositions of glass tesserae were defined and discussed in detail, in relation to their colors.

4.7.3.1. Yellow Glasses

XRF analysis results indicated that yellow tessera contained high amounts of PbO (19.31wt %) and low amounts of Sb_2O_5 (1.01 wt %). This revealed that yellow tessera was opacified and colored with Pb-antimonate in the form of bindheimite ($Pb_2Sb_2O_7$) that was indicated by XRD analysis (Figure 4. 31, Table 4. 13).

Bindheimite crystals were densely and homogenously dispersed in glassy matrix (Figure 4. 32). The sizes of crystals varied between 0.9 μm-1.2 μm. They had well defined edges and angles (euhedral) (Figure 4. 33). They contained high amounts of PbO and Sb_2O_3 and low amounts of SnO_2 to be found as impurities in the PbO (Figure 4. 34).The presence of tiny acicular crystals in the glass compositions indicated that they were manufactured with ex situ crystallization (Silvestri et. al. 2012).

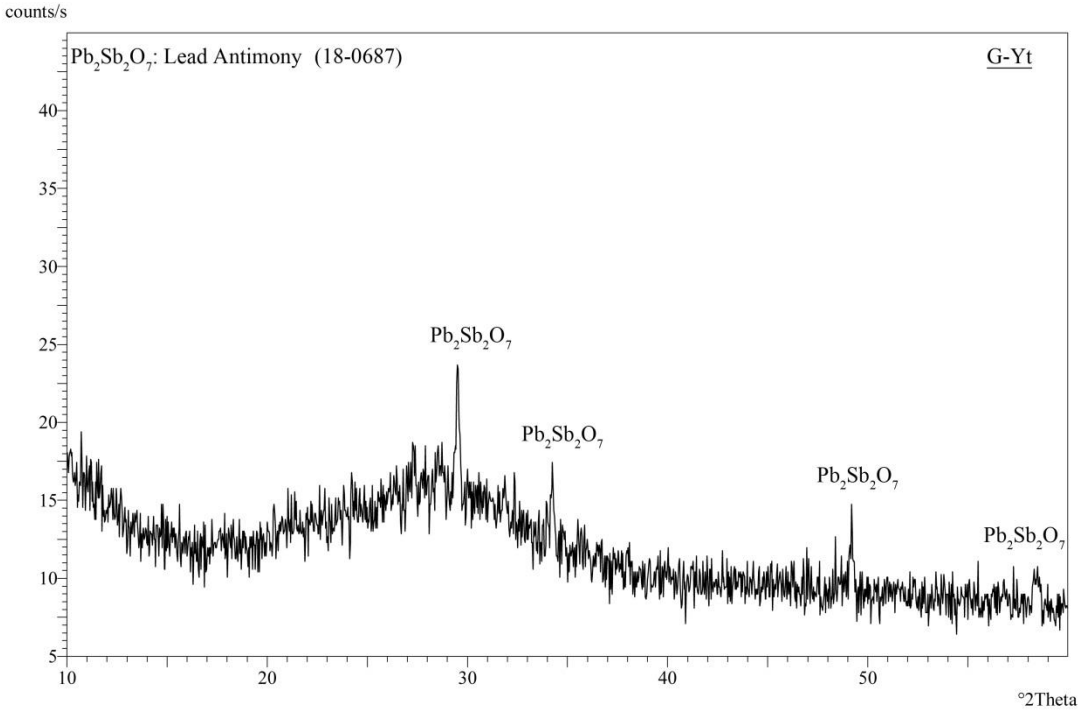

Figure 4. 31. XRD pattern of yellow glass tessera

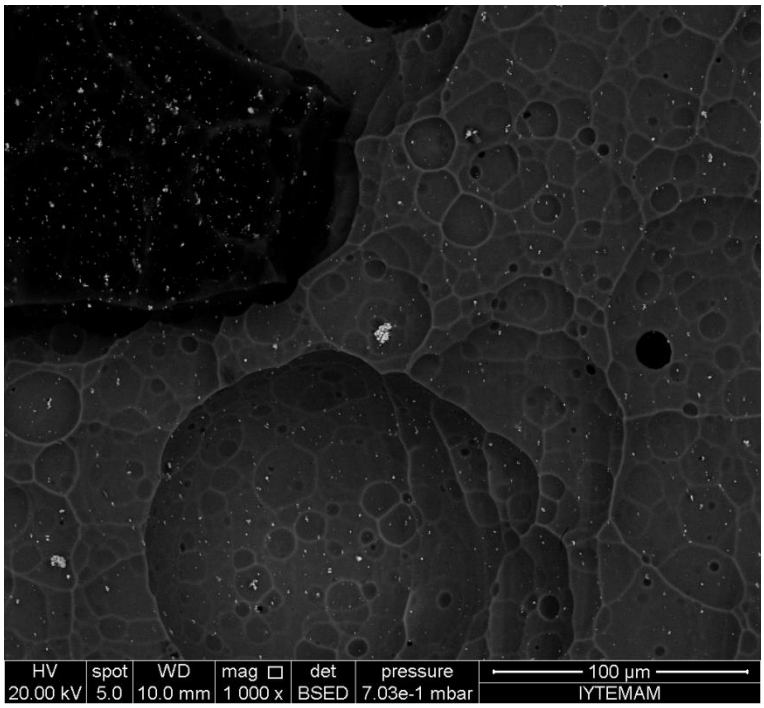

Figure 4. 32. SEM image of bindheimite crystals (10000x) in yellow glass tessera (G-Yt)

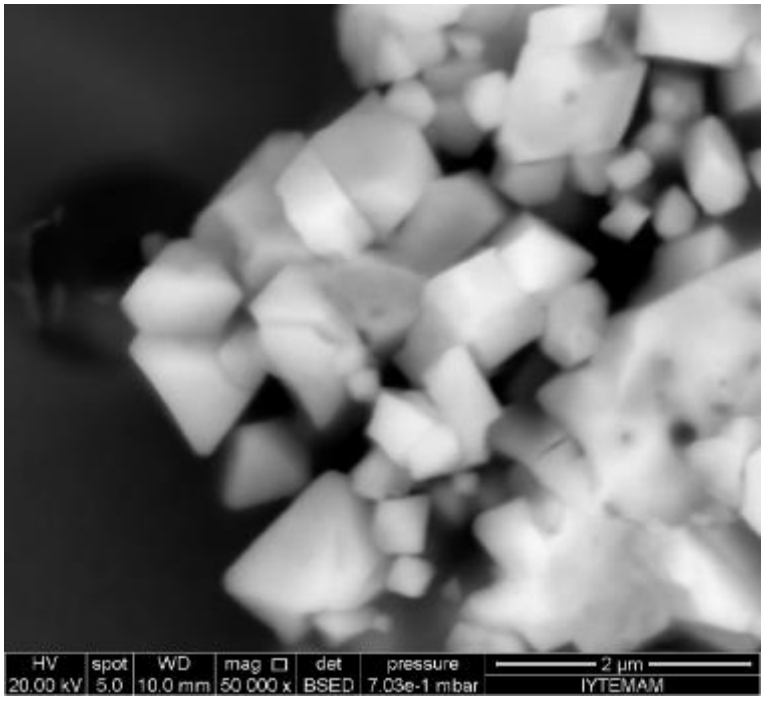

Figure 4. 33. SEM image of bindheimite crystals (50000x) in yellow glass tessera (G-Yt)

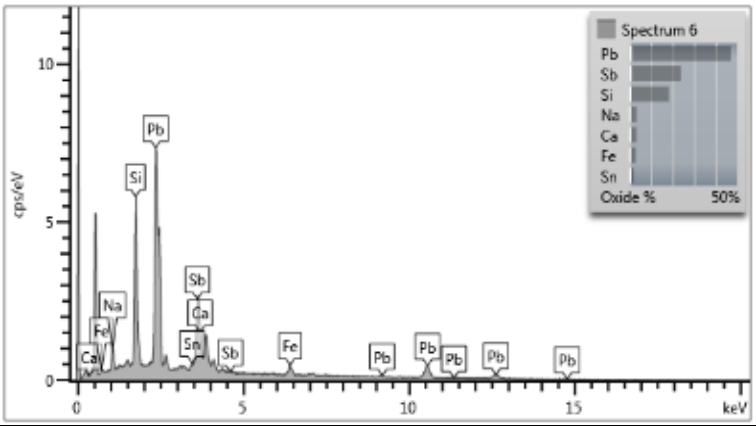

Sp6-Oxide	Sb_2O_3	SiO_2	PbO	Na_2O	CaO	FeO	SnO_2	
%	23.77	18.26	47.02	3.16	3.09	2.77	1.94	100.00

Figure 4. 34. EDS spectrum of yellow glass tesserae (G-Yt)

Microstructural analyses of yellow tesserae indicated that they have a spongy texture with air bubbles and micro cracks on the surface (Figure 4. 35). The spongy microstructure with air bubbles and micro cracks observed on the glass surfaces can be explained by low melting temperature of glass and deterioration process of mosaics during burial and after excavation.

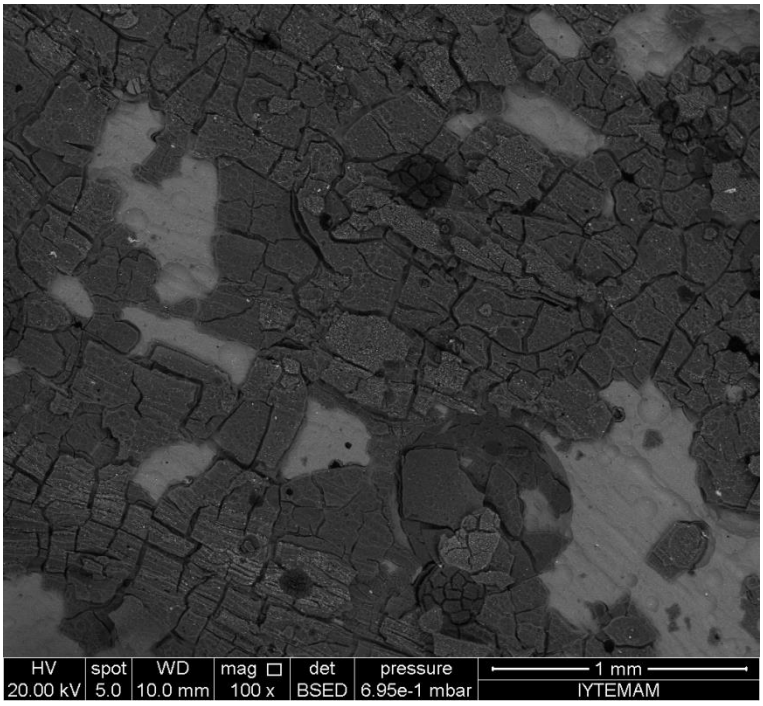

Figure 4. 35. SEM image of air bubbles and micro cracks in yellow glass tessera (G-Yt)

4.7.3.2. Green Glasses

XRF analysis results indicated that green tesserae contained high amounts of PbO (6.61- 22.66 wt %) and low amounts of Sb_2O_5 (0.64-0.86 wt %) and SnO_2 (0.04-0.2 wt %). High amounts of lead in the compositions of the tesserae indicated that green tesserae were manufactured with lead oxide to decrease the melting temperature of the glass and opacified with Pb-antimonate in the form of bindheimite that was indicated by XRD analysis (Figure 4. 36, Table 4. 13) (Werf et. al. 2009).

Bindheimite crystals were densely and homogenously dispersed in glassy matrix (Figure 4. 37). The sizes of crystals varied between 0.5 μm-3μm in G-Dgt2 and 0.3 μm-1.2 μm in G-Gt2. They were tiny acicular crystals in sample G-Dgt2 (Figure 4. 38) whereas in sample G-Gt2 crystals had well defined edges and angles (Figure 4. 39). They contained high amounts of PbO and Sb_2O_3 and low amounts of SnO_2 to be found as impurities in the PbO (Figure 4. 40). Recent studies suggested that previously synthesized Pb-antimonate was added to transparent glass to obtain an opaque glass (ex situ) (Shortland 2002, Lahlil et. al. 2011, Silvestri et. al. 2012). In some cases well-formed Pb-antimonate crystals were determined in green glasses this may explain by precipitation of Pb-antimonates from glass melt during cooling of the glass (Mass et. al. 1998, Silvestri et. al. 2012).

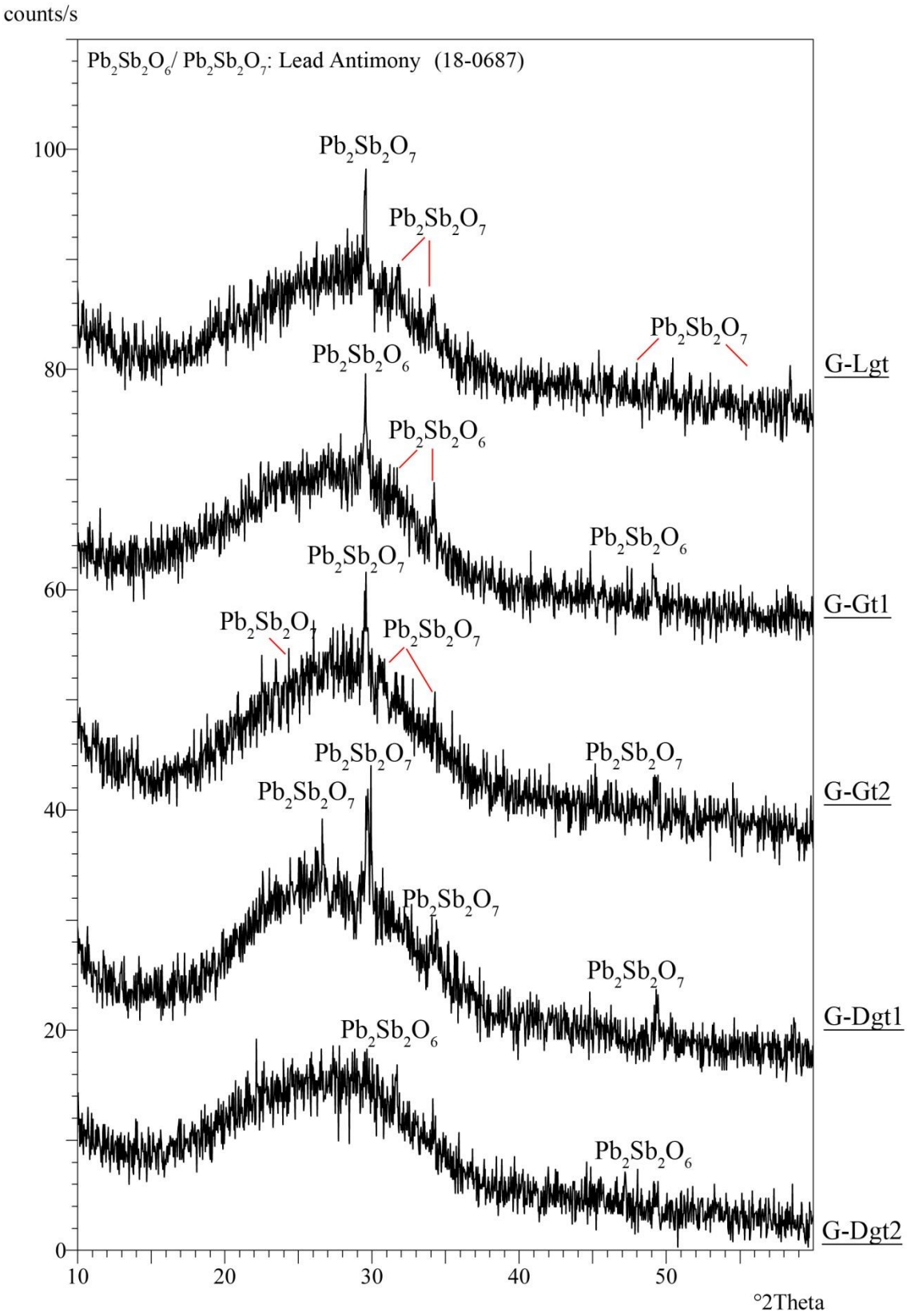

Figure 4. 36. XRD pattern of green glass tesserae

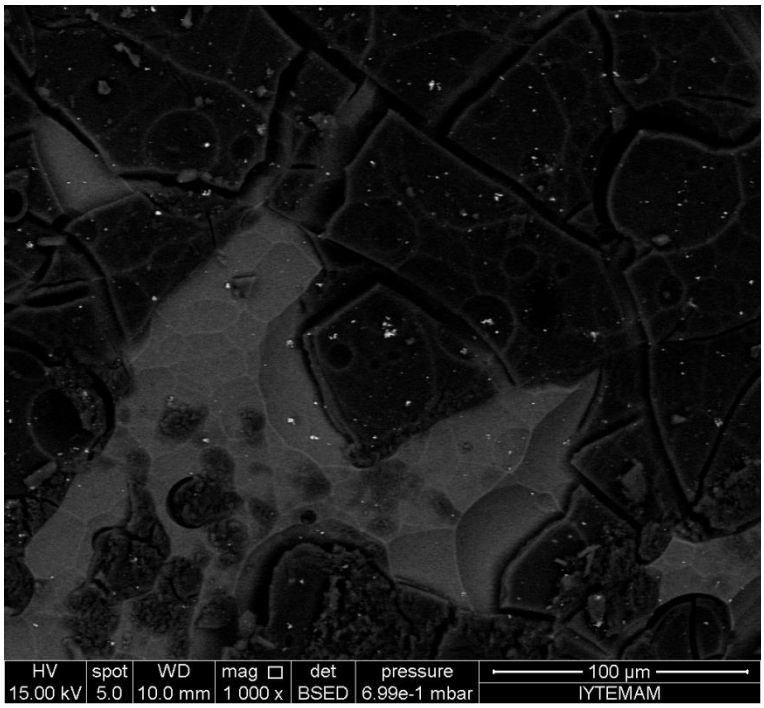

Figure 4. 37. SEM image of bindheimite crystals (1000x) in green glass tessera (G-Gt2)

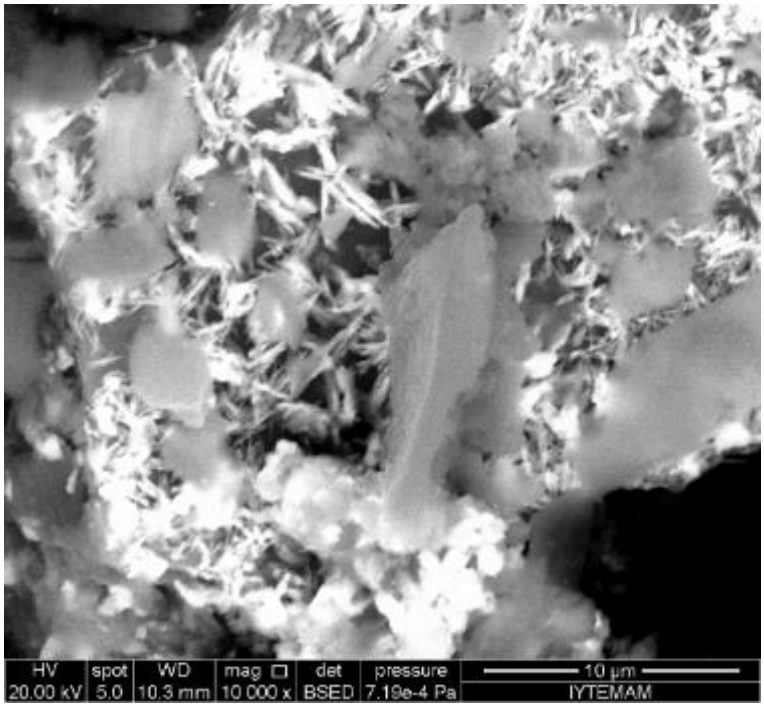

Figure 4. 38. SEM image of bindheimite crystals (10000x) in green glass tessera (G-Dgt2)

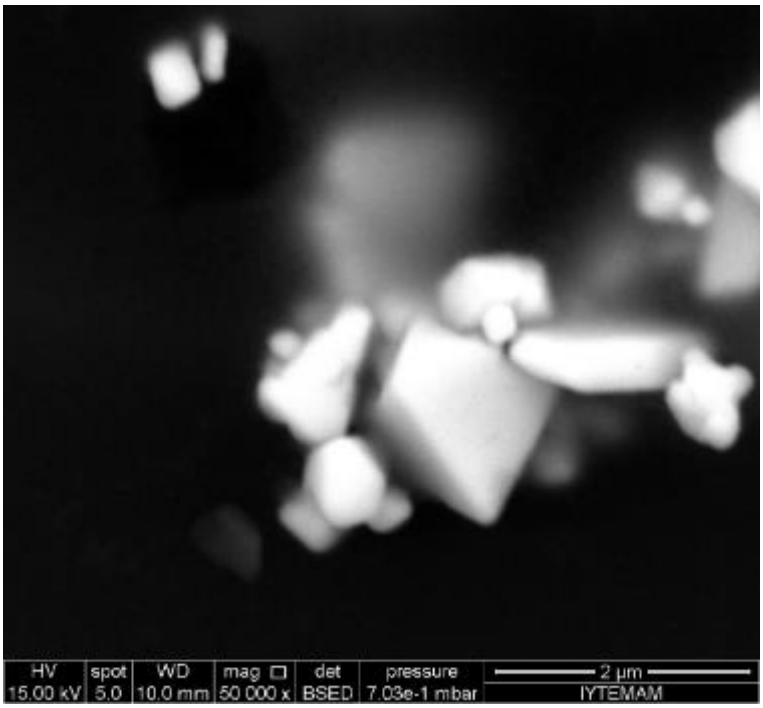

Figure 4. 39. SEM image of bindheimite crystals (50000x) in green tessera (G-Gt2)

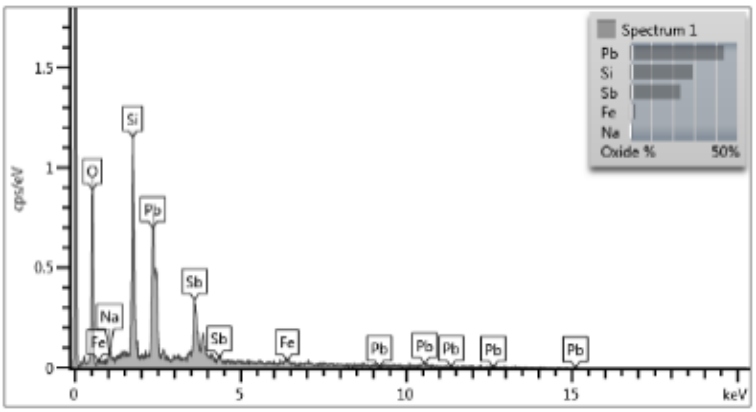

Sp1-Oxide	Sb_2O_3	SiO_2	Na_2O	FeO	PbO	
%	23.53	29.13	1.05	2.52	43.77	100.00

Figure 4. 40. EDS spectrum of green tessera (G-Dgt2)

Microstructural analysis of green tesserae indicated that they had spongy texture with air bubbles and micro cracks on the glass surface and in the air bubbles (Figure 4. 41). The spongy texture with air bubbles and micro cracks occurred due to low melting

temperatures of glass and deterioration process of mosaics during burial and after excavation.

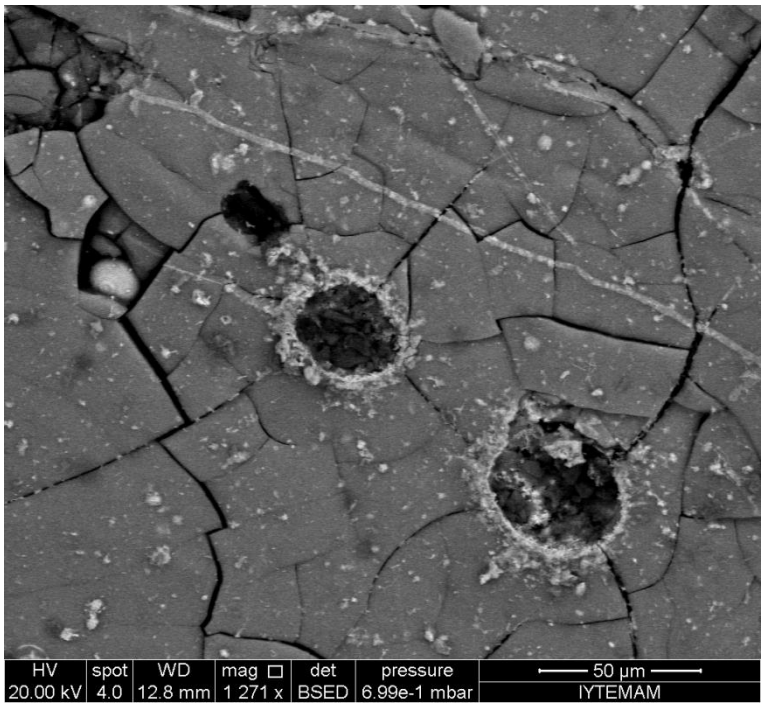

Figure 4. 41. SEM image of air bubbles and micro cracks in the surface of green glass tessera (G-Gt2)

Differently all tones of green tesserae, dark one (G-Dgt1) contains high amounts of ZnO (0.38 wt %). The ratio of PbO/ZnO in the composition of dark green tessera was lower than the other green ones (Table 4. 16.). This shows that dark green tesserae produced by the use of lead-zinc ore (galena). (Shugar 2000, Henderson 2000, Mirti et. al. 2002, Shortland 2002, Rehren 2003, Werf et. al. 2009).

Basic chemical compositions of green tesserae with different hues were close to yellow tessera. However, they had lower PbO and higher CuO (0.88-2.65 wt %) that added as chromophore (Werf et. al. 2009, Croveri et. al. 2010). The SiO_2/CuO ratios might explain the color hues of the green tessera (Table 4. 16). As it is seen in Table 4. 16, SiO_2/CuO ratios were lower than yellow and light green tesserae. This indicated that CuO were used as chromophore in green tesserae.

It can be suggested that the source of CuO might be tin bronze (Brill and Cahill 1988, Shortland and Tite 2000, Mirti et. al. 2001, 2002, Werf et. al. 2009).

Table 4. 16. Differences of PbO/ZnO% and SiO_2/CuO% values of green and yellow tesserae

	PbO/ZnO%	**SiO_2/CuO%**
Dark Green (G-Dgt1)	17.39	25.01
Light Green (G-Lgt)	755.33	63.69
Green (G-Gt1)	631.67	24.42
Green (G-Gt2)	582.67	34.88
Dark Green (G-Dgt2)	406.75	33.77
Yellow (G-Yt)	643.67	120.78

4.7.3.3. White Glasses

XRF analysis results indicated that white tessera contained high amounts of SiO_2 (76.21 wt %) and low amounts of PbO and Sb_2O_5 compared to yellow and green tesserae. This suggested that they were soda lime silica glasses and opacified with Ca-antimony as indicated by XRD analysis (Figure 4. 42, Table 4. 13).

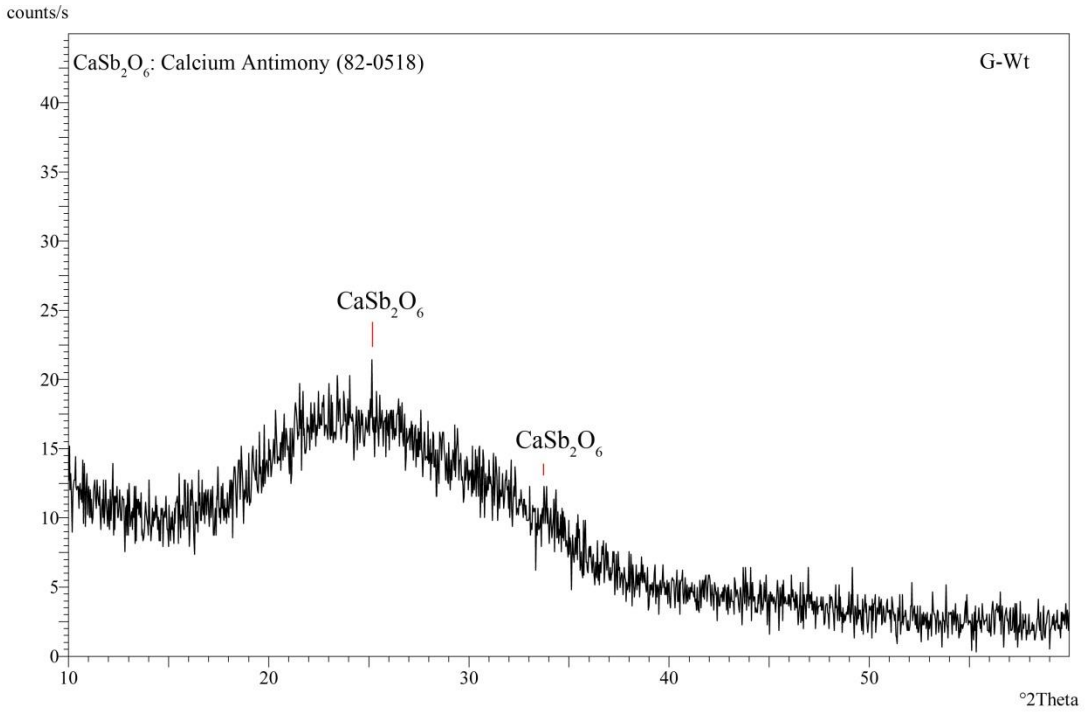

Figure 4. 42. XRD pattern of white glass tesserae

Ca-antimony crystals were less densely and homogenously dispersed in the glass matrix (Figure 4. 43) compared to the other opaque glasses. The sizes of crystals varied between 0.2 μm - 1 μm and they had amorphous shapes (Figure 4. 44). They contained high amounts Sb_2O_3 and CaO (Figure 4. 45).

The presence of amorphous crystals in the glassy matrix indicated that glass was manufactured by adding stibnite (Sb_2O_5) to the raw materials of the glass to obtain an opaque glass (in situ) (Mass et. al. 1997, Shortland 2002, Lahlil et. al. 2010a, Schibille et. al. 2012). The absence of transition elements in their compositions made the tesserae white.

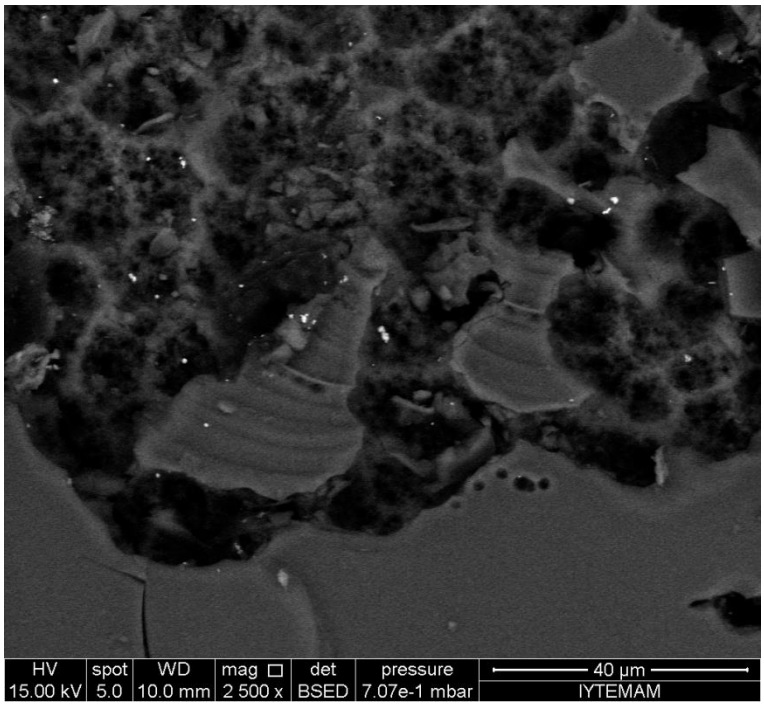

Figure 4. 43. SEM image of Ca-antimonate crystals (2500x) in white glass tessera (G-Wt)

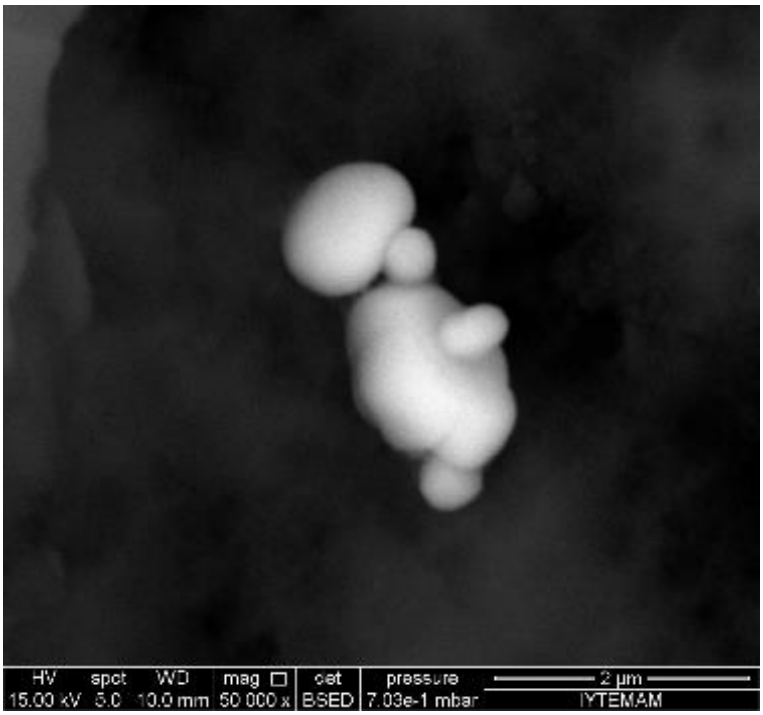

Figure 4. 44. SEM image of Ca-antimonate crystals (50000x) in white glass tessera (G-Wt)

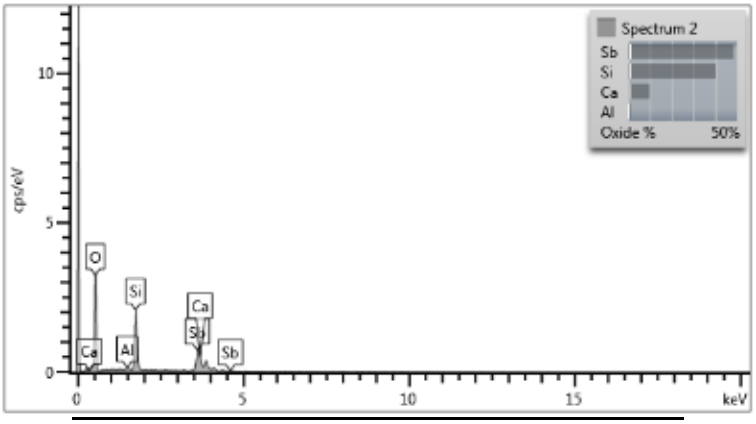

Sp2-Oxide	Sb_2O_3	SiO_2	Al_2O_3	CaO	
%	48.31	40.33	1.41	9.95	100.00

Figure 4. 45. EDS spectrum of Ca-antimonate crystals in white glass tessera (G-Wt)

Microstructural analysis of white tesserae indicated that they had semi-porous structure composed of micro cracks and pitting on their surface (Figure 4. 46). White tesserae were less deteriorated than other opaque glass tesserae since they had less air bubbles in its glassy matrix.

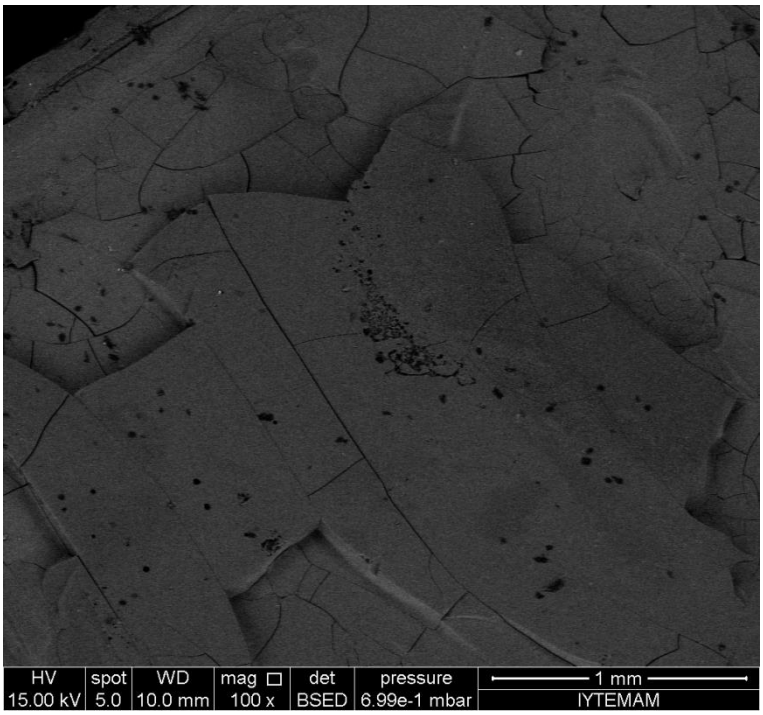

Figure 4. 46. SEM image of micro cracks on the surface of white glass tessera (G-Wt)

4.7.3.4. Turquoise Glasses

XRF analysis results indicated that turquoise tesserae contained high amounts of SiO_2 and Sb_2O_5 and low amounts of PbO revealed that they were soda lime silica glasses and opacified with Ca-antimony that was indicated by XRD analysis (Figure 4. 47, Table 4. 13).

In SEM analysis of light, turquoise and dark turquoise tesserae (G-Tt2, G-Tt1 and G-Dtt), Ca-antimony crystals were densely and homogenously dispersed to the glassy matrix (Figure 4. 48). The size of crystals varied between 0.1 μm – 0.4 μm crystals had well defined edges and angles (euhedral) (Figure 4. 49). They contained high amounts of Sb_2O_3 and CaO (Figure 4. 50).

The presence of euhedral crystals in the glass compositions indicated that Ca-antimony crystals were glass was manufactured with ex situ crystallization.

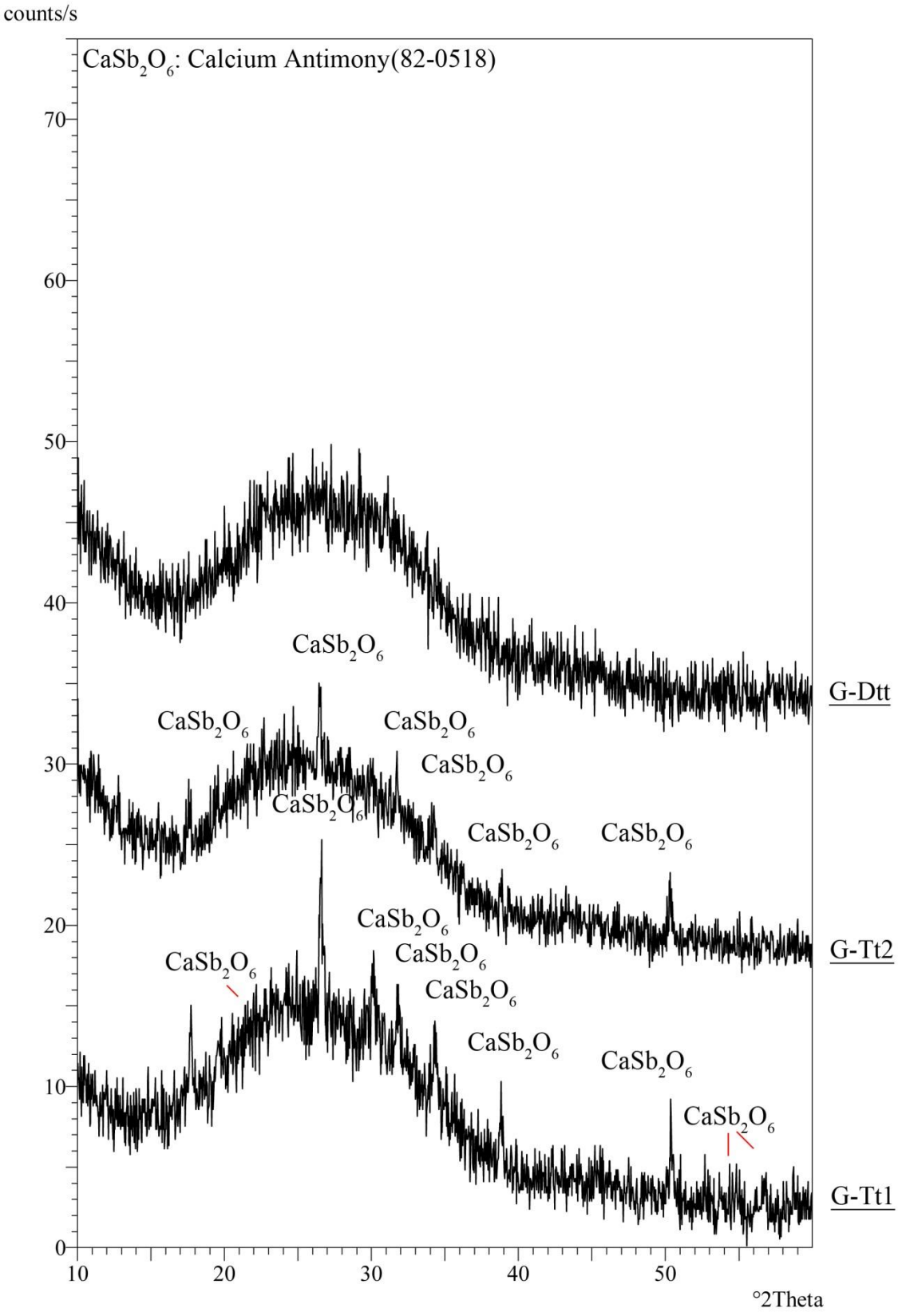

Figure 4. 47. XRD pattern of turquoise glass tesserae

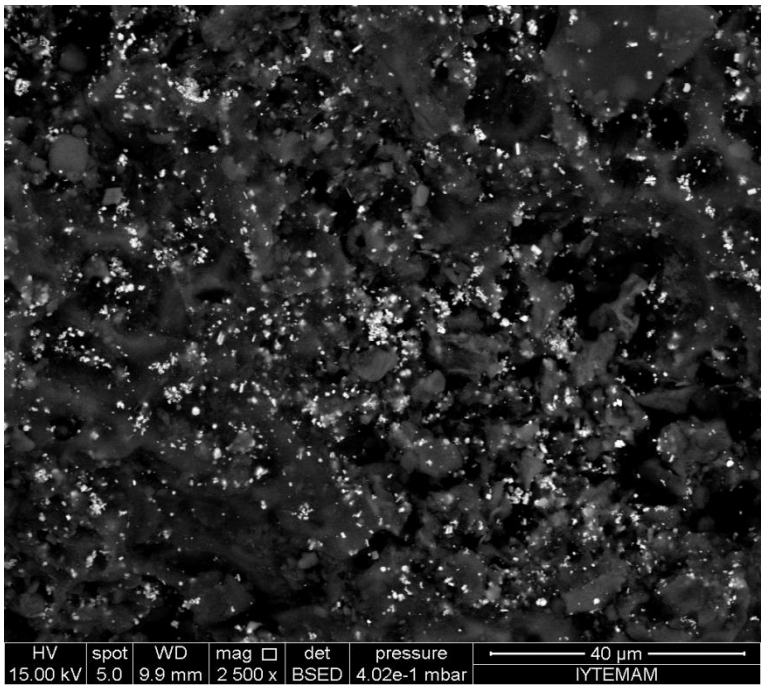

Figure 4. 48. SEM image Ca-antimonate crystals (2500x) in turquoise glass tessera (G-Tt2)

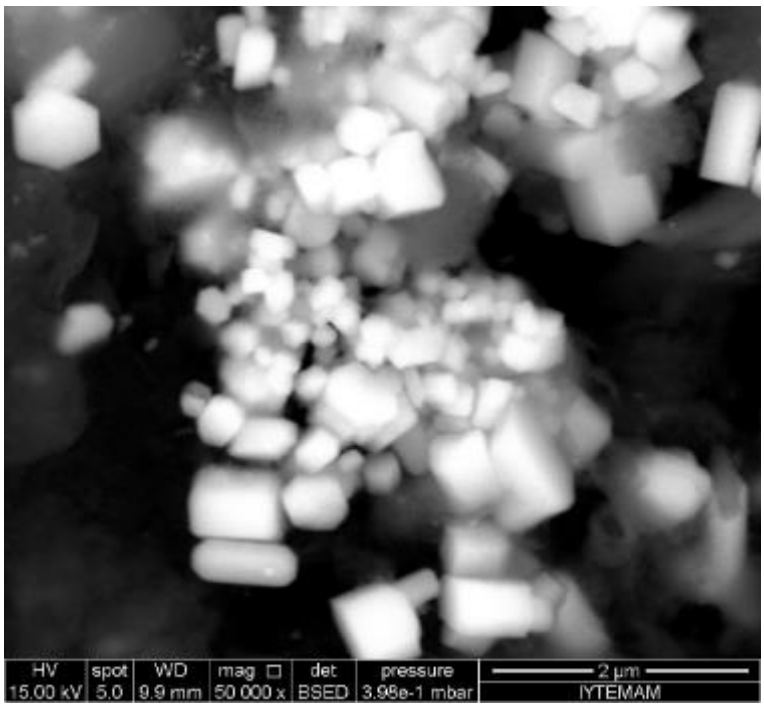

Figure 4. 49. SEM image of Ca-antimony crystals (50000x) in turquoise glass tesserae (G-Tt2)

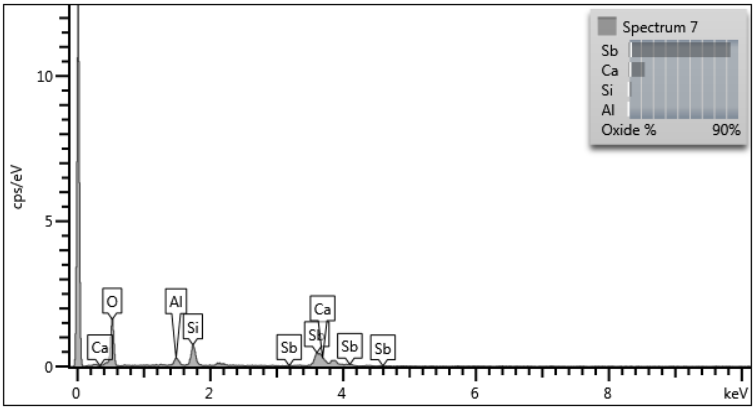

Sp7-Oxide	Al_2O_3	SiO_2	CaO	Sb_2O_3	
%	0.59	2.36	13.44	83.61	100.00

Figure 4. 50. EDS spectrum of Ca-antimony crystals in dark turquoise tesserae (G-Dtt)

Microstructural analysis of turquoise tesserae indicated a spongy microstructure with air bubbles and micro cracks on the surface of the glass (Figure 4. 51).

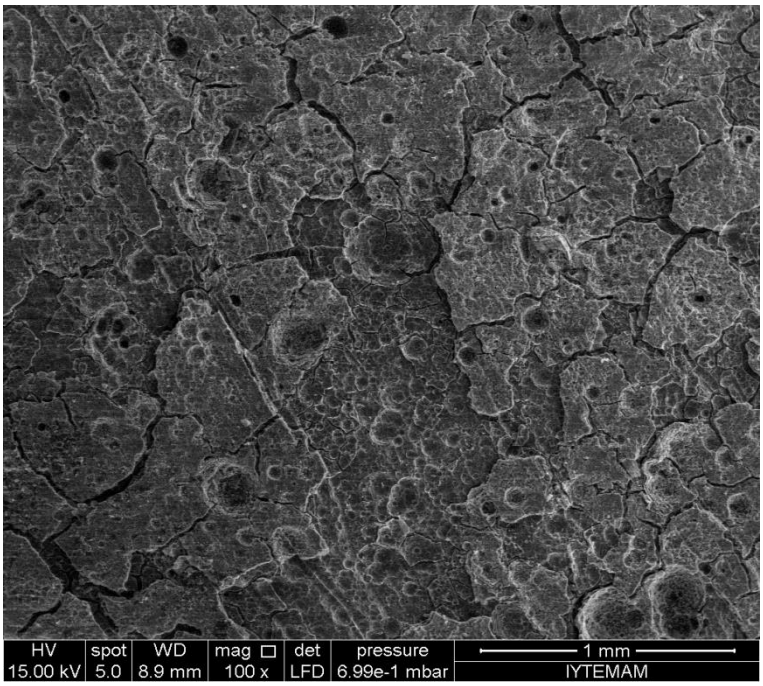

Figure 4. 51. SEM image of Ca-antimony crystals (100x) in turquoise glass tessera (G-Tt2)

In previous studies CuO was found to be a colorant for turquoise tesserae. In XRF analysis of turquoise tesserae, high amounts of CuO determined. It was suggested that CuO was responsible for turquoise color. High amounts of CuO indicated that turquoise tesserae were colored with copper. As seen in Table 4. 17 the SnO_2/CuO ratios of turquoise tesserae were high and their ratios are nearly the same, suggesting that the use of tin bronze for the source of copper as chromophore (Werf et. al. 2009). The dark tone of the turquoise tessera (G-Dtt) originated from different tin bronze source that contains high amounts of SnO_2 compared to the other turquoise glass tesserae. Tin oxide crystals that were determined in dark turquoise tesserae with SEM-EDS analysis supporting the bronze source contained high amounts of tin oxide that were responsible for the color of the tesserae.

Table 4. 17. CuO% and SnO_2% values and their ratios of turquoise tesserae

	CuO%	**SnO_2%**	**SnO_2/CuO**
G-Tt1	3.25	0.39	0.12
G-Tt2	0.74	0.09	0.12
G-Dtt	2.56	0.44	0.17

4.7.3.5. Blue Glasses

XRF analysis indicated that blue tesserae contained high amounts of SiO_2 and Sb_2O_5 and low amounts of PbO implied that they were soda lime silica glasses and opacified with Ca-antimony except light blue sample (G-Lbt1). Ca- antimonate crystals were observed by XRD analysis in all blue samples (Figure 4. 52, Table 4. 13).

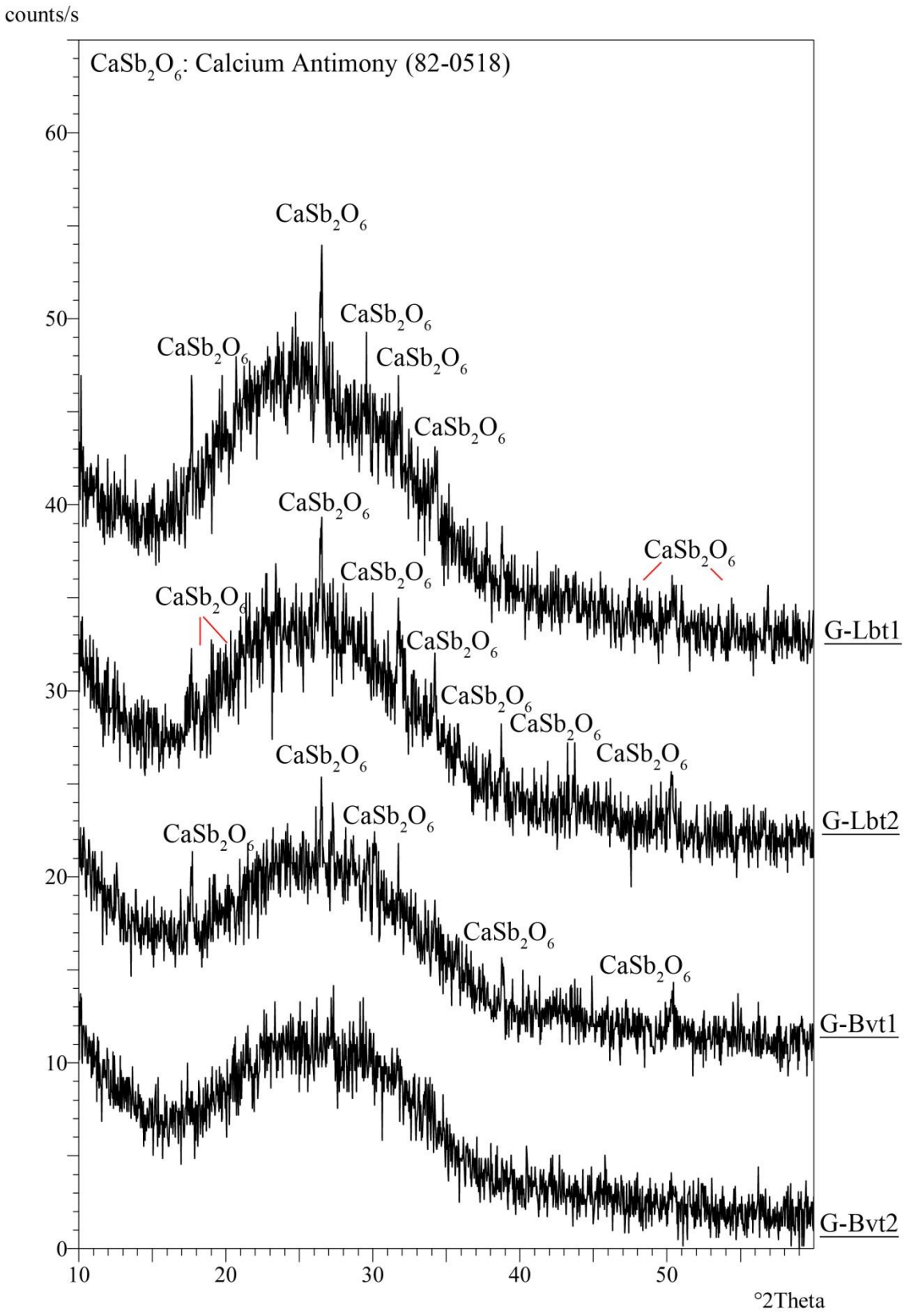

Figure 4. 52. XRD patterns of blue glass tesserae

In SEM analysis of light blue tesserae (G-Lbt2), Ca-antimony crystals were densely and homogenously dispersed in the glassy matrix (Figure 4. 53) whereas in semi opaque blue tesserae crystals were less densely dispersed. The sizes of crystals varied between 0.1 μm-0.5 μm. They had well defined edges and angles (euhedral) both in light blue and semi opaque blue tesserae (Figure 4. 54, Figure 4. 55). Ca-antimony crystals contained high amounts of Sb_2O_3 and CaO (Figure 4. 56).

The presence of euhedral crystals in the glass compositions indicated that glass was manufactured with ex situ crystallization.

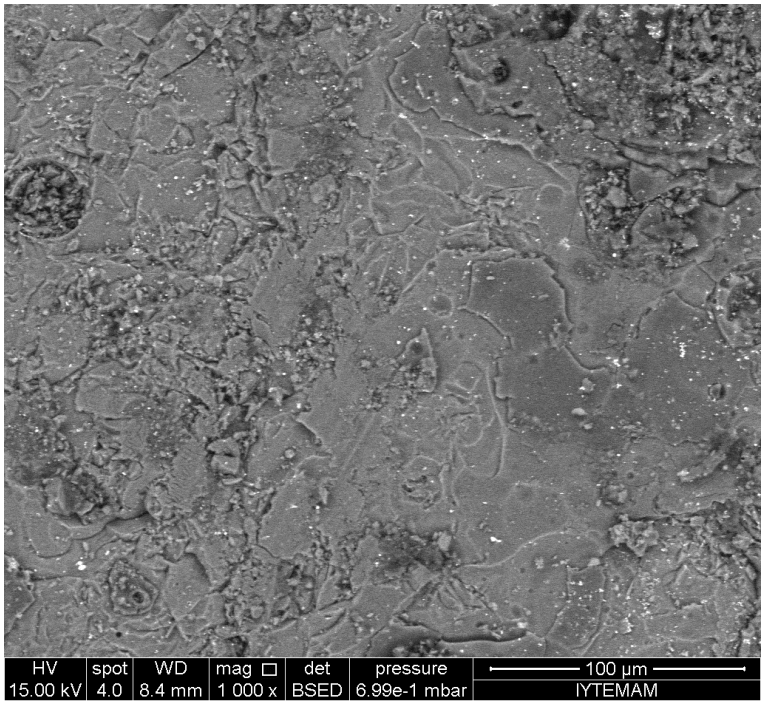

Figure 4. 53. SEM images of Ca-antimony crystals (1000x) in light blue tesserae (G-Lbt2)

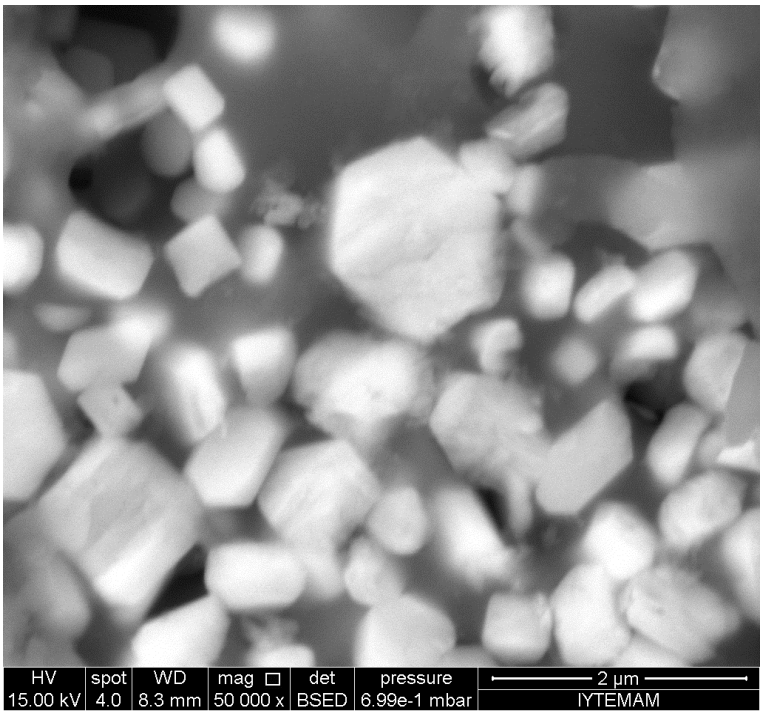

Figure 4. 54. SEM image of Ca-antimony crystals (50000x) in light blue tessera (G-Lbt2)

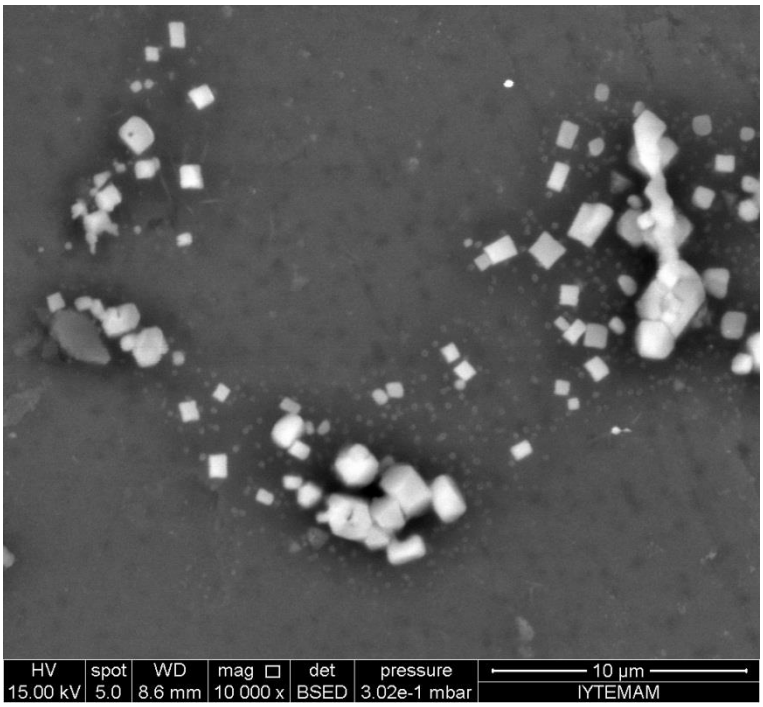

Figure 4. 55. SEM image of Ca-antimonate crystals (10000x) in semi opaque glass tessera (G-Bvt2)

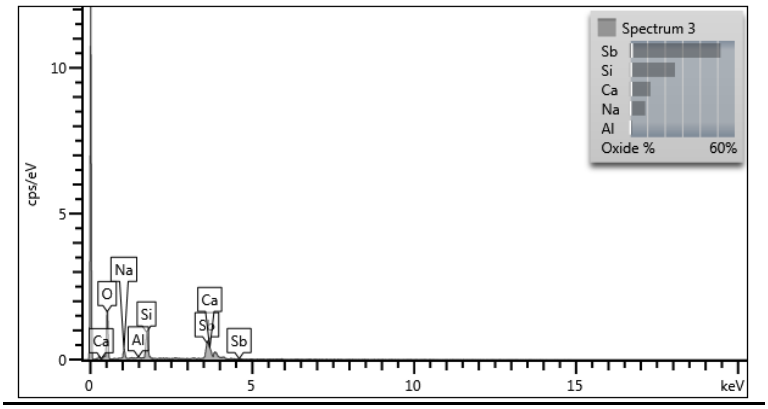

Sp3-Oxide	Al_2O_3	Na_2O	SiO_2	CaO	Sb_2O_3	
%	1.39	8.93	25.92	11.89	51.86	100.00

Figure 4. 56. EDS spectrum of Ca-antimonate crystals of blue glass tesserae (G-Lbt2)

Microstructural analyses of light blue and semi opaque blue tesserae indicated spongy texture with less air bubbles (Figure 4. 57). However, in semi opaque blue tesserae in addition air bubbles pitting were observed on the glass surface (Figure 4. 58). Therefore, it can be suggested that blue tessera were less deteriorated like white tesserae and less deteriorated than other opaque glass tesserae since it had less air bubbles.

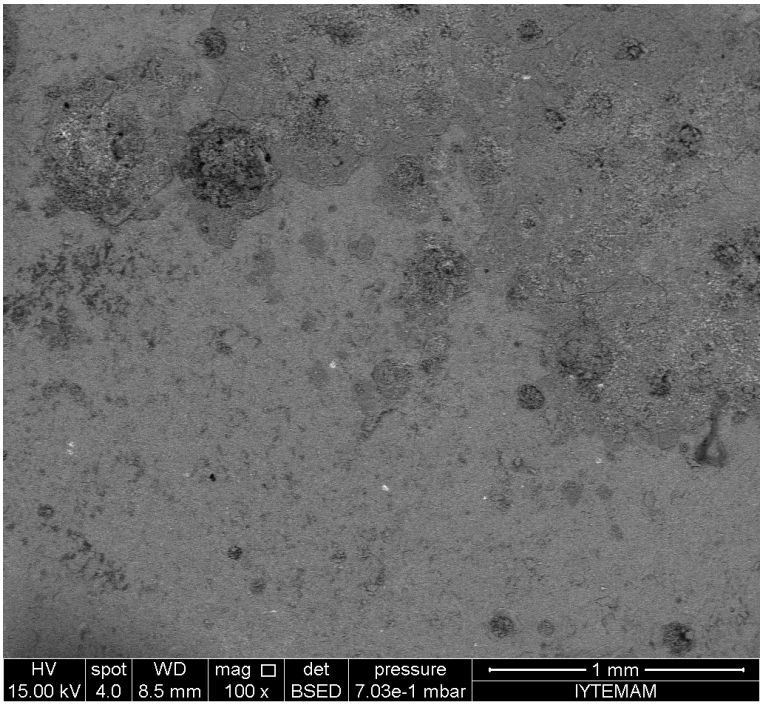

Figure 4. 57. SEM image of the surface of light blue tessera (G-Lbt2)

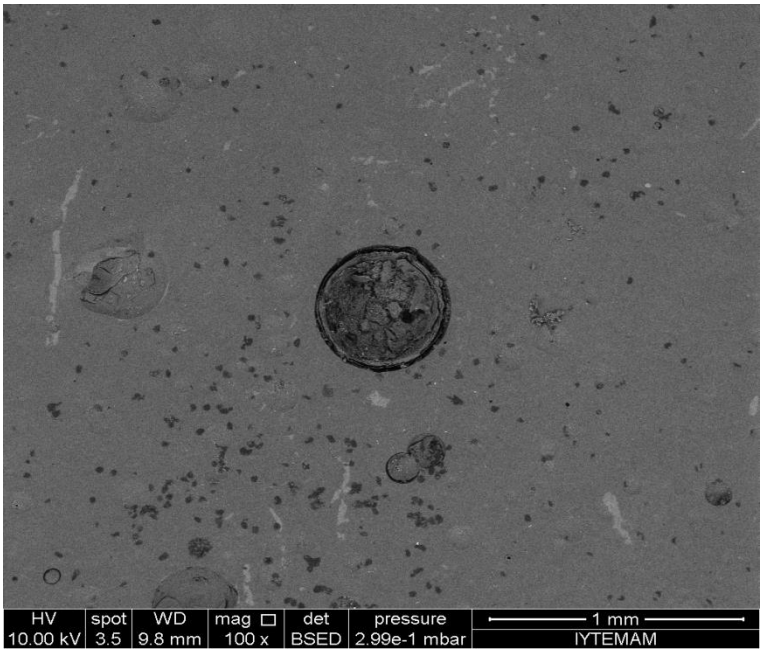

Figure 4. 58. SEM image of less spongy structure and air bubble in semi opaque blue glass tessera (G-Bvt2)

In previous studies, copper, cobalt and iron were determined as colorants in blue tesserae. The light blue tessera (Lbt2) colored with CoO (0.02 wt %) and Fe_2O_3 (0.42 wt %). In addition, light blue tesserae (G-Lbt2) was decolorized with MnO (0.22 wt %) (Croveri et. al. 2010).

Other blue tesserae (G-Lbt1, G-Bvt1 and G-Bvt2) were colored with copper and iron oxides (Table 4. 18). In the production of light blue and blue tesserae (G-Lbt2, G-Bvt1) tin bronze source was used as chromophore.

Table 4. 18. CuO% and SnO_2% values and their ratios of blue tesserae

	CuO%	**SnO_2%**	**SnO_2/CuO**
G-Lbt1	_	_	_
G-Lbt2	0.07	0.03	2.33
G-Bvt1	0.16	0.02	8.00
G-Bvt2	0.10	_	_

4.7.3.6. Cyan Glasses

XRF analysis results indicated that cyan tesserae contained high amounts of SiO_2 and Sb_2O_5 and low amounts of PbO revealed that they were soda lime silica glasses and opacified with Ca-antimony that were indicated by XRD analysis (Figure 4. 59, Table 4. 13).

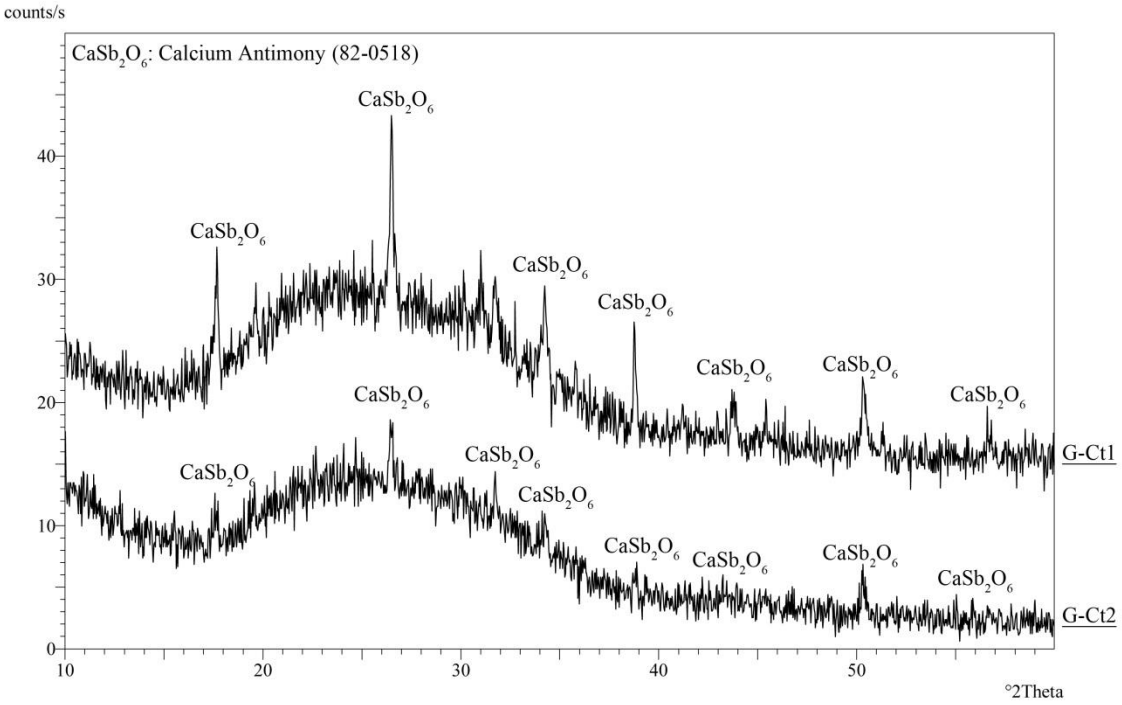

Figure 4. 59. XRD pattern of cyan glass tesserae

Ca- antimony crystals were densely and homogenously dispersed to the glassy matrix (Figure 4. 60). Their size varied between 0.1 μm – 0.6 μm. They had well defined edges and angles (euhedral) (Figure 4. 61). Ca-antimony crystals contained high amounts of Sb_2O_3 and CaO. The presence of euhedral crystals indicated that they were manufactured ex situ crystallization.

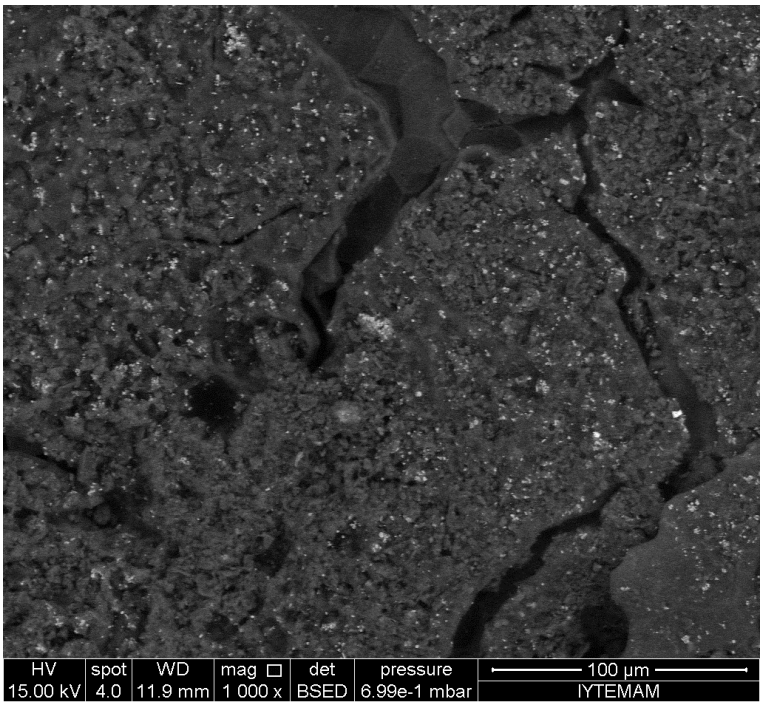

Figure 4. 60. SEM image of Ca-antimony crystals (1000x) in cyan glass tessera (G-Ct2)

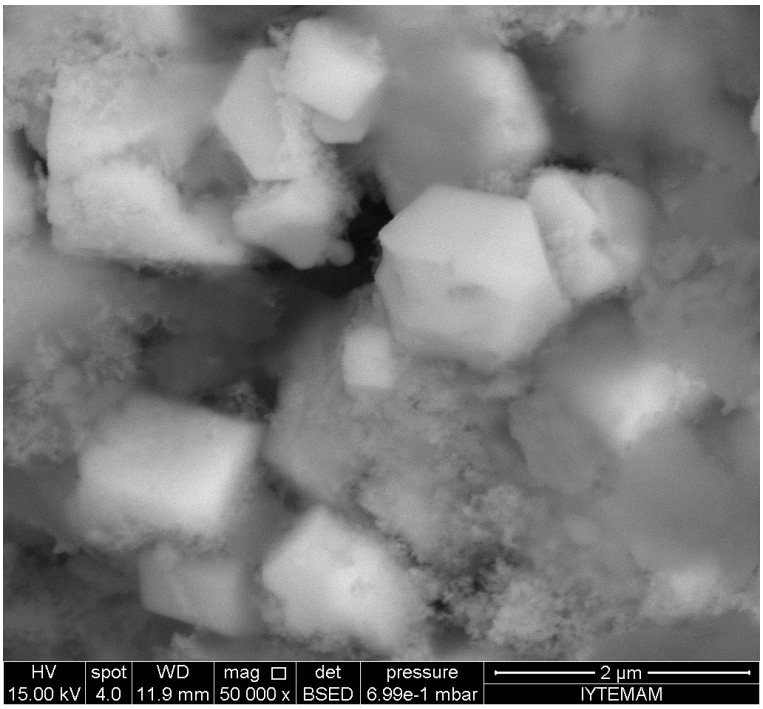

Figure 4. 61. SEM image of Ca-antimonate crystals (50000x) in cyan glass tessera (G-Ct2)

Microstructural analysis of cyan tesserae indicated have spongy texture with air bubbles and micro cracks on the glass surface (Figure 4. 62). The spongy microstructure with air bubbles and micro cracks can be explained by low melting temperatures in the glass manufacture and deterioration process during burial and after excavation of mosaics.

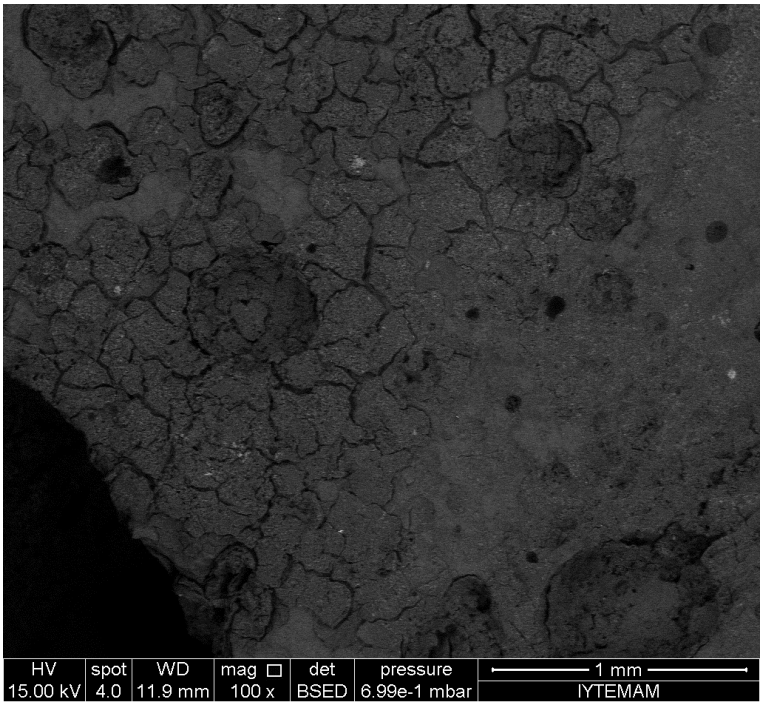

Figure 4. 62. SEM image of spongy structure and micro cracks of cyan glass tessera (G-Ct2)

The greenish colors of the tesserae were derived from copper. Tin bronze was used for the source of copper as chromophore.

Table 4. 19. CuO% and SnO_2% values and their ratios of cyan tesserae

	CuO%	**SnO_2%**	**SnO_2/CuO**
G-Ct1	0.35	0.07	5.00
G-Ct2	0.30	0.07	4.29

4.7.3.7. Black Glasses

XRF analysis results indicated that black tessera contained high amounts of SiO_2 but did not contain PbO and antimony revealed that they were soda lime silica glasses. The black tessera was opaque, although antimony was not observed in XRF analysis and also XRD analysis (Figure 4. 63, Table 4. 13). The opacity of the black tessera might be obtained by low temperature of the furnace that could not reach the melting point of the glass.

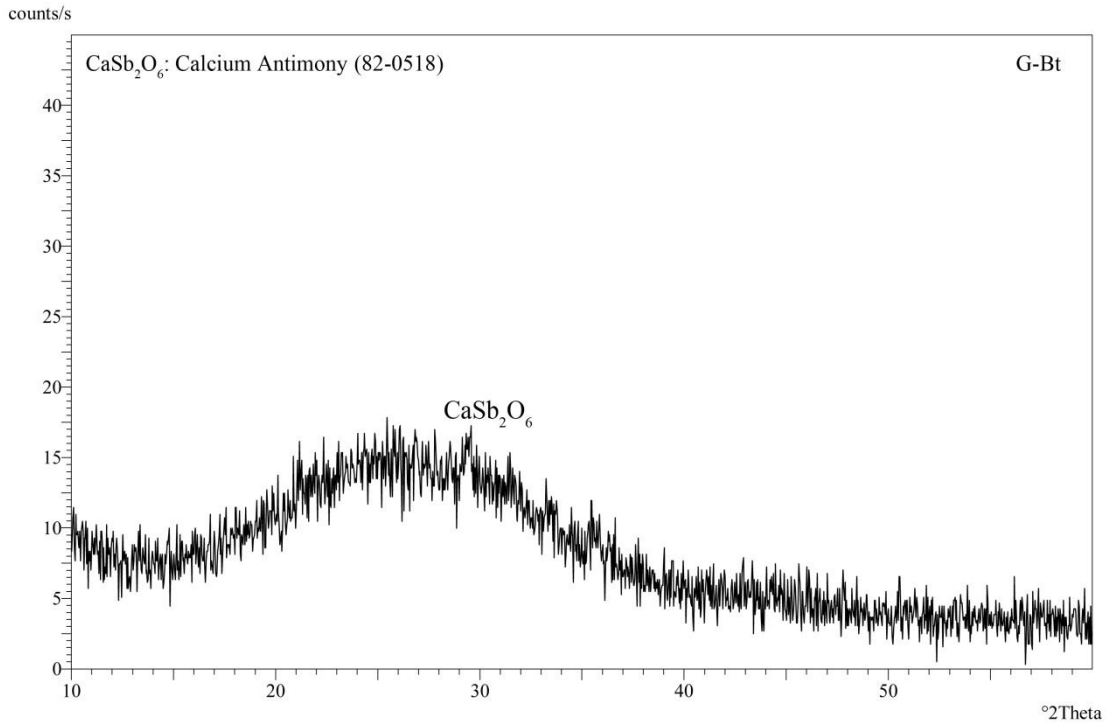

Figure 4. 63. XRD pattern of black tessera

Microstructural analysis of black tessera indicated that it had porous structure with the air bubbles and micro cracks on the surface of the glass (Figure 4. 64). The spongy structure with air bubbles and micro cracks were produced due to low melting temperature of glass and deterioration process of mosaic.

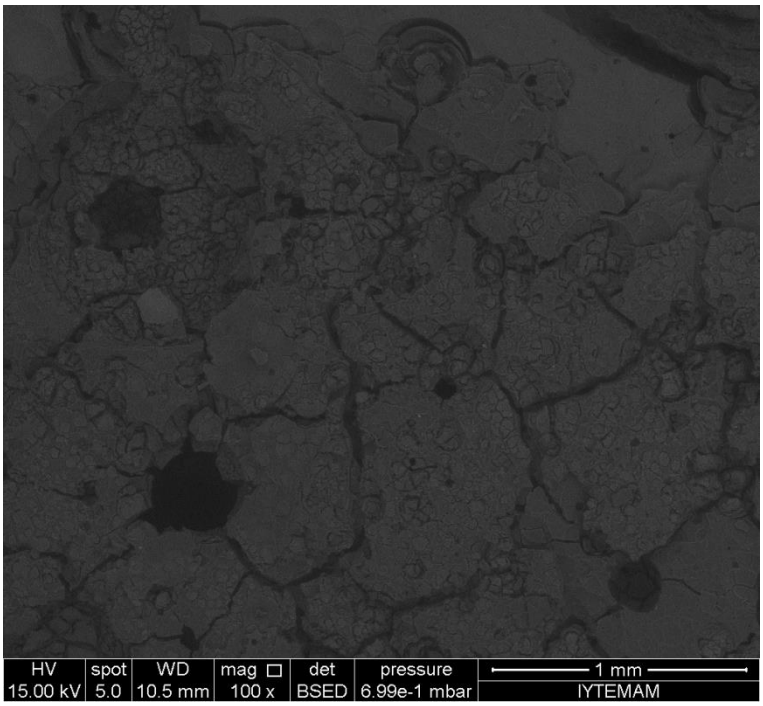

Figure 4. 64. SEM image of spongy microstructure with air bubbles in black tessera

Black tessera contained significant amounts of iron oxide (5.61 wt %) compared to the other glasses, suggesting iron oxide was intentionally added to obtain black color of the tessera as chromophore (Arletti et. al. 2011).

4.7.3.8. Brown Glasses

XRF analysis results indicated that light brown tessera contain high amounts of SiO_2 and low amounts of PbO and Sb_2O_5 revealed that they were soda lime silica glasses and opacified with Ca-antimony (Figure 4. 65, Table 4. 13).

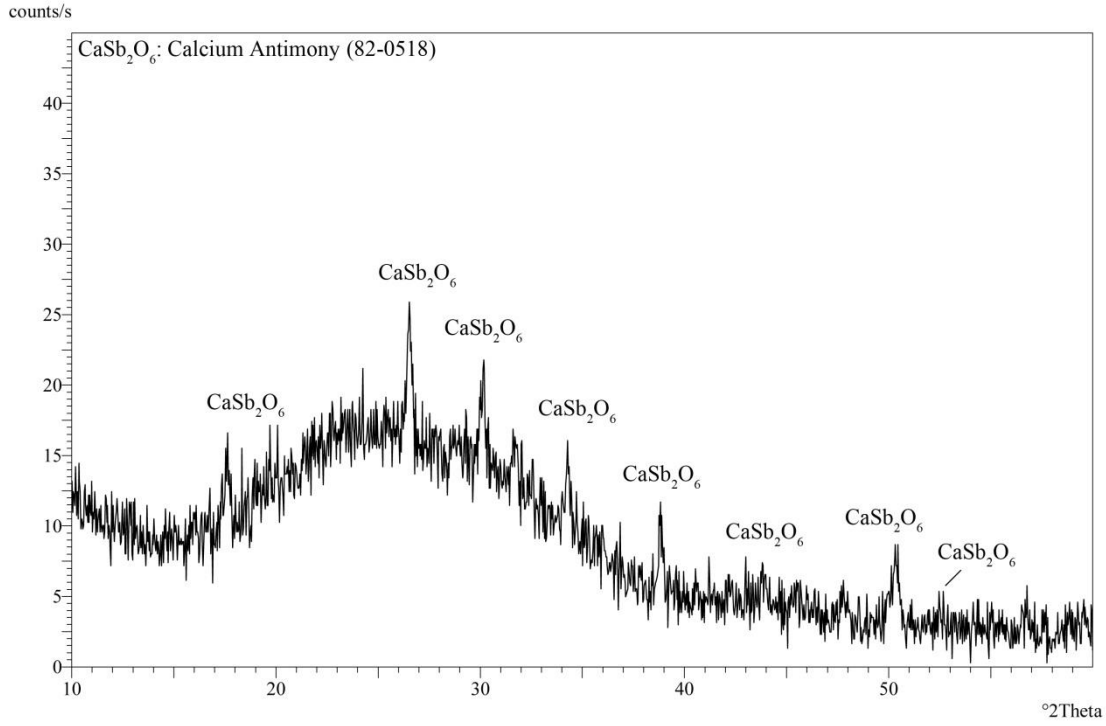

Figure 4. 65. XRD pattern of light brown glass

MnO was used as chromophore determined in previous studies. High amounts of MnO in the composition of the brown tessera indicated that MnO was used as chromophore.

4.7.3.9. Dark Red Glasses

XRF analysis results indicated that dark red tesserae contained high amounts of SiO_2 and low amounts of PbO and Sb_2O_5 revealed that they were soda lime leaded glasses.

In XRF analysis of red glass tessera high amounts of CuO (1.07 wt %) with FeO oxide (3.81 wt %) and PbO (2 wt %) were determined. The dark red tessera colored and opacified due to the presence of metallic copper which was reduced by high levels of iron oxide that added to the batch and precipitates in the form of metallic copper (Ahmed and Ashour 1981, Brill and Cahill 1988, Brun et. al. 1991, Mirti et. al. 2002, Arletti et. al. 2006a, b, Santagostino Barbone et. al. 2008).

Similar results were indicated by XRD analysis and previous studies (Figure 4. 66, Table 4. 13) (Brill and Cahill 1988, Barber et. al. 2009, Werf et. al. 2009, Arletti et. al. 2011, Schibille et. al. 2012). In previous studies typical Roman red glass tesserae can be obtained by using low amount of lead, copper and iron (% PbO=2.63, $\%CuO_2$=1.2, $\%Fe_2O_3$=2) (Croveri et. al. 2009).

In SEM analysis, densely and homogenously dispersed iron oxide crystals were observed to the glassy matrix (Figure 4. 67). They were anhedral (Figure 4. 68). In addition to iron oxide crystals, tin oxide (Figure 4. 70) and Ca-antimony crystals (Figure 4. 71) were determined in dark red tesserae.

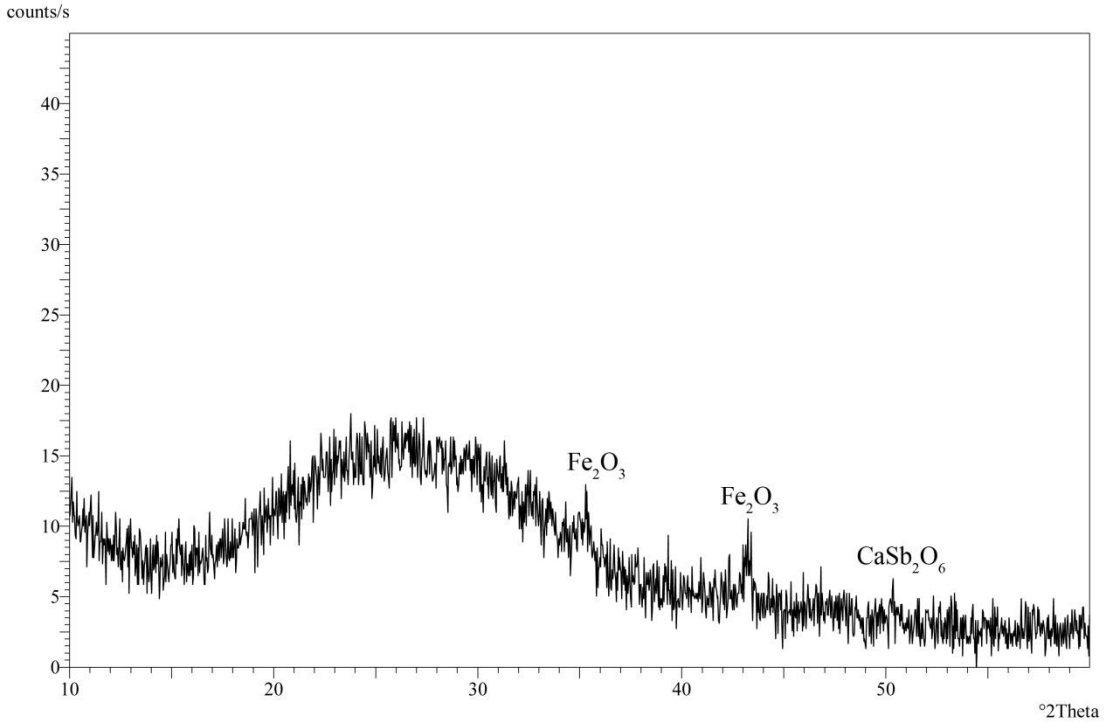

Figure 4. 66. XRD pattern of dark red glass tesserae

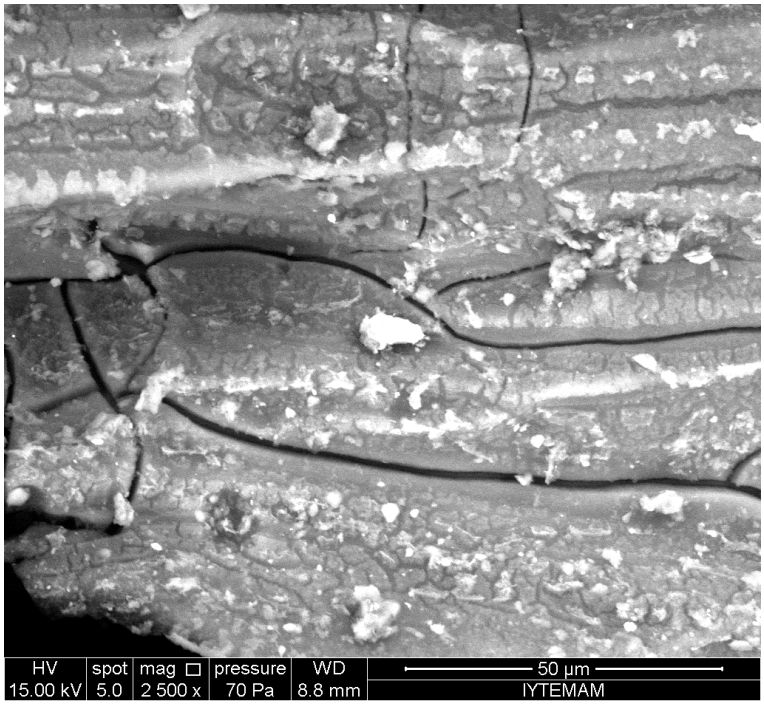

Figure 4. 67. SEM image of iron oxide crystals (2500x) in dark red glass tessera (G-Drt)

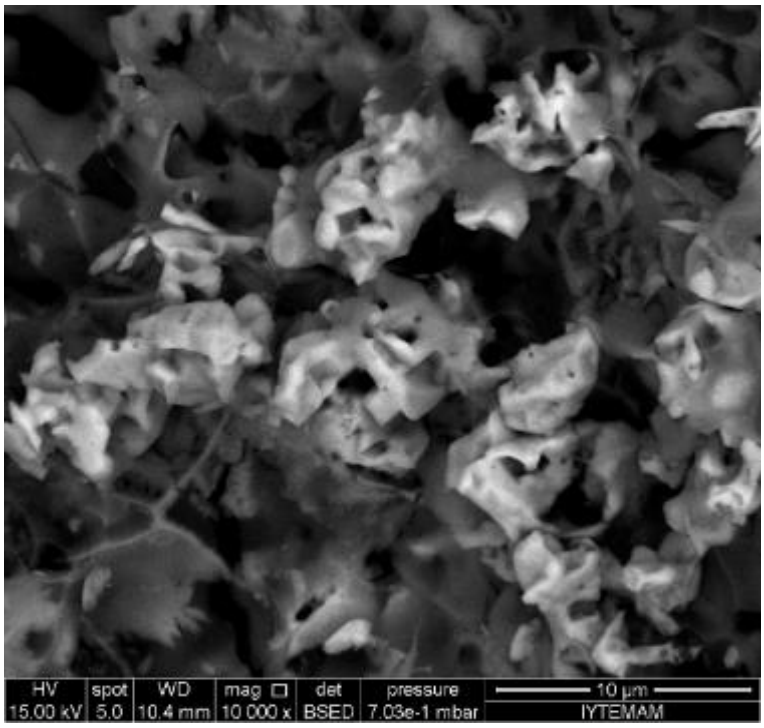

Figure 4. 68. SEM image of iron oxide crystals (10000x) in dark red glass tesserae (G-Drt)

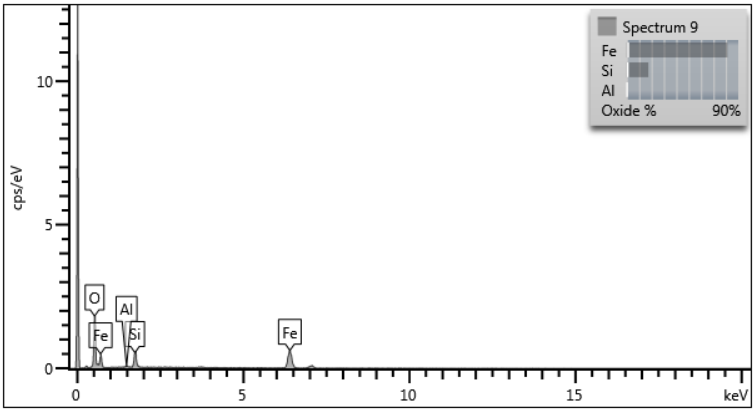

Sp9-Oxide	FeO	SiO_2	Al_2O_3
%	81.24	17.53	1.23

Figure 4. 69. EDS spectrum of iron oxide crystals in dark red tesserae

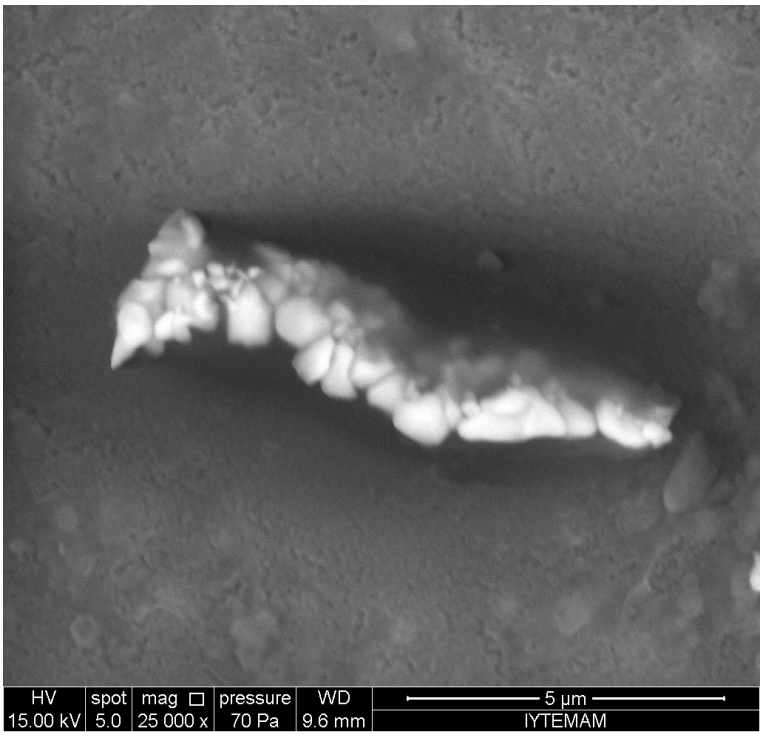

Figure 4. 70. SEM image of tin oxide crystals in dark red tesserae

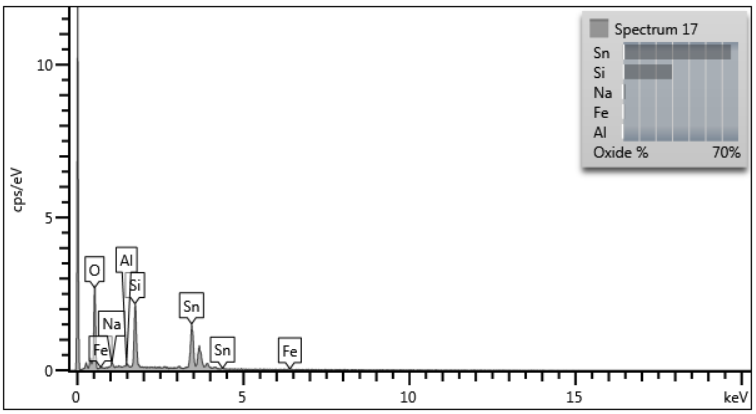

Sp17-Oxide	SnO_2	Al_2O_3	Na_2O	SiO_2	FeO	
%	65.53	1.04	1.94	29.98	1.50	100.00

Figure 4. 71. EDS spectrum of tin oxide crystals in dark red glass tesserae (G-Drt)

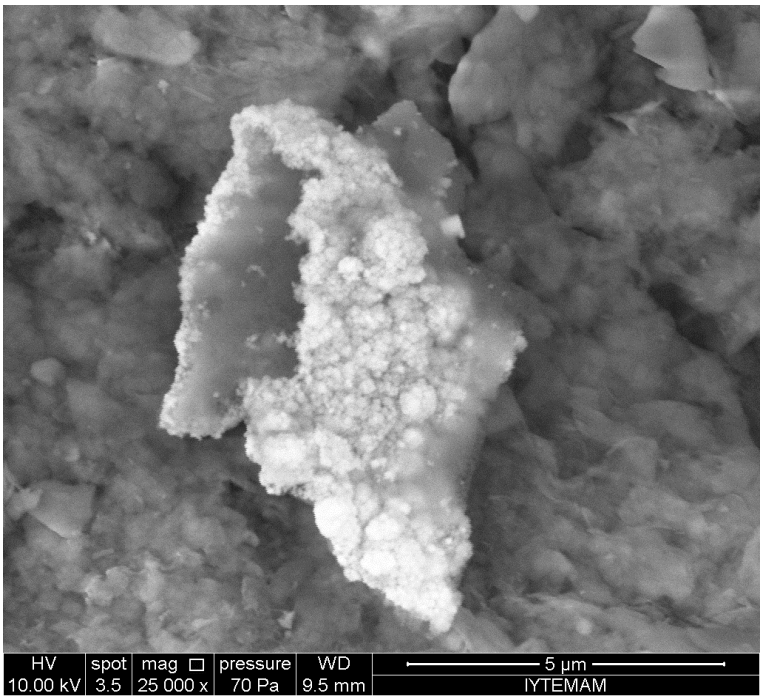

Figure 4. 72. SEM image of Ca-antimony crystal in dark red tesserae

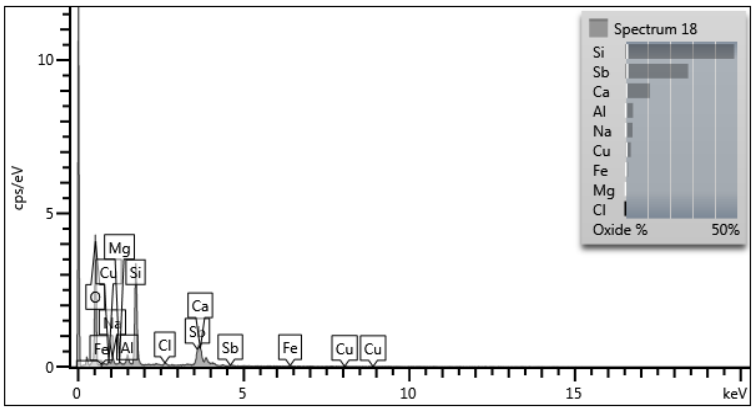

Sp18-Oxide	Sb_2O_3	CaO	CuO	Al_2O_3	Na_2O	SiO_2	FeO	MgO	
%	28.08	11.00	2.56	3.54	3.32	48.57	1.28	0.79	100.00

Figure 4. 73. EDS spectrum of Ca-antimony crystals in dark red glass tessera (G-Drt)

Microstructural analysis of dark red tessera indicated had a spongy structure due to air bubbles (Figure 4. 74) and micro cracks (Figure 4. 75) same as yellow and black glasses. However, in dark red tesserae whole glass was not deteriorated as seen in Figure 4. 88. The high porosity values of dark red tesserae can be explained by low

melting temperatures that could be reached at the ancient glass furnaces and deterioration process of glass.

Red tessera had different mineralogical and chemical compositions than the other colored tessera, similar with the ones analyzed in previous studies (Henderson 1991, Cable and Smedly 1987, Brill and Cahill 1988, Freestone 1987, 1990, 2003 a, b, Shugar 2000, Barber 2009, Werf et. al. 2009, Paytner and Kearns 2011, Schibille et. al. 2012).

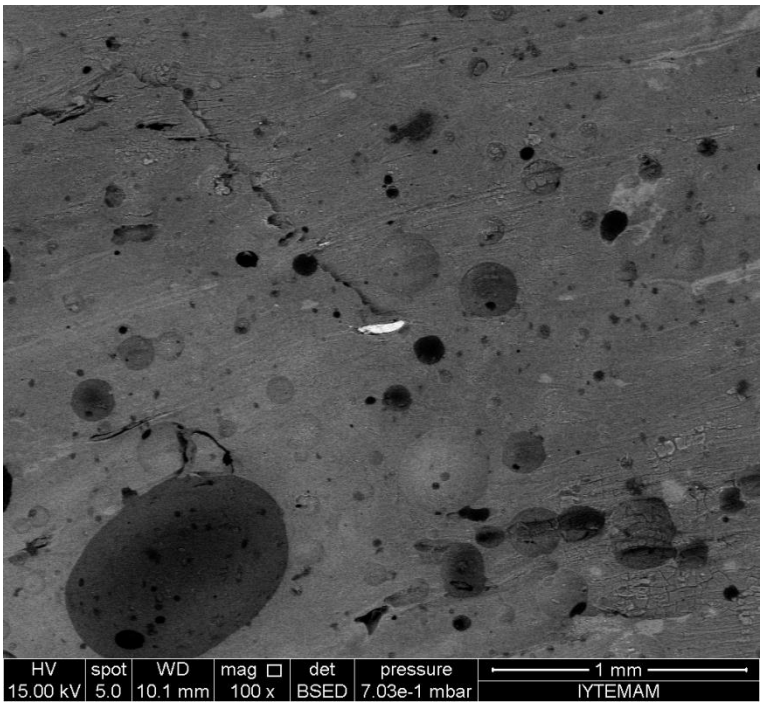

Figure 4. 74. SEM image of spongy structure of dark red glass tessera (G-Drt)

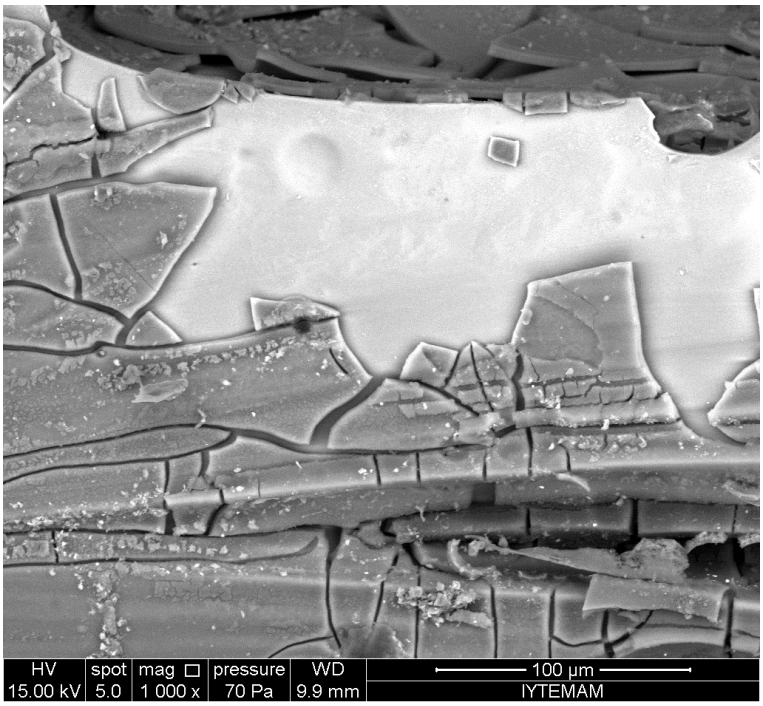

Figure 4. 75. SEM image of micro cracks on the surface of dark red glass tessera (G-Drt)

4.8. Deterioration Problems of Mosaics

Deterioration processes of the mosaics in archaeological sites takes place in inadequate or faulty drainage systems, settlement in the mosaic floors, changes in temperature and humidity, the presence of soluble salts, biological colonization, material characteristics of mosaics, presence of clay minerals and the use of incompatible materials in the cleaning, consolidation and the protection of mosaics.

The original surface water drainage systems of Antandros were demolished and new ones were not sufficient to keep water away from the site. However, mortars of the mosaics were not severely affected from water due to water-resistance properties of brick-lime mortars used in the rudus and nucleus layers of the mosaics (Uğurlu and Böke 2009).

In this study, soluble salt contents of the preparatory mortars and tesserae, type of deposits formed on the outer surfaces of tesserae and microstructure of outer and inner surfaces of tesserae were determined to estimate the deterioration processes of the mosaics.

Soluble salts of preparatory mortars and tesserae were determined with electrical conductivity measurements and spot analysis. The minor amounts of soluble salts less than % $5x10^{-3}$ were found in mortars and tesserae (Table 4. 20). Main ions such as NO_3^-, SO_4^{-2}, Cl^- and PO_4 ions were not detected in any of the soil or stone samples. These results showed that soluble salts were not effective for the deterioration of mosaics.

Table 4. 20. Soluble salt contents of preparatory mortars and tesserae

	Soluble Salts (%)
Glass	($9x10^{-4}$)
Stone	($3x10^{-4}$)
Bedding	($4x10^{-4}$)
Nucleus	($4x10^{-4}$)
Rudus	($4x10^{-4}$)

Mineralogical compositions of the deposit layers that form on the tesserae were mainly composed of calcite and clay minerals (Figure 4. 76).

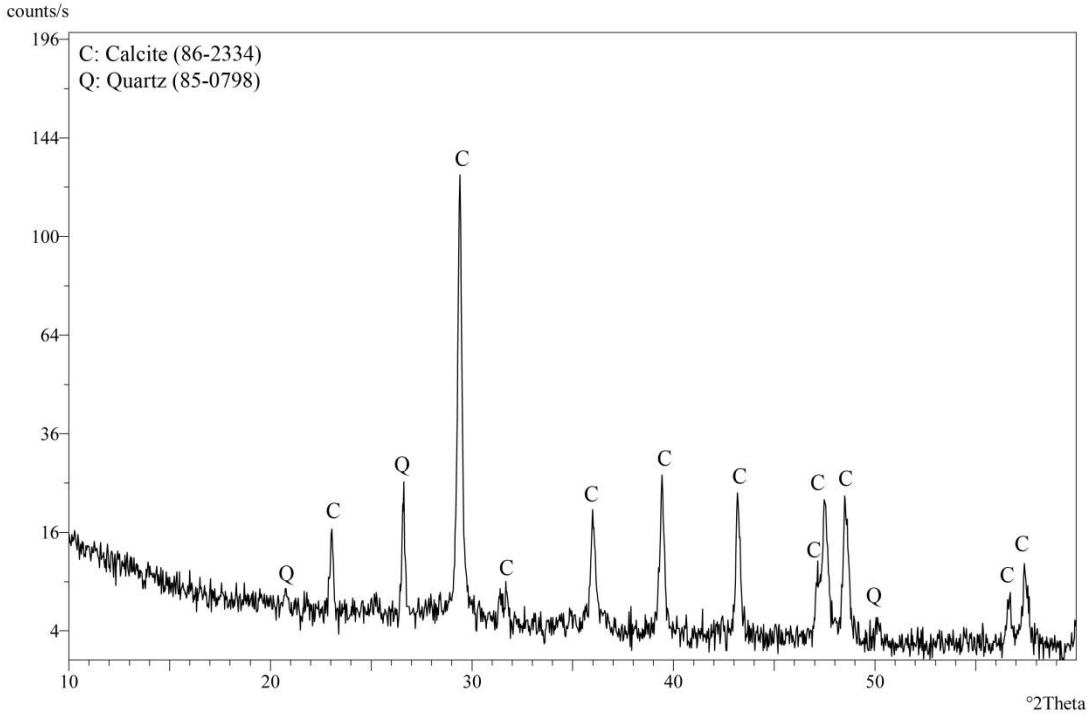

Figure 4. 76. XRD pattern of patina on mosaic surface

Calcite could be formed by the subsequent dissolution and precipitation of bedding mortars. Subsequent dissolution and precipitation process on the mosaics cause a lack of adhesion between the tesserae and bedding mortars. Clay minerals found in the deposits swell and shrink with wetting and drying processes that cause micro cracks, and pitting on the tesserae and promote the biological formations. The thickness of the layers varies from approximately 50 – 500 μm in the SEM-EDS analysis (Figure 4. 77-Figure 4. 79).

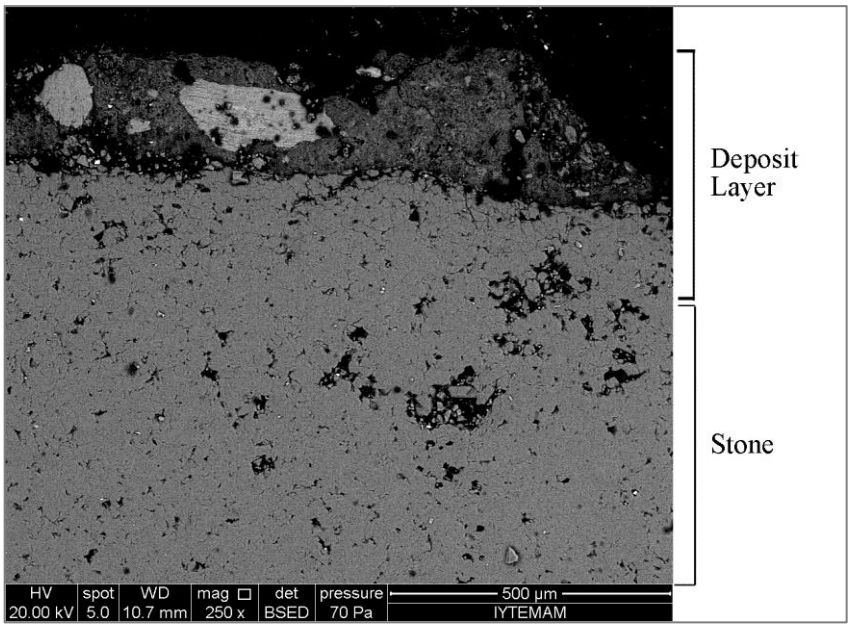

Figure 4. 77. SEM image of deposit layer of stone tesserae

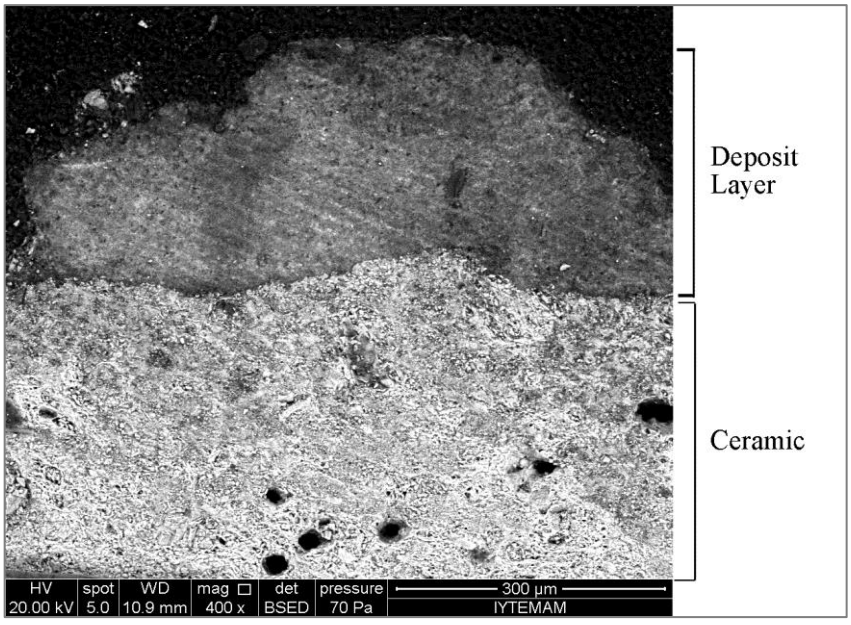

Figure 4. 78. SEM image of deposit layer of ceramic tessera

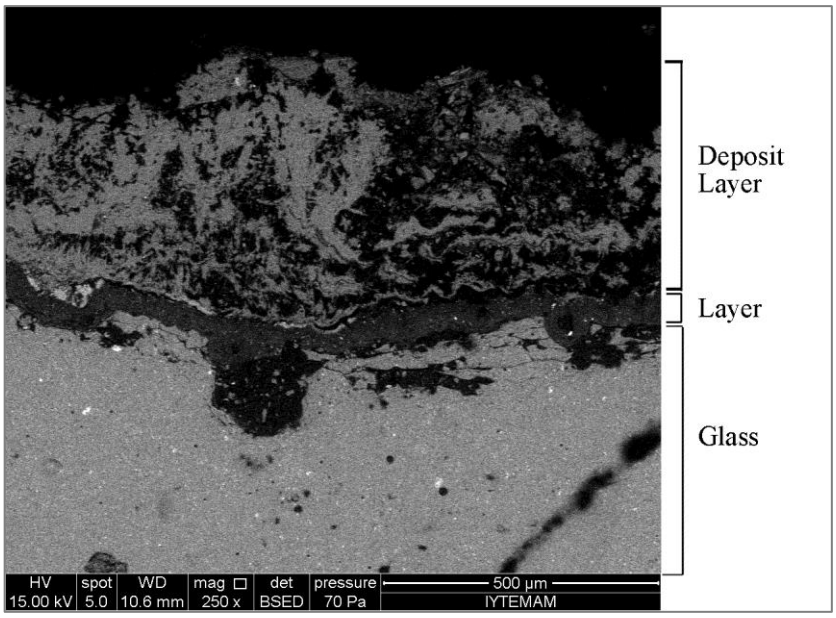

Figure 4. 79. SEM image of deposit layer of blue glass tessera

Microstructural analyses of all glass tesserae indicated a spongy texture with air bubbles (Figure 4. 80) and micro cracks on the surfaces (Figure 4. 81) of glass that could also be seen with the naked eye. The spongy microstructure with air bubbles and micro cracks observed on the glass surfaces can be explained by low melting temperature of glass and the leaching of glass components due to water penetrations.

The leaching of glass is governed by the reaction of hydronium ions in water ($H3O^+$) with the alkalis (leaching) (Reaction 4.1) in the compositions of glass during wetting–drying cycles (Palomar et. al. 2013). This can be called ion-exchange of the glass alkaline ions.

$$Si – O - M + H_3O^+ \rightarrow Si – O - H + M^+ + H_2O \quad (4.1)$$

$$M^+ = Na^+ \text{ or } K^+$$

The ion-exchange causes a thin layer near the glass surface which contains high amount of silica and low amount of sodium-ions. It is brittle and easily detached. Leaching causes corrosion, micro cracks and pittings (Figure 4. 82) on the surface of the glass tesserae. Micro cracks allow water to penetrate inside the tesserae. These processes can increase the propagation of micro-cracks, blistering (Figure 4. 83) and cause biological colonization in detached surfaces.

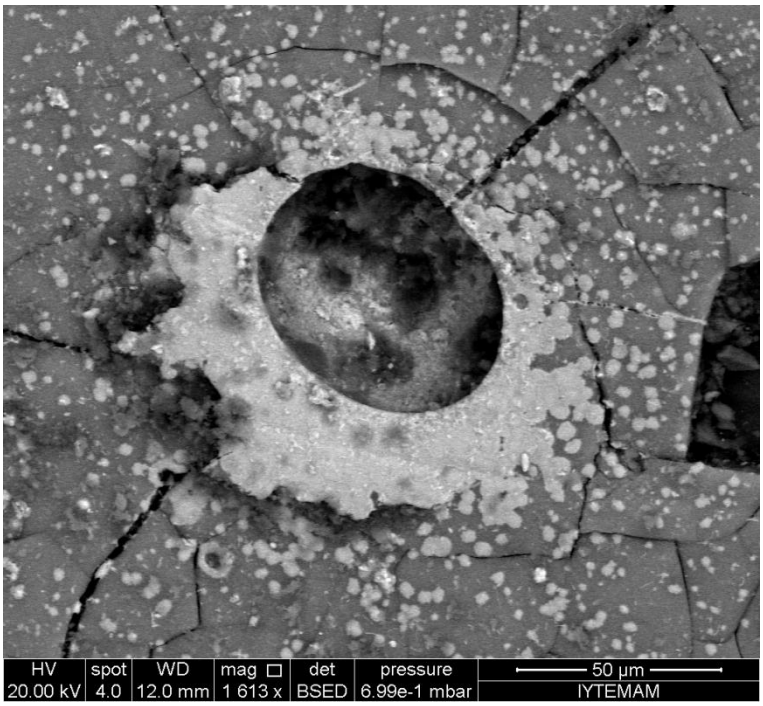

Figure 4. 80. SEM image of air bubbles in green glass tesserae (G-Dgt2)

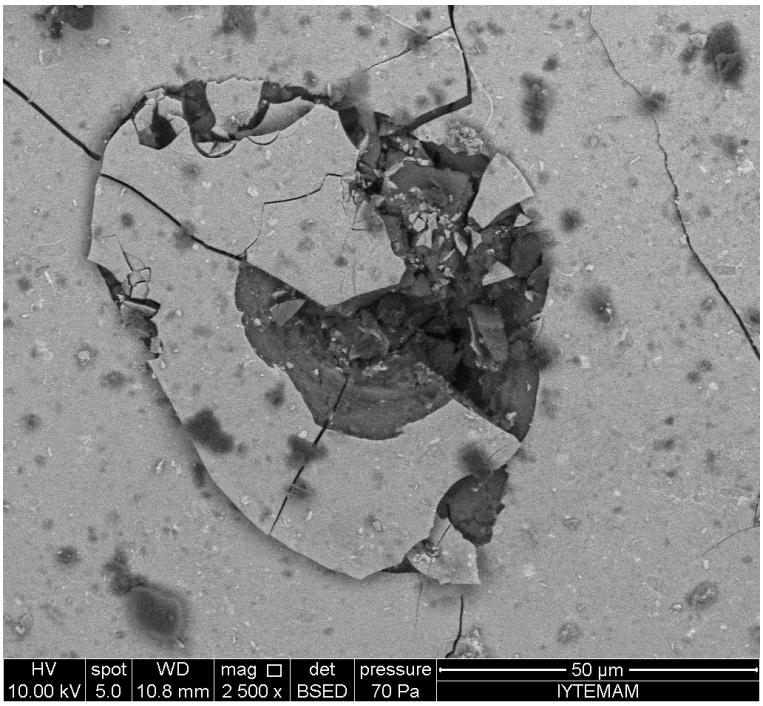

Figure 4. 81. SEM image of micro-cracks in green glass tesserae (G-Dgt2)

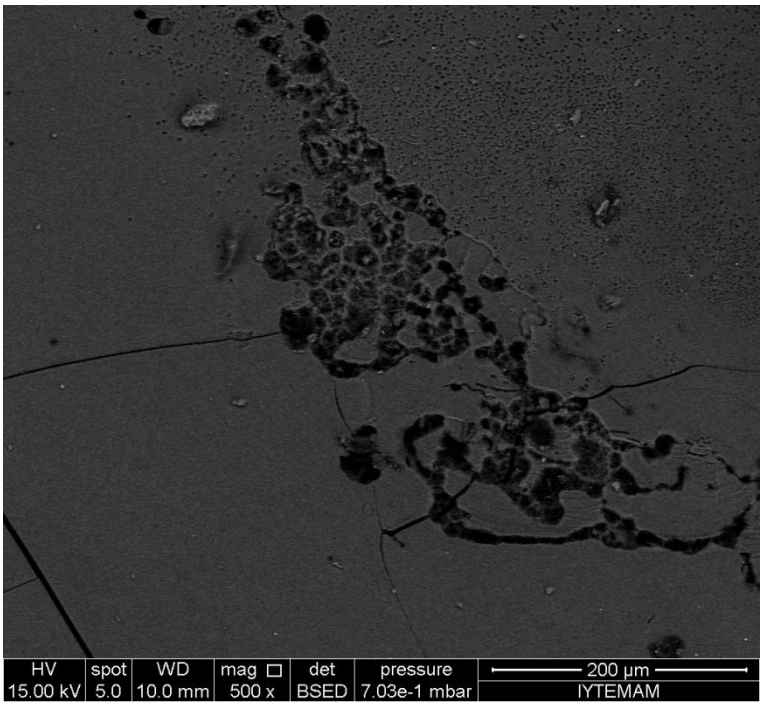

Figure 4. 82. SEM image of pitting in white glass tesserae (G-Wt)

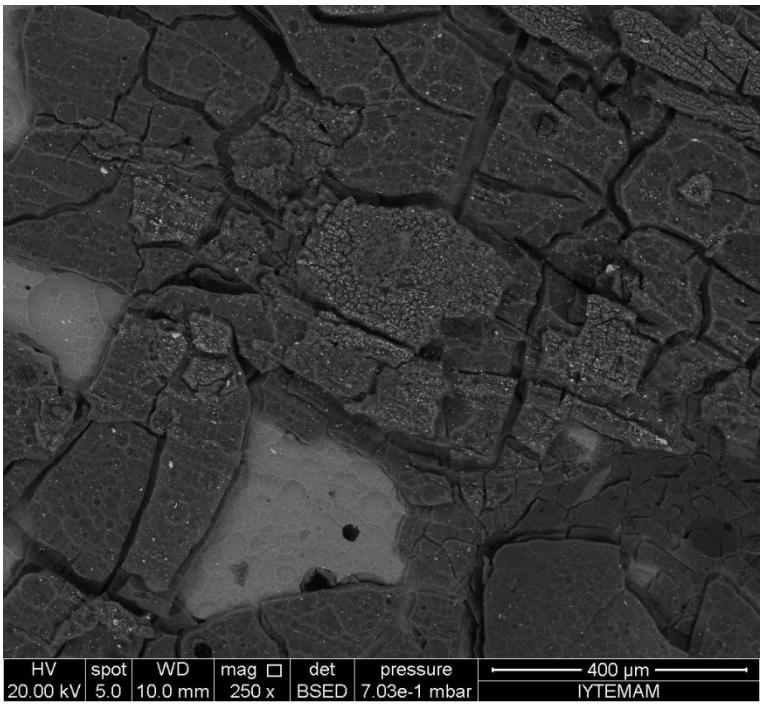

Figure 4. 83. SEM image of blistering in yellow glass tessera (G-Yt)

CHAPTER 5

CONCLUSION

In this study, material characteristics of Roman mosaics found in Antandros Ancient city (Altınoluk, Balıkesir) as well as their deterioration problems have been determined in order to define the properties of mosaics and the main characteristics of the intervention materials, which will be used in the conservation works of the mosaics.

The experimental studies involve determination of colours of tesserae, raw material compositions and hydraulicity of mosaic mortars, pozzolanic activities of brick aggregates, mineralogical and chemical compositions of tessera and mosaic mortars, microstructural characteristics of tesserae, soluble salt content of the mortars and tesserae as well as the problems of deterioration were determined.

Mosaics had a multilayered system composed of tesserae, bedding layer, nucleus and rudus from the surface to bottom. Tesserae were small cubes of stone, ceramic and opaque glass tesserae. The thin bedding layer in which the tesserae were embedded was non-hydraulic lime rich mortar. Nucleus and rudus layer mortars were composed of brick aggregates and lime. The nucleus layer was thinner and made of fine brick aggregates than the rudus one. Manufacturing of rudus and nucleus mortars were not the same when considering the particle size distribution of the brick aggregates in the mortars. Nucleus and rudus layer mortars were hydraulic due to the use of pozzolanic brick aggregates manufactured by using raw materials containing high amounts of clay minerals in their production. The nucleus and rudus mortar layers had high porosity and low density.

Tesserae had a higher density and lower porosity than mortars. The colours of the stone tessera were white, grey, beige and yellow. Beige and yellow stone tesserae were mainly composed of dolomite and tridymite composed of a high-temperature polymorph of quartz. White and grey ones were composed of mainly fine-grained calcite and quartz minerals.

The colors of the ceramic tesserae, used for the mosaics execution, were pink and red. They mainly consisted of quartz, calcite, albite and muscovite minerals. They contained high amounts of SiO_2 and Al_2O_3, and low amounts of MgO, CaO, Fe_2O_3,

Na_2O and K_2O. Red ceramic tesserae had high iron content while pink ones had low iron content. The red color of the ceramic was resulted from the effects of high amounts of iron oxide content. Pink and red ceramic tesserae were made from different raw clay sources by heating them at high temperatures. Red ones were made from calcium rich clay and pink ones from calcium poor clay.

The glass tesserae used in the mosaics could be provided from glass producing sites in Assos (Behramköy) in Roman time. Their colors were white, yellow, different hues of green and blue, turquoise, light brown, dark red and black. They were produced by melting silica sand (SiO_2), sodium carbonate (Na_2CO_3), calcium carbonate ($CaCO_3$) and lead oxide (PbO) as raw materials.

Tesserae were composed mostly of SiO_2, Na_2O, CaO and PbO. Depending upon chemical composition, they were classified into three groups. They were soda lime, lead and soda lime lead glasses. Natron was used in glass production during Roman period. It was mined in Egypt (Wadi Natrun, North-West of Cairo) and traded from Egypt to local glass workshops (Pliny 77 AD, Jacoby 1991, 1993, James 2006).

Soda-lime glasses were turquoise, dark turquoise, cyan, light blue, blue, light brown and black tesserae. Soda-lime-lead glasses were dark green and red tesserae and lead glasses were yellow, light green and dark green tesserae.

Glass tesserae were opacified with Ca and Pb-antimonates with in situ and ex situ crystallizations. Yellow and green tesserae were opacified with Pb-antimonate in the form of bindheimite ($Pb_2Sb_2O_7$) by ex-situ crystallization. White, turquoise, blue and cyan glass tesserae were opacified with $CaSb_2O_6$ crystals by in situ crystallization. However, black tessera was opacified by air bubbles. Dark red tesserae were opacified with copper and iron oxides.

White tesserae were colored with Ca-antimony, while yellow tesserae were colored with Pb-antimony and green tesserae with copper and lead oxides. Turquoise and cyan tesserae were colored with copper oxides and blue tesserae were colored with combinations of copper, cobalt and iron oxides. Black tessera was colored with iron oxides. Brown tessera was colored with manganese oxide and dark red tesserae were colored with copper and iron oxides.

Deterioration processes of the mosaics in Antandros Ancient city caused by destroyed original drainage systems, settlement in the mosaic floors, changes in temperature and humidity and biological colonization. The soluble salts were not effective for the deterioration of mosaics.

Glass tesserae were leached by water during burial and after excavation. Leaching causes corrosion, micro cracks and pitting on the surface of the glass tesserae. Micro cracks allow water to penetrate inside the tesserae and increase. These processes increase the propagation of micro-cracks, blistering and cause to biological colonization in detached surfaces.

All tesserae surfaces had deposit layers composed mainly of calcite and clay minerals due to subsequent dissolution and precipitation reaction of bedding mortar layers.

Taking into account the interventions made in the light of the results obtained from this study, the following recommendations can be made;

- The original surface water drainage systems should be investigated and all proper repairs should be made.
- Mosaics should be protected from rain and sunlight with proper shelters.
- The filling of cracks or gaps observed in rudus and nucleus layers will be treated by mortars produced by pure aged lime putty and pozzolanic brick aggregates.
- Use of sea sand and cement in the filling of cracks or gaps of rudus, nucleus and bedding layer mortars leads to rapid deterioration of the mosaics.
- The deteriorated bedding layer will be consolidated with the pure aged lime putty.
- The detached tesserae will be re-bedded by injection with the pure aged lime putty.
- Deposit layers formed on the tesserae surfaces can be removed by a soft nylon brush, scalpels or dental instruments after softening with pure water. Acids or bases should not be used to remove the deposited layers.

REFERENCES

Adam, J.P. 1984. *La Construction Romaine, Matériaux et Techniques*. Editions et J. Picard, Paris.

Alberti, L.B. 1965. *Of Pavements according to the Opinion of Pliny and Vitruvius, and the Works of the Ancients*. Ten Books on Architecture, (Translated into English by J. Leoni) London, pp. 61-63.

Anthony, E.W. 1965. *A History of Mosaics*. New York, Hacker Art Books.

Aslan Ö., Böke H. 2009. *Properties of Roman bricks and mortars used in Serapis Temple in the City of Pergamon.* Materials Characterization 60, pp. 995-1000.

Atik, Ş. 2004. *MÖ. I. Binde Anadolu'da Cam Üretimi Ve Tasarımı*. Phd Thesis, Mimar Sinan Üniversitesi, Fen Bilimleri Enstitüsü, Endüstri Ürünleri Tasarimi Ana Bilim Dalı Tasarim, İstanbul.

Bakolas, A., Biscontin, G., Moropoulou, A., Zendri, E. 1998. *Characterization of Structural Byzantine Mortars by Thermogravimetric Analysis*, Thermochimica Acta, Vol. 321, No.1-2, p. 151-160.

Barber, D.J., Freestone, I.C., Moulding, K.M. 2009. *Ancient copper red glasses: investigation and analysis by microbeam techniques*, in From Mine to Microscope, Advances in the Study of Ancient Technology. Shortland, A., Freestone, I., Rehren, T., (Eds.), Oxbow Books, Oxford, pp. 115–127.

Bimson, M., Werner, A.E. 1967. *Two problems in ancient glass: opacifiers and Egyptian core material*. Annales of the 4th Congress of the AIHV, Ravenna, Venise (Italy), pp. 262-266.

Blake, E.M. 1930. The pavements of the Roman Building of the Republic and Early Empire, Memoirs of the American Academy in Rome VII, p. 70.

Boschetti, C., Corradi B.A., Fabbri, B., Leonelli, C., Macchiarola, M., Ruffini, A., Santoro S., Speranza, M., Veronesi, P. 2007. *Caratterizzazione archeometrica dei mosaici del ninfeo della Domus del Centenario*, in Pompei: Insula del Centenario (IX, 8). Indagini diagnostiche e geofisiche e analisi archeometriche su muri, malte, pigmenti, colori, mosaici, ed. Sara Santoro Bianchi, Studi e Scavi, v. 16, Bologna, pp. 259–308.

Böke H., Akkurt S., İpekoğlu B., Uğurlu E. 2006. *Characteristics of brick used as aggregate in historic brick-lime mortars and plasters.* Cement and Concrete Research 36, p. 1115–1122.

Braidwood, R.J., and Çambel H. 1983. *Çayönü*, Arkeoloji ve Sanat, 18/19, pp. 3-8.

Brett, G. 1942. *The Mosaic of the Great Palace in Constantinople*. Journal of the Warburg and Courtauld Institutes, vol. 5, pp. 34-43.

Brill, R.H. 1968. *The scientific investigation of ancient glasses*. Proceedings of the 8th International Congress on Glass, pp. 47–68.

Brill, R.H. 1976. *Scientific studies of the panel materials*, in Kenchreai: Eastern Port of Corinth. II. The Panels of the Opus Sectile in Glass, L. Ibrahim, R. Scranton, R.H. Brill (Eds.), Brill Academic Publishers, Leiden (1976), pp. 227–255

Brill, R.H., Cahill, N.D. 1988. *A red opaque glass from Sardis and some thoughts on red opaques in general*. The Journal of Glass Studies vol. 30, pp. 16-27.

Brill, R.H. 1988. *Scientific Investigations of the Jalame Glass and Related Finds*. Chapter 9 of Excavations at Jalame: site of a glass factory in late Roman Palestine. Ed. G. D. Weinberg. Columbia: U of Missouri P,. pp. 257-294.

Brun, N., Mazerolles, L., Pernot, M. 1991. *Microstructure of opaque red glass containing copper*. Journal of Materials Science Letters, Volume 10, Issue 23, pp. 1418-1420.

Butler, K.H., Bergin, M.J., Hannaford, J. 1950. *Calcium antimonates*. Journal of the Electrochemical Society 97, 117-122.

Cable, M. and Smedley, J. 1987. *The replication of an opaque red glass from Nimrud*. In: Early Vitreous Materials. Bimson, M., Freestone, I.C. (Eds.), British Museum Occasional Paper 56, London, pp. 151-164.

Campbell, D.S. 1979. *Roman Mosaic Workshops in Turkey*Author. American Journal of Archaeology, Vol. 83, No. 3, pp. 287-292.

Chlouveraki, S.N. and Politis, K.D. 2003. *The documentation and conservation of the nave mosaic in the basilica of Agios Lot at Deir, Ain, Abata, Jordan. In Mosaics make a site: The Conservation in Situ of Mosaics on Archaeological Sites*: Proceedings of the VIth Conference of the International Committee for the Conservation of Mosaics, Nicosia, Cyprus, 1996, ed. D. Michaelides, Rome, ICMM, pp. 149-156.

Costagliola, P., Baldi, G., Cipriania, C., Pecchionic, E., Bucciantic, A. 2000. *Mineralogical and chemical characterisation of the Medicean glass mosaic tesserae and mortars of the Grotta del Buontalenti, Giardino di Boboli, Florence, Italy*, Journal of Cultural Heritage 1, p.p 287–299.

Cronyn, J.M. 1990. *The Elements of Archaeological Conservation*. London.

Davison, S. 1989. *Conservation and Restoration of Glass.* The Conservation Studio, Thame, Oxfordshire.

Dierks, L. 2004. *Making Mosaics: Designs, Techniques & Projects*. Sterling Publishing Company, Inc., New York.

Dunbabin, K.M. 1999. *Mosaics of the Greek and Roman World*. Cambridge University Press, Cambridge.

Efe, N. 2009. *Analysis of Materials Used in Mosaic Making.* M.Sc. Thesis, Istanbul Technical University, İstanbul.

Erkan, O. 2006. *Mozaik Sanati ve Büyük Saray Mozaikleri Restorasyon Çalışmaları.* M.Sc. Thesis, Maltepe Üniversitesi, İstanbul.

Fawcett, J. 1998. *Historic Floors: Their History and Conservation*. Butterworth-Heinemann, Oxford, in association with ICOMOS UK.

Fiori, C., Donati, F., Mambelli, R., Racagni, P. 1988. *A study of the structure and materials found in the different layers of two mosaic pavements in the archaeological zone of Ravenna*, in: Mosaico e Restauro Musivo, Quaderni Irtec 1, C. Fiori, R. Mambelli, L., Faenza, pp. 66-79.

Fiori, C., Vandini, M., Mazzotti, V. 2003. *Colore e tecnologia degli smalti musivi dei riquadri di Giustiniano e Teodora nella Basilica di San Vitale a Ravenna*. Ceramurgia *XXXIII*, 135-154.

Freestone, I.C., Bimson, M., Buckton, D. 1990. *Compositional categories of Byzantine glass tesserae.* Annales du 11e Congrès de l'Association Internationale pour l'Histoire du Verre, Amsterdam, pp. 271-279.

Freestone, I.C. 1987. *Composition and microstructure of early opaque red glass*. In: Early Vitreous Materials. Bimson, M., Freestone, I.C. (Eds.), British Museum Occasional Paper 56, London, pp. 173-191.

Freestone, I.C., Leslie, K.A., Thirlwall, M. and Gorin-Rosen, Y. 2003a. *Strontium isotopes in the investigation of early glass production: Byzantine and early Islamic glass from the near east.* Archaeometry *45*, pp. 19-32.

Freestone, I.C., Stapleton, C.P., Rigby, V. 2003b. *The production of red glass and enamel in the Late Iron Age, Roman and Byzantine periods*. In: Through a Glass

Brightly - Studies in Byzantine and Medieval Art and Archaeology Presented to David Buckton. Entwistle, C. (Ed.). Oxbow Books, Oxford, pp. 142-154.

Galli, S., Mastelloni, M., Ponterio, R., Sabatino, G., Triscari, M., 2004. *Raman and scanning electron microscopy and energy-dispersive X-ray techniques for the characterization of coloring and opaquening agents in Roman mosaic glass tesserae*. Journal of Raman Spectroscopy 35, 622-627.

Gauckler, P. 1897. Domaine des Laberii a Uthina in Monuments Piot, III.

Genç, A. 1994. *Bizans ve Roma'da Mozaik Sanatı*, Dokuz Eylül Üniversitesi Güzel Sanatlar Fakültesi Dergisi, VIII-IX, p. 87-93.

Haga, K., Shibata, M., Hironaga, M., Tanaka, S., Nagasaki, S. 2002. *Silicate Anion Structural Change in Calcium Silicate Hydrate Gel on Dissolution of Hydrated Cement*, Journal of nuclear Science and Technology, Vol. 39, No. 5, p. 540-547. doi: 10.1080/18811248.2002.9715232.

Harden, D. B. 1968. *Ancient glass I: Pre-Roman*. Archaeological Journal 125, pp. 46-72.

Haswell, J. M. 1973. *Mosaic*. The Thames and Hudson, London, p. 184.

Hartmann, G. 1994. *Late-medieval glass manufacture in the Eichsfeld region (Thuringia, Germany).* Chemie der Erde 54, pp. 103-128.

Henderson, J. 1991. *Chemical characterization of Roman glass vessels, enamels and tesserae in Vandiver,* Material Issues in Art and Archaeology II, Materials Research Society 185, Pittsburgh, Pennsylvania, pp. 601-7.

Henderson, J. 1988. *Electron probe microanalysis of mixed-alkali glasses.* Archaeometry , vol. 30, no. 1, pp. 77-91.

Henderson, J. 1991. *Chemical characterization of Roman glass vessels, enamels and tesserae.* Materials Research Society, Symposium Proceedings, Pittsburgh, vol. 185, pp. 601–607. doi: 10.1557/PROC-185-601.

Herodotos, 1991. *Herodot Tarihi, (*Translated into Turkish by M. Ökmen), Remzi Kitabevi, İstanbul.

Henderson, J. 2000. *The Science and Archaeology of Materials: an Investigation of Inorganic Materials*. Routledge, London.

ICCROM, 1983. *Mosaics No.2: Safeguard, Carthage 1978, Périguez 1980.* ICCROM, Rome.

Işıklıkaya, R. Işıl. 2010. *Perge Mozaikleri, Macellum, Güney Hamam ve Geç Dönem Meydanı Doğu Portiği, Cilt 1*, Unpublished Phd. Thesis, İstanbul Üniversitesi, İstanbul.

İdil, A. Ç. 1982. *Conservation and restoration of mosaics at Aphrodisias, Turkey*, International Committee for Mosaics Conservation, Newsletter/Chronique. Comite International pour la Conservation des Mosaiques 5, pp. 14-18.

Jacoby, D. 1991. *Research on the Venetian glass industry in the Middle Ages*, Journal of Glass Studies 33. pp. 119-20.

Jacoby, D. 1993. *Raw materials for the glass industries of Venice and the Terrafirma*, c.1370–c.1460', Journal of Glass Studies 35. pp. 65-90.

James, L. 2006. *Byzantine glass mosaic tesserae: some material considerations*, Byzantine and Modern Greek Studies Vol. 30 No. 1. Pp. 29-47

Jansssens, K.H.A. 2013. *Modern Methods for Analysing Archeological and Historical Glass.* John Wiley&Sons, Ltd, United Kingdom.

Jobst, W. 1978. *Romische Mosaiken aus Ephesos I*, Die Hanghauser des Embolos. Corpus der antiken Mosaiken in der Türkei I.

Kaletsch, H. 1958. Zur Iydischen Chronologie. *Historia*.

Kaplan,. M., Matero, F., Hinchman, J., Keller, M., Thompson, T. 2011. *Conservation of Gordion's Pebble Mosaic Pavement.* Architectural Conservation Laboratory School of Design, University of Pennsylvania.

Kiepert, H. 1889. *Die alten Ortslagen am Sudfufse des Idagebirges*, Zeitschrift des Gesellschaft fur Erdkunde zu Berlin, 24, pp. 290-303.

Lahlil, S., Biron, I., Galoisy, L., Morin, G. 2008. *Rediscovering ancient glass Technologies through the examination of opacifier crystals*, Applied Physics. A 92, pp. 109-116.

Lahlil, S., Biron, I., Cotte, M., Susini, J., Menguy, N. 2010 b. *Synthesis of calcium antimonate nano-crystals by the 18th dynasty Egyptian glassmakers.* Applied Physics A 98, pp. 1-8. Doi: 10.1007/s00339-009-5454-1 pp.1-8

Lahlil, S., Cotte, M., Biron, I., Szlachetko, J., Menguy, N., Susini, J. 2011. *Synthesizing lead antimonate in ancient and modern opaque glass*, Journal of Analytical Atomic Spectrometry, Volume 26, issue 5 p. 1040-1050. Doi: 10.1039/c0ja00251h

Lauwers, V., Patrick, D.W.M. 2007. *Evidence for Anatolian glassworking in Antiquity: the case of Sagalassos (Southwestern Turkey)*, Journal of Glass Studies vol49, pp 39-46.

Leaf, W. 1923. *Strabo on the Troad*, Cambridge.

Lemke, C. 1998. *Reflections of the Roman Empire: the first century glass industry as seen through traditions of manufacture*. In: Prehistory and History of Glassmaking Technology. McCray, P., Kingery, W. (Eds.). Ceramics and Civilization, vol. VIII. The American Ceramics Society, Westerville, pp. 269-291.

Lovoos, J., Paramore, F. 1969. *Modern Mosaic Techniques*. Watson-Guptill Publications, New York.

Lopreato, P., Fiori, C., Perpignani, P. 2003. *Basilica di Santa Eufemia a Grado: storia, restauro e indagine scientifica, in:* Mosaics, Conserve to Display? VIIth Conference of the International Committee for the Conservation of Mosaics: Proceedings, ed. P. Blanc, 177-90. Arles: Musee de l'Arles et de la Provence antiques.

Luxán, M.P., Madruga, F., Saavedra, J. 1989. *Rapid Evaluation of Pozzolanic Activity of Natural Products of Conductivity Measurement*, Cement and Concrete Research, Vol. 19, p. 63-68. Doi: 10.1016/0008-8846(89)90066-5.

Malay, H. 1992. *Helenistik Devirde Pergamon ve Aristonikos Ayaklanması*, Bergama Belediyesi Kültür Yayınları, İzmir.

Marchese B. and Garzillo V., 1983. *An Investigation of The Mosaics In The Cathedral of Salerno Part I. Characterization of Binding Materials,* Studies in Conservation, pp. 28, 127-132.

Macchiarola, M. and Fiorella G. 2005. *The study of hydraulic lime mortars for the conservation of mosaics.* In: Lessons Learned: Reflecting on the Theory and Practice of Mosaic Conservation. Proceedings of the 9th ICCM conference, Hammamet, Tunisia, pp. 273-280.

Mass, J.L., Stone, R.E., Wypyski, M.T. 1997. *An investigation of the antimony containing minerals used by the Romans to prepare opaque colored glasses.* In: Materials Issues in Art and Archaeology V. Materials Research Society,

Vandiver, P.B., Druzik, J.R., Merkel, J.F., Stewart, J. (Eds.), Warrendale, pp. 193-204. Doi: http://dx.doi.org/10.1557/PROC-462-193

Mass, J., Stone, R.E., Wypyski, M.T. 1998. *The mineralogical and metallurgical origins of Roman opaque colored glasses*, in: The Prehistory and History of Glassmaking Technology, Ceramics and CivilisationVIII McGray, P., Kingery, W. (Eds.). The American Ceramics Society, Westerville (Ohio), pp. 121-144.

Mass, J.L., Wypyski, M.T., Stone, R.E. 2001. *Evidence for the metallurgical origins of glass at two ancient Egyptian glass factories.* Materials Research Society Bulletin, pp. 26-38. Doi: http://dx.doi.org/10.1557/mrs2001.17

Mass, J.L., Wypyski, M.T., Stone, R.E. 2002. *Malkata and Lisht glassmaking technologies: towards a specific link between second millennium BC metallurgists and glassmakers.* Archaeometry 44, 1, pp. 67- 82.

Mirti, P., Davit, P., Gulmini, M. 2002. *Colorants and opacifiers in seventh and eighth century glass investigated by spectroscopic techniques,* Analytical and Bioanalytical Chemistry, 372, pp. 221-229. doi: 10.1007/s00216-001-1183-9

Montanaro, M., Barboni, R., Macchiarola, M. 1998. Trasporto *e restauro del mosaico con tigre marina proveniente dall'area archeologica dell'antica Histonium (Vasto, Chieti),* in Atti del V colloquio dell'Associazione italiana per lo studio e la conservazione del mosaico, F. Guidobaldi, A. Paribeni, Edizioni del Girasole, Ravenna, pp. 385-398.

Moretti, C., Gratuze, B. 2002. *Vetri romani di Aquileia e di altri siti europei: analisi chimiche e studio comparativo.* Riv Staz Sper Vetro 32, 19–28.

Moropoulou, A., Bakolas, A., Bisbikou K. 2000a. *Investigation of the Technology of Historic Mortars,* Journal of Cultural Heritage, Vol. 1, pp.45-48.

Newton, E.G. 1980. *Recent views on ancient glass*, Glass Tech., 21, 173-183.

Newton, R.G. and Davison, S. 1989. *Conservation of Glass*. Butterworth Heinemann, Oxford.

Nicholson, P.T. 1993. *Ancient Egyptian faience and glass, Shire Egyptology,* London.

Ödekan, A. 1997. *Mozaik*. Eczacıbaşı Sanat Ansiklopedisi, 2.cilt, YEM Yayınları, pp. 1300-1302.

Özügül, A. 1996. *Antik Döşeme Mozaiklerinde Bordür Motifleri*., Unpublished Msc Thesis. İstanbul Teknik Üniversitesi, İstanbul.

Palomar, T., Oujja, M., Garcia-Heras, M., Villegas, M.A., Castillejo, M. 2013. *Laser induced breakdown spectroscopy for analysis characterization of degradation pathologies of Roman glasses.* Spectrochemica Acta Part B: Atomic Spectroscopy. Doi:10,1016/j.sab.2013.05.004

Peltenberg, E.J. 1987. *Early faience: recent studies, origins and relations with glass*, in: Early vitreous materials. Bimson M. and Freestone I. C., (Eds.). British Museum Occasional Papers, 56, London.

Pliny, 1962. *Natural History, 10, Book XXXVI* (Translated into English by Eicholz) Loeb Classical Library.

Polat, G. 2002. *Antandros 2001 Yılı Kazıları*, 24. Kazı Sonuçları Toplantısı, Cilt 2, Ankara.

Polat, G., Polat, Y. 2003. *Antandros 2002 Yılı Kazıları*; 25. Kazı Sonuçları Toplantısı, Cilt 1, Ankara.

Polat, G., Polat, Y. 2005. *Antandros 2003-2004 Yılı Kazıları*; 27. Kazı Sonuçları Toplantısı, Cilt 2, Antalya.

Polat, G., Polat, Y., Yağız, K. 2006. *Antandros 2005 Yılı Kazıları*; 28. Kazı Sonuçları Toplantısı, Cilt 2, Çanakkale.

Polat, G., Polat, Y., Yağız, K., Küçük, T. 2007. *Antandros 2006 Yılı Kazıları*; 29. Kazı Sonuçları Toplantısı, Cilt 2, Kocaeli.

Polat, G., Polat, Y., Yağız, K., Küçük, T. 2009. *Antandros 2008 Yılı Kazıları*; 31. Kazı Sonuçları Toplantısı, Cilt 4, Denizli.

Polat, G., Polat, Y., Yağız, K., Küçük, T. 2011 *Antandros 2010 Yılı Kazıları*; 33. Kazı Sonuçları Toplantısı, Cilt 1, Malatya.

Rehren, T. 2003. *Comments on J.L. Mass, M.T. Wypyski and R.E. Stone 'Malkata and Lisht glassmaking technologies: towards a specific link between second millennium BC metallurgists and glassmakers. Archaeometry 44 (1), 67–82. reply (2002).* Archaeometry 45(1), 185–190.

Ricciardi, P., Colomban, P., Aure´ lie Tournie´, Macchiarola, M., Ayed N. 2009. *A non-invasive study of Roman Age mosaic glass tesserae by means of Raman spectroscopy*, Journal of Archaeological Science 36. 2551–2559.

Ruffini, A., Fiori, C., Vandini, M. 1999a. *Caratterizzazione chimica di vetri musivi antichi Parte 1: metodologie d'analisi e risultati,* Ceramurgia XXIX (4), 285–295.

Ruffini, A., Fiori, C., Vandini, M. 1999b. *Caratterizzazione chimica di vetri musivi antichi Parte 2: Elaborazione dei dati analitici*, Ceramurgia XXIX (5–6), 361–368.

Saltuk, S. 1997. *Arkeoloji Sözlügü 3.b*. İnkılap Kitabevi, İstanbul.

Santagostino, B.A., Gliozzo, E., D'Acapito, F., Memmi T.I., Turchiano, M., Volpe, G. 2008. *The Sectilia panels of Faragola (Ascoli Satriano, Southern Italy): a multi-analytical study of the red, orange and yellow glass slabs*, Archaeometry 50, pp. 451-473.

Sayre, E.V. and Smith R.W. 1961. *Compositional Categories of Ancient Glass*, American Association for the Advancement of Science, Vol. 133, No. 3467

Sayre, E.V. 1963. *The Intentional use of antimony and manganese in ancient glasses*. In: Advances in Glass Technology, Part 2. Matson, F.R., Rindone, G.E. (Eds.), Plenum Press, New York, pp. 263-282.

Sekban, B. 2007. *Antandros Yamaç Evleri Terra Sigillata Buluntuları*. M.Sc. Thesis, Ege Universitesi, İzmir.

Schaffer, R.J. 1932. *The Weathering of Natural Building Stones, Special Report No: 18.* Garston Watford: Building Research Establishment.

Schibille, N., Degryse, P., Corremans, M., Christian G., Specht D. 2012. *Chemical characterisation of glass mosaic tesserae from sixth-century Sagalassos (south-west Turkey): chronology and production techniques*. Journal of Archaeological Science 39, pp. 1480-1492.

Shortland, A., Schachner, L., Freestone, I., Tite, M. 2006a. *Natron as a flux in the early vitreous materials industry: sources, beginnings and reasons for decline*, Journal of. Archaeological Science 33, pp. 521–530.

Shugar, A.N. 2000. *Byzantine opaque red glass tesserae from Beit Shean, Israel*. Archaeometry 42 (2), pp. 375–384.

Smith, J.T. 1998. *Roman Villas.* A Study in Social Structure. Routledge, London.

Sözen, M., Tanyeli, U. 1999. *Sanat Kavram ve Terimleri Sözlügü*, *5.b*. Remzi Kitabevi, İstanbul.

Starinieri, V. 2009. *Study of Materials and Technology of Ancient Floor Mosaics Substrate,* PhD Thesis, Università di Bologna.

Stephanos Byzantion, Etnikon, Chicago, İllinois, MCMXCII.

Strabon. 2005. *Antik Anadolu Coğrafyası - Geographika*. İstanbul: Arkeoloji ve Sanat Yayınları.

Strong, E. 1929. *Art in Ancient Rome, vol II,* London. p. 33.

Şahin, M. 2010. *Mozaik Sanatı, Antakya ve Zeugma Mozaiklerinin Resim Analizleri*. M.Sc. Thesis, Anadolu Üniversitesi, Eskişehir.

Şirin, M. 2011. *Anadolu'da Roma Dönemi Mozaik Sanatinda Konu Biçim Anlayişi, Bu Anlayişi Oluşturan Kültürel Etkiler ve Bu Etkilerin Erken Hiristiyanlik Sanatina Kadarki Evrimi*. Msc Thesis, Mimar Sinan Güzel Sanatlar Üniversitesi, İstanbul.

Tabanlı D. 2007. *Roma Dönemi Mozaiklerinin Efes Örneğinde incelenmesi*. M.Sc. Thesis Dokuz Eylül Üniversitesi, İzmir.

Tait, H. 1991. *Five Thousand Years of Glass*. BMP, London.

Tite, M., Pradell, T., Shortland, A. 2008. *Discovery, production and use of tin-based opacifiers in glasses, enamels and glazes from the late iron age onwards: a reassessment*. Archaeometry 50, pp. 67-84. Doi: 10.1111/j.1475-4754.2007.00339.x

The Getty Conservation Institute. 2002. *Newsletter, Conservation 17* (3), p. 26.

The Getty Conservation Institute and the Israel Antiquities Authority. 2003. *Mosaics in Situ Project: Illustrated Glossary*.

The Getty Conservation Institute. 2011. *Technician Training for the Maintenance of in Situ Mosaics*, J. Paul Getty Trust and Institut National du Patrimoine de Tunisie.

Thukydides, 1976. *Peloponnesos Savası*, (Translated into English by T. Gökçöl). İstanbul.

Todua, T.I. 1975. *Removal and restoration of the Bichvinta mosaic*, in Icom committee for conservation. 4th triennial meeting, Venice, 13-18 October. Preprints, Icom, Paris, 75113-1-7.

Torraca, G. 2009. *Lectures on Materials Science for Architectural Conservation.* The Getty Conservation Institute. Los Angeles.

Triscari, M., Quartieri, S., Sabatino, G., Vezzalini, G., Arletti, R., Mastelloni, M.A. 2005. *Analisi archeometrica di tessere musive in pasta vitrea da un pavimento di Lipari*. Quaderni del Museo Regionale di Messina 11.

Tsakirgis, B. 1990. *The Decorated Pavements of Morgantina II: The Opus Signinum*. American Journal of Archaeology, Vol. 94, No. 3. Archaeological Institute of America. pp. 425-443.

Turner, W.E.S., Rooksby, H.P. 1959. *A study of the opalising agents in ancient opal glassesthroughout three thousand four hundred years*. Glastechnische Berichte Heft 8, Sonderband: V. Internationaler Glaskongress, pp. 17-28.

Quien, M.Le. 1958. *Oriens Christianus I,* Graz.

Uboldi, M., Veritá, M. 2003. *Scientific analyses of glasses from late Antique and early medieval archaeological sites in northern Italy*. Journal of Glass Studies 45, pp. 115-137.

Uğur, T. 2011. *Perge Antik Kentine Ait Mozaik Harçlarinin Karakterizasyonu*. M.Sc. Thesis İstanbul Üniversitesi, İstanbul.

Uğurlu, E. and Böke H. 2009. *The use of brick–lime plasters and their relevance to climatic conditions of historic bath buildings*. Construction and Building Materials 23, pp. 2442–2450.

Uğuryol, M.F. 2005. *Arkeolojik Taban Mozaiklerinin, Restorasyonu, Konservasyonu ve Sergilenmesi*. M.Sc. Thesis, Yıldız Teknik Üniversitesi, İstanbul.

Üstüner, A.C. 2002. *Mozaik Sanatı*, Engin Yayıncılık, First Edition İstanbul.

Vance, P. and Goodrick-Clarke, C. 1994. *The Mosaic Book: Ideas, Projects and Techniques*. Conran Octopus Limited, London.

Vandini, M., Fiori, C., Cametti, R. 2006. *Classification and technology of byzantine mosaic glass*. 96(9-10), Annali di chimica. pp. 587-99.

Vergilius. 1998. *Aeneis*, (Translated into English by T.Uzel), Ankara.

Verita, M. 2000. *Technology and deterioration of vitreous mosaic tesserae.* Reviews in Conservation, Volume 1, pp. 65-76.

Verita, M., Arena, M.S., Carruba, A.M., Santopadre, P. 2008. *Roman glass: art and technology in a 4th century AD opus sectile in Ostia (Rome).* Journal of Cultural Heritage 9, pp. 16-20.

Vitruvius. 1914. *The Ten Books on Architecture*. (Translated into English by Morris Hicky Morgan), Harvard University.

Von Saldern, A. 1974. *Gläser der Antike*. Museum fur Kunst und Gewerbe, Hamburg.

Werf, Inez van der., Mangone, A., Giannossa, L.C., Traini, A., Laviano, R., Coralini, A., Sabbatini, L. 2009. *Archaeometric investigation of Roman tesserae from Herculaneum (Italy) by the combined use of complementary micro-destructive analytical techniques,*Journal of Archaeological Science 36, pp. 2625-2634.

Xenophon, 1999. *Hellenika*, (Translated into English by Prof. Dr. S. Sinanoglu), Ankara.

Young, R.S. 1965a. *Early Mosaics at Gordion*, Expedition / (spring) 4-13.